AN ARTIFICIAL SKELETAL MUSCLE FOR USE IN PEDIATRIC REHABILITATION ROBOTICS

by

Ahad Behboodi

A dissertation submitted to the Faculty of the University of Delaware in partial fulfillment of the requirements for the degree of Doctor of Philosophy in Biomechanics and Movement Science

Summer 2019

AN ARTIFICIAL SKELETAL MUSCLE FOR USE IN PEDIATRIC REHABILITATION ROBOTICS

by

Ahad Behboodi

Approved: _____
Samuel C.K. Lee, Ph.D.
Director of the Interdisciplinary Program in Biomechanics and Movement Science

Approved: _____
Kathleen S. Matt, Ph.D.
Dean of the College of Health Science

Approved: _____
Douglas J. Doren, Ph.D.
Interim Vice Provost for Graduate and Professional Education and Dean of the Graduate College

I certify that I have read this dissertation and that in my opinion it meets the academic and professional standard required by the University as a dissertation for the degree of Doctor of Philosophy.

Signed: _____

Samuel C.K. Lee, PT, Ph.D.
Professor in charge of dissertation

I certify that I have read this dissertation and that in my opinion it meets the academic and professional standard required by the University as a dissertation for the degree of Doctor of Philosophy.

Signed: _____

Stuart Binder-Macleod, PT, Ph.D.
Member of dissertation committee

I certify that I have read this dissertation and that in my opinion it meets the academic and professional standard required by the University as a dissertation for the degree of Doctor of Philosophy.

Signed: _____

Federico Carpi, Ph.D.
Member of dissertation committee

I certify that I have read this dissertation and that in my opinion it meets the academic and professional standard required by the University as a dissertation for the degree of Doctor of Philosophy.

Signed: _____

Fabrizio Sergi, Ph.D.
Member of dissertation committee

ACKNOWLEDGMENTS

Studying in one of the greatest biomechanics program in US and worldwide was a dream come true. My PhD study in the Biomechanics and Movement Science program in the Physical Therapy Department, #1 nationally, gave me the unique opportunity to learn from some of the greatest scientists and students in the field, which provided me with an invaluable foundation for more scientific achievements in the coming years. My PhD not only enhanced my scientific life, but also it shaped my personality and mentality; the most extensive and significant experience I have been through so far. Thus, I will do my best in my career to add to the fame and reputation of the program, department, and university.

This dissertation would not have been possible without my advisor, Dr. Samuel Lee. The level of autonomy and support, and thereby creativity, in his lab was exceptional in comparison to many other labs I know. I will never forget his support during my final presentation for the first grant I was awarded as the principle investigator. In addition, I was so lucky to benefit from the mentorship of Dr. Stuart Binder-Macleod whom I have always looked up to during my academic career. I could not have asked for better committee members. Without Dr. Carpi's consultants and guidance the artificial muscle project would not be able to proceed. Dr. Sergi was the last added member; nonetheless, his guidance substantially improved the dissertation, especially the third aim.

Many thanks to my present and previous lab-mates, especially Henry Wright. His patience and LabVIEW skills helped me through the several projects I have

accomplished throughout these six years. More importantly, he was always there when I needed a pickle back. Nicole Zahradka and Anastasia Zarkou, who substantially helped me acclimate to my PhD life. James Alesi, his LabVIEW skills substantially improved mine and the messy codes I had written. Khushboo Verma and Ashwini Sansare, who joined the lab during the last year of my PhD, but helped me go through the most stressful year of my life. I will never forget the taste of the Indian food they brought me when I was writing my dissertation document. I was truly lucky to be part of this lab.

I would like to take the opportunity to thank my parents in Iran, who trained me to be a trooper, and have been guiding me through all of my best decisions. My special brother, who has believed in my capabilities like no other, and when nobody did; I truly owe all of my scientific achievements to him more than anybody else. I was so blessed to have a loving and caring family in US. Amoo Nader, Khale Lida, Taraneh, AmirAli, Amoo Shahryar , Khale Nadi, and Ame Farah: without you my life in US would be miserable with all the distance and the travel ban. My family's unconditional love has made me a happy, empathic, caring and, hopeful person.

I am truly speechless when it comes to Bahareh and Ali and their tremendous love and support. I am ever grateful for having you guys in my life.

A special shout out to my amazing friends, who made my PhD study an absolutely awesome experience. Mohammadam and Tiphanie; Ali Abdolali and Hosna; Reza and Elham; Amoo Erfan; Amoo Sina; Sina Bebeto, and Mohammad Shaf;. Thanks to them, I can confidently claim that I had the best PhD life among all international PhD students in US.

I want to thank my lovely girlfriend, Erin Kelleher, who made the stressful last couple of years of my PhD so wonderful. I really appreciate your support, JB.

This dissertation is dedicated to my grandma, Azizam. Once I started elementary school, she left her hometown, Shiraz, after 50 years living there, to come and take care of me while my mother was at work. I owe her a significant part of my personality, culture, and academic achievements. We shared many wonderful memories, which we could still laugh at last time I was back in Iran, three years ago. I have lost all of them now to Alzheimer's disease.

This dissertation work was supported by NIH DE-CTR ACCEL program, #U54-GM104941, Shriners Hospitals for Children-Philadelphia, # 87500-PHI-17.

Dear President Trump, at end I want to thank you for your maximum pressure policy on Iranians, which helped me grow emotionally and scientifically. Through your travel ban, I settled down better in US and got to visit your country in unprecedented detail for a PhD student. Hope I can help to keep America great.

TABLE OF CONTENTS

LIST OF TABLES

LIST OF FIGURES

ABSTRACT

Perceptual-motor experience is critical in early childhood for learning and cognition. By exploring object properties and relations among objects, infants develop visual-motor coordination, spatial skills, memory, language, cognition, and problem solving abilities. Such development and performance of activities of daily life (ADLs) rely heavily upon upper extremity function; and those with impaired reaching ability are at great risk for delays in these areas. While increasing user ADL independence, automated assistive devices may potentially increase the dose of interaction, which may enhance cognitive, social and motor development.

Many actuator materials and devices are used to power automated assistive devices, however, in orthotics and prosthetics, the requirement for a "natural" look and feel, to make the artificial or assisted limb feel integrated with the body, is limited by current technology. Bulky, heavy, noisy electrical motors are typically used, which substantially reduce user compliance of powered orthoses. For greater acceptance of such devices, the desired requirements include: low weight, quiet operation, soft feel, and size and shape approximating that of a natural limb, with cost being an important factor. Dielectric elastomer actuators (DEAs) feature great promise in fulfilling these requirements. Nonetheless, so far only a few studies have attempted to explore rehabilitation applications, and at a very preliminary level.

The overall goal of this dissertation is to develop a powered unilateral exoskeleton using a commercially available DEA that works as "artificial skeletal

muscle", and thereby, assess DEAs' capabilities and limitations to actuate rehabilitation robots.

In Aim 1, by assessment of the state of soft actuators technology, Stacked Dielectric Elastomer was chosen to form an artificial skeletal muscle for actuating an upper extremity rehabilitation exoskeleton. This was accomplished through comparison of five novel groups of soft actuators: Coiled Nylon Fiber, Ethanol-Based Phase-Change, Poly Vinyl Chloride Gel, Stacked Dielectric Elastomer and Hydraulically Amplified Self-Healing Electrostatic.

In Aim 2, the electro-mechanical properties of a commercially available CTsystems' stacked DEA (CT-SDEA) were benchmarked. CT-SDEA observed properties were then compared with the reported values for mammalian skeletal muscle and performance metrics, such as its length-tension properties and force generation hysteresis were assessed. Thereby, an artificial skeletal muscle using multiple CT-SDEAs in series and parallel was configured.

In Aim 3, the capability of adding proprioception to the configured artificial muscle was evaluated. This was done by measuring the length-dependent variation in capacitance of the CT-DEA, via a previously established length self-sensing technique. This length self-sensing technique then was added to an artificial muscle consisting of three CT-SDEAs in series. To mimic the muscle spindle's function in mammalian skeletal muscle, the length modulation of the middle CT-SDEA was then sensed, while the artificial muscle was contracting.

In Aim 4, the capability of the configured artificial muscle in actuation of a phantom upper extremity model's elbow joint was assessed. Multiple artificial muscle configuration were tested to actuate the joint. The artificial muscle consisting a bundle

of 3 myofibrils, each which containing five actuators in series, generated 22º of elbow flexion in the sagittal plane with 224 º/s angular velocity, under 1 N of tensile load.

These results demonstrated CT-SDEAs' potentials and limitations in rehabilitation applications. Using the benchmark testing results, appropriate assistive devices can be designed, which fit the capabilities of these versatile soft actuators. Further investigation is needed to assess CT-SDEAs capabilities in actuating joints with range of motion smaller than that of elbow, such as ankle.

.

Chapter 1

INTRODUCTION

1.1 Background and Significance

For young children, exploration using their arms significantly impacts cognitive, language, social, and perceptual-motor development[1–3]. Children demonstrating impaired or delayed use of their upper extremities often display developmental delays in the above areas. For example, infants with delayed reaching onset and less object exploration are not as successful at exploring and problem solving[4,5]. The ability to move one's arms against gravity is important for independent performance of countless activities of daily living (ADLs)[4,6]. Additionally, surveys of major impairments and disabilities in individuals with tetraplegia indicate that improving arm function rated high or very high in improving quality of life and would have high impact and priority[7,8]. Thus, the development of a powered, pediatric exoskeleton that can improve upper extremity function and may have profound immediate and long-term implications for populations with severe impairments.

Interventions exist to enhance upper extremity function in pediatric populations with severe impairment[9–13], however, there are a limited number of robotic devices available to enhance movement, exploration, and learning ADLs for these populations[14–16].

Positive outcomes of physical rehabilitation of neurologically based disorders depend heavily on the, duration, intensity, and task orientation of the training[17,18]. Additionally motor learning strategies that incorporate high-intensity practice, cognitive

engagement, and functional relevance are considered essential to successful therapy for pediatric movement disorders[19,20]. Such interventions, however, require a high level of hands-on assistance and supervision by a trained caregiver, which may be limited by clinical and insurance constraints, or caregiver accessibility. The durations of rehabilitation are getting shorter[21] and one approach to combat this problem is to develop devices that one can use in the home on a daily basis. By increasing the independence of the user in performance of ADLs, automation will potentially increase the dosage of interaction that consequently results in greater cognitive, social and development improved motor performance. Robot-assisted therapy is considered to be as effective or better than conventional therapy[22,23], because, 1) it is less labor intensive for therapists; 2) it is more challenging for patients; 3) robots can produce repetitive movements, allowing increased intensity of rehabilitation[24]; 4) they can provide a large variety of exercises for the therapist to choose from; 5) the man-machine-interaction allows an objective measure of progress, which itself can condition changes in the interaction by altering control parameters; 6) they can be combined with virtual reality interfaces to motivate patients and increase active participation; and 7) sophisticated control strategies can provide assist-as-needed[14]. In adult rehabilitation, specifically post-stroke, arm training is increasingly provided by rehabilitation robots[14]. There are two main applications of rehabilitation robotics, 1) support to perform ADLs, which we call assistive robots, and 2) providing physical training, the most common application, which we call training robots.

Although a handful of active and passive pediatric exoskeletons exist, major improvements are needed to develop a wearable assistive exoskeleton for ADLs.

Based on the definition by Dollar et al., an exoskeleton is defined as “an active mechanical device that is essentially anthropomorphic in nature, is “worn” by an

operator and fits closely to his or her body, and works in concert with the operator's movements"[25]. They enable the users to increase their range of motion (RoM) and provide a safe environment in which each joint is mechanically constrained to stay in the anatomical range to induce physiological rather than compensatory movements[14]. The possibility to train 3-D reaching movements in space is among their potential benefits[14]. Exoskeletons have been studied as rehabilitation robots since 1983[26] and showed promising results in upper extremity rehabilitation of adults. Robots such as ARMin[27] for post-stroke rehabilitation and WOTAS[28] for tremor suppression are two examples of such exoskeletons. Nonetheless, there are only a handful of exoskeletons specifically

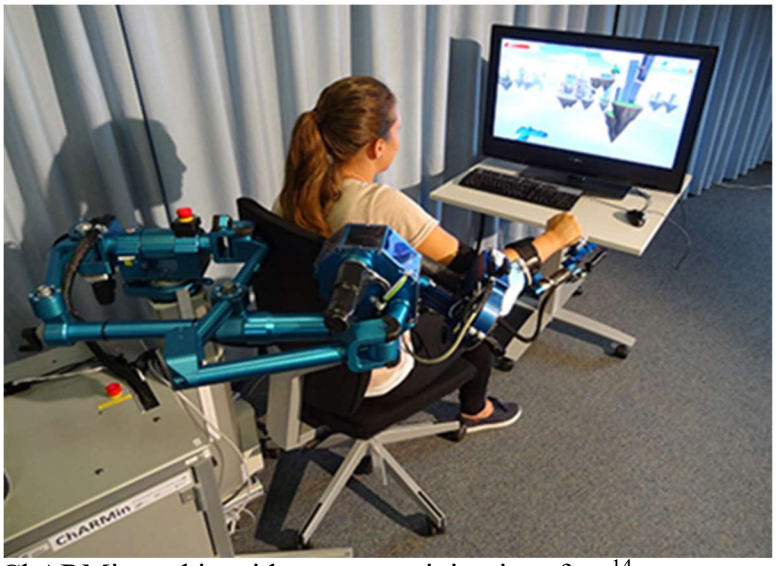

Figure 1.1 ChARMin and its video game training interface[14].

designed for pediatric populations. The ChARMin, the pediatric version of the widely studied ARMin rehabilitation robot, is one of the only actuated upper extremity exoskeletons for children. Its adaptable and patient-cooperative controller, which

supports arm movements during game-like scenarios, have shown great potential in preliminary evaluations on five children with variety of upper extremity movement disorders. Due to using DC motors to actuate four degrees of freedom of movement, its bulky and heavy structure, however, prohibits its use as wearable assistive exoskeleton (Figure 1.1). Conversely, using a less complex approach, Rahman et al. proposed a wearable pediatric version of WREX exoskeleton, called the P-WREX[29]. The P-WREX is based upon the WREX mechanical structure, but is comprised of 3D-printed plastic parts mounted to a wearable molded back plate and harness. This passive assistive exoskeleton provides support of the arms against gravity by using elastic bands to produce counter torques to unweight the arms (Figure 1.2, left panel). Use of the WREX showed improved upper extremity function, within one session, for older children with muscular dystrophy, and spinal muscular atrophy[30–32]. Similarly, use of the P-WREX showed both immediate effects while using the device and additionally, therapeutic effects post-training on a subject with arthrogryposis. Positioning the arms against gravity was effective in enhancing the reachable workspace and allowed for enhanced play, exploration and mid-line manipulation of objects (Figure 1.2, right panel.), however, the level of support that P-WREX creates, is static and does not dynamically change based on the needs of the users[13]. Additionally the device showed poorly assisted elbow flexion[13] and the child cannot lift a substantial weight, mainly because of its passive structure[33]. Passive devices, i.e., devices without active actuators, are cheaper, lighter, aesthetic and less complex for at home usage, however, they cannot actively create motion, therefore their applicability is limited in children with severe movement disorders. Passive exoskeletons are mostly useful for stabilizing or supporting tasks and cannot provide any fluid motion[34], thus, development is driven toward powered

exoskeltons[24]. Accordingly, attempts to actuate the WREX have included series elastic[33] and pneumatic actuators[35].

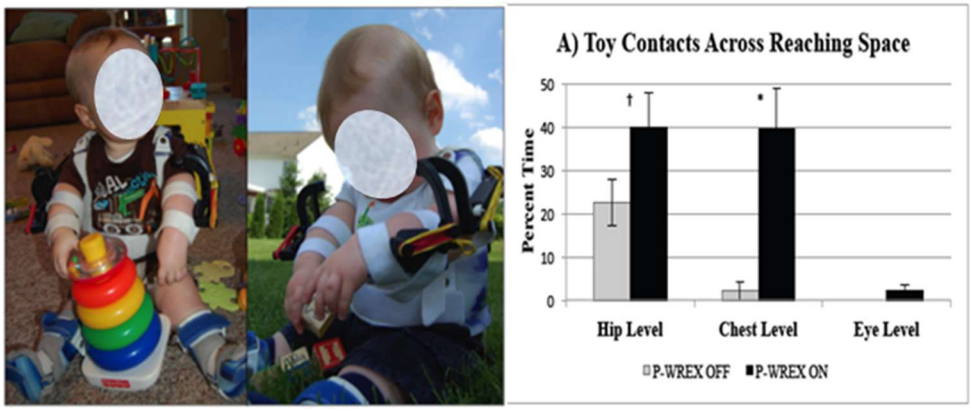

Figure 1.2 An infant with arthrogyposis using the P-WREX 3D printed exoskeleton (black plastic components, - left). Greater toy contacts while donning the P-WREX at hip, chest and eye level (right)[13].

Despite the shortcomings of conventional actuators in proposed wearable active exoskeletons for assistive ADLs in pediatric population, none have used alternative soft actuators to enhance their impediments of weight, volume and natural feel to increase their acceptability.

Although there is a significant need for at home rehabilitation robots, only a few rigid upper extremity exoskeletons have been tested to support ADLs, perhaps due to complexity and economic restrictions[24,36]. Moreover, these robots can be physically uncomfortable due to their rigid structure dictated by their actuation technique[37]. Additionally, their conspicuous designs are potentially stigmatizing for users and their families by drawing unwanted attention to users' impairments[38]. Portability is also often expected from devices assisting individuals to perform basic ADLs, thus limiting the volume and weight of such devices should be included in their design[24]. If an exoskeleton is to support movements of multiple joints, the number of needed actuators

increases as well as does the weight of the device thus complicating potential designs[24]. Collectively, it is the properties of the actuation system, which define and limit fundamental characteristics of the prosthesis such as weight, response time, noise level, and power[34]. Notably, if an assistive robot does not significantly improve, or if it hinders the lives of its users, they become dissatisfied and discontinue its use shortly after, which is the case for most of the proposed assistive robots[24]. Thus, an alternative soft and light actuator, which can align inconspicuously with skeletal structure to develop an acceptable exoskeleton by pediatric population, is highly important.

Skeletal muscle is an evolutionary masterpiece in its mechanical properties and is superior to conventional actuators in a variety of mechanical properties including; power to mass ratio, power density, i.e., power to volume ratio, strain, stress, , strain-rate, and electro-mechanical delay i.e., response time. Engineered alternatives often fall short in mimicking skeletal muscle[34,39]. Thus, the need to closely mimic the mechanical characteristics of skeletal muscle is of a high importance in developing an actuator for exoskeletons where the main focus is the augmentation of musculoskeletal system. Table 1.1 shows some of these properties for mammalian skeletal muscle[39,40].

The widely studied DC motor is the most common actuator in upper-limb exoskeletons. This is due to their fast operation, precision, and controllability[41]. More than 70% proposed active upper extremity exoskeletons, used DC motors as their actuators[41]. The low power to mass ratio of DC motors, however, makes these type of exoskeletons bulky and heavy[40]. Additionally, unlike skeletal muscle, conventional DC motors usually cannot align in parallel with bones due to their rotary actuations and require transmission mechanisms, which further increases the size of the robot. Moreover, the need for gears to meet the low speed, high torque needs in robotic

applications further exacerbate the weight and volume issues[42]. Pneumatic actuators are the second most common actuators in rehabilitation robotics and power about 20% of the proposed exoskeletons[41]. These contractile linear actuators- that is an actuator that creates motion in straight line in contrast to rotary DC motors- are soft and their work density and power to mass ratio are closer to biological muscle, however, they generally require a heavy and noisy energy resource equipment (air compressors) needed to drive them[40].

Soft actuators, i.e., actuators having Young's modulus in the range of soft biological material (104-109 Pa) such as muscle and tendon, are highly desirable in assistive robotics because, they increase the safety of the device and adapt more readily to various objects[37]. When natural feel combines with acoustically noiselessness operation, the resultant actuator may substantially increase the acceptability of the assistive robots, which use them. These features may even more significant in pediatric population. Additionally, a soft contractile linear actuator can closely follow any complex origin and insertion point of a target muscle, e.g., a supinator muscle, to augment its complex motion while occupying more minimal space. These continuously deformable muscle like actuators can be configured to virtually obtain unlimited degrees of freedom in contrast to their hard-bodied counterparts [37,43]. Among all proposed soft linear actuators only a few of them have shown to be capable of generating comparable force to human skeletal muscle. In this proposal, we call this group of soft actuators artificial skeletal muscle.

Despite numerous proposed novel actuators, their capability to be deployed as artificial skeletal muscle in rehabilitation robotics has not been compared.

A variety of electronic, ionic, and photo activated soft actuators with interesting muscle-like characteristics have been proposed. Nonetheless, due to their scalability,

manufacturing and structural complexity a few of them have shown promise as artificial skeletal muscle. Recently, polymer based actuators have attracted great attention due to their unique mechanical characteristics, which can be tailor made for the targeted applications[40]. Many electro-active polymer (EAP) and thermally driven polymer actuators have shown promising capability to act as artificial skeletal muscle.

Thermally activated actuators usually have large strain and high force generation capability, which surpass human skeletal muscle[44–46]. The most studied and commercially available actuators of this kind are Shape memory alloys (SMAs), which due to their mechanically rigid nature (Young's modulus $2x10^{10}$) are not soft actuators. Among thermally driven polymer actuators, shape memory polymers (SMPs) have limited force generation capability[47]. Conversely, thermally driven polymer fibers and phase change actuators are soft linear actuators, with large strain and power to weight ratios, which make them potentially versatile artificial skeletal muscles. Haines et al.[44] proposed an inexpensive, (~$5/kg), thermally activated polymer fiber actuator, that could generate up to 20% longitudinal strain under 40 MPa load with little or no hysteresis. Despite its versatility, this actuator was not easy to manufacture. In the remerging phase change actuators category, Miriyev et al.[46] proposed another uncomplicated group of thermally driven soft actuators that combined the elastic properties of a silicone elastomer and the extreme volume change in liquid–vapor phase transition of ethanol. When heated these light-weight actuators expanded up to 900%. These actuators can be 3D printed in various shapes. In a more complex approach Lima et al.[45] presented a group of liquid-solid phase change actuators, which used volume change of a guest material trapped in carbon nanotube (CNT) yarn. These hybrid CNT actuators delivered up to 3% longitudinal strain, while lifting a tensile load of 14.3-MPa

with acceptable cycle life. Unlike most previous CNT actuators these group phase change actuators did not need electrolyte and special packaging, however, it was expensive to manufacture[44]. Similar to most thermally driven actuators, despite high power to mass generation capability, these three aforementioned actuators have limited response times, actuation frequency, and efficiency.

Table 1.1 Properties of mammalian skeletal muscle[39,40].

Property	**Typical**	**Max**
Strain (%)	20[48]	>40
Stress (MPa)	0.1	0.35
Strain-rate (%/s)		500
Power to mass (W/kg)	50	200
Efficiency (%)		40
Cycle life (M Cycle)		1000
Axial Young Modulus (MPa)	10-60	
Electro-mechanical delay (ms)	54[49]	

Activation mechanism is prominent criteria in choosing a suitable actuator for any applications. For active exoskeletons, light and magnetically activated actuators are less interesting because their source of activation decreases their power to mass ratio and complicates their structural design. Electrical stimulation, however, is consider the most promising activation mechanism, because of its speed, availability, advances, and control systems[50]. Thus, even thermally driven actuators use electro-thermal activation[44,46]. Furthermore, since natural muscle is a electro-active actuator, for biomimetic applications and artificial muscles electrical activation may be more preferable.

Electro-active polymer (EAP) actuators is an emerging class of electro-mechanical transducers that show unique combination of functional and structural properties that have no equals among alternative actuation technologies, such as large active strains, high power density, high mechanical compliance, scalability, no acoustic noise, and, in most cases, low cost[51]. EAPs are commonly classified into two major families: ionic EAPs, and electronic EAPs. Ionic EAP actuation mechanisms are mostly based on ion commute between two electrodes thus they usually need to operate either in a gel or a wet state electrolyte[52]. The performance of the latter, e.g. conductive polymers, CNT and Ionic Polymeric Metallic/Composites (IPMC), is adversely affected by their low efficiency, short lifespan, and high response time[45,52]. Additionally, their need for a wet state electrolyte, limits their operating temperature, increases their structural and packaging complexity. Conversely, Plasticized Poly Vinyl Chloride (PVC) gel actuators are inexpensive ionic EAP actuators, with strain, efficiency, and power to mass ratio surpassing many artificial skeletal muscles alternatives[53,54]. A 50 × 10 × 6 mm PVC Gel artificial muscle showed up to 9 Hz full actuation frequency, 12% of no-load tensile strain and 39 N of maximum isometric force generation capablity[53]. Although PVC Gel is a soft EAP, most proposed packaging for high force generation PVC actuators are rigid as well. Furthermore, life cycle testing of these actuators showed decrease in performance after short period of actuation[53].

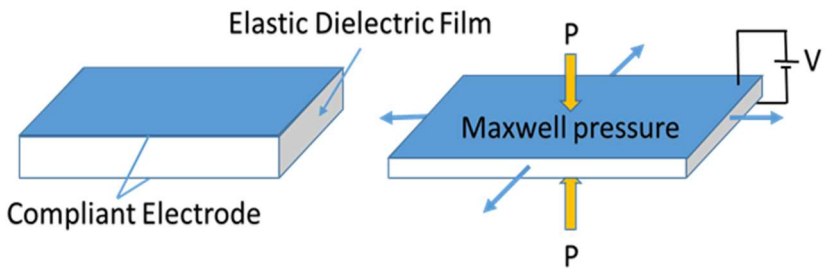

Figure 1.3 DEA actuation mechanism. When DC voltage is applied, Maxwell pressure squeez the elsatic dielectric between the electrodes.

Figure 1.4 Rolled DEA acting as a bicep on a full-size human skeletal muscle[55].

Electronic EAPs (AKA, 'dry' EAPs or field-activated EAPs) are polymers that respond to an applied electric field by either reorientation of their internal structure, AKA, electrostrictive polymers, or electrostatic interaction of opposite charges, i.e., Maxwell pressure, as opposed to charge or mass transport of ionic EAPs. Maxwell pressure is the electrostatic pressure between the charged electrodes of a capacitor. Although they need high activation electrical field (~150 MV/m), large strains and stresses, fast response times, high actuation rate and long lifetime are some of their prominent properties[50–52]. Despite these outstanding features, currently there are not many electronic EAPs suitable to act as artificial skeletal muscle. Ferroelectric polymers are mechanically rigid [54]. Liquid crystal elastomers, which are capable of producing large strain (up to the order of %100) have limited response time and are more suitable

for micro applications[51]. The existing CNT aero gels have low force generation capability[51].Alternatively, dielectric elastomer actuators (DEAs) are a promising solution for artificial skeletal muscles.

DEAs are soft, acoustically noiseless, and lightweight actuators with outstanding muscle like features. High power to mass ratios that can surpass human skeletal muscles, length self-sensing and energy recuperation capability are among their unique features[42,56]. The inverse relationship between force and displacement, however, is one of the major drawbacks of these actuators. DEAs consist of a thin elastomer film, which is coated on both sides with compliant electrodes forming a capacitor. When a high DC voltage is applied to this compliant capacitor, the electrodes squeeze the elastomeric dielectric in the thickness direction (Figure 1.3). DEAs have already shown some promise as artificial skeletal muscles for orthotic and prosthetic devices[34,57]. These actuators have been formed into cylindrical rolls that have strain, shape, and performance similar to natural skeletal muscles[58]. One such actuator was configured to be a similar shape to a biceps muscle and to act on a life-size skeletal arm (Figure 1.4)[55]. Although showing great potential, there are a few proposed DEA configurations that can generate enough force to deploy in an assistive upper extremity exoskeleton. The Hydraulically Amplified Self-Healing Electrostatic (HASEL) actuators proposed by Acome's group[59] combined the power of hydraulic actuators and muscle-like behavior of DEAs. The HASEL actuators showed interesting capabilities such as, high force and tensile actuation generation, e.g., 16% strain under 1.5 kg load, in addition to high efficiency at 21%. However, high activation voltage (~40 kV vs <5 kV in other proposed DEAs), their complex controllability, packaging, and risk of leakage are discouraging

properties. Furthermore, among all proposed soft actuators hydraulic ones show the least similarity to biological muscle in terms of actuation mechanism.

Stacked DEAs proposed by Kovacs et al.[60] is a powerful versatile DEA configuration that shows the most similarity to human skeletal muscle compared with other soft actuators. Kovacs group stacked multiple layers of thin enhanced DEAs to create this novel actuator. In this configuration, each layer can be considered as sarcomere within a myofibril. This group of inexpensive tensile actuators were capable of producing 32N of isometric force and 15% strain while lifting a 11 N tensile load. These capabilities led these actuators to become the first and only commercially available DEA that can be deployed as artificial skeletal muscle[61].

The main goal of this project is to develop an artificial skeletal muscle composed of soft actuators and assess its capabilities in rehabilitation robotics applications. To do so we connect multiple Stacked DEAs in series, to magnify the displacement by increasing the number of DEA layers (representing sarcomeres in skeletal muscle), to create artificial myofibrils. Then, multiple artificial myofibrils will be connected in parallel to magnify the force generation, analogous to the skeletal muscle fibers in parallel. To add proprioception, the length self-sensing capability of DEAs will be added to this artificial skeletal muscle. This will finalize the development of our artificial skeletal muscle. In the second phase, length modulation controllability of this muscle will be assessed. Finally, this muscle will actuate the elbow joint of a phantom model to provide proof of concept as a wearable robotic device.

1.2 Specific Aims

This proposal will develop an artificial skeletal muscle using soft actuators that can replace commonly used DC motor and fluidic actuators in rehabilitation robotics.

Developing such actuators is of high importance, especially for infants and children, because commonly used actuators in rehabilitation robotics are noisy, bulky and rigid in structure. These factors often lessen the acceptability and practicality of rehabilitation robotic device use despite the positive impact such devices have in rehabilitation outcomes.

Robot-assisted therapy has increased the dose of mass practice beyond that which can be provided during supervised therapy sessions and has been found to be as good as or better than conventional therapy in promoting motor leaning in impaired upper extremities. We believe that the development of a soft, low-noise artificial skeletal muscle be the first step in realizing devices better suited for pediatric populations. This proposal represents a novel first step in developing bioinspired mechatronic devices for pediatric populations with severe upper extremity impairments. To achieve our goal, we plan to use an advanced soft actuator to develop "artificial skeletal muscles" to automate control of an exoskeleton elbow joint to assist and expand the types of tasks that the user can actively engage. Unlike bulky, heavy and noisy electric motor and fluid actuators currently used in rehabilitation robotics, our artificial skeletal muscle design will be muscle-like in their operation, light weight, compact in size, mechanically compliant, and have low power consumption and noiseless operation. Such features are attractive characteristics that may help with translation to real world devices. First, this proposal will compare potential soft actuator candidates that can form an artificial skeletal muscle and select the one whose characteristics most resemble function of biological muscle. Second, we will benchmark test a soft, muscle-like transducer composed of the chosen actuator to use as an "artificial skeletal muscle". Third, length-sensing capability, mimicking length proprioception of biological muscle spindles, will

be added to the artificial skeletal muscle. Finally, we will design and manufacture a unilateral pediatric upper extremity exoskeleton, and use the proprioceptive artificial skeletal muscle to actuate its elbow joint. Proof of concept will be demonstrated by controlled elbow flexion of the designed exoskeleton on an anatomic-like form that simulates the weight of the extremity and its center of mass (COM).

Aim 1: To assess the state of soft actuator technology for use as artificial muscles in pediatric exoskeletal rehabilitation devices; and thereby, choose a soft actuator to test in the powering of such a device.

Purpose: Due to variety in soft actuator technology, choosing the suitable actuator for a specific application is nontrivial. To our knowledge, there are no studies that compare existing soft actuator capabilities for potential use to power exoskeletons. Therefore, this aim will compare soft actuator candidates that can be used in rehabilitation exoskeletons.

Hypothesis 1.1: Soft actuator technology development has sufficiently progressed to allow muscle-like actuation of rehabilitation robots. Such technology has acoustically noiseless operation and its reported mechanical properties including stress, longitudinal strain, power to mass ratio, strain-rate, and efficiency, are comparable to those of human skeletal muscle.

Aim 2: To configure an artificial muscle, which is capable of lifting a tensile load equivalent to that of a 2-year-old boy's forearm and hand, through benchmark testing of the chosen actuator.

Purpose: This aim will measure the mechanical properties of the chosen CT-SDEA to assess its capabilities and limitations for rehabilitation robots. An artificial muscle will be configured to have sufficient force and longitudinal displacement capabilities to actuate an exoskeleton for flexing a 2-year-old boy's elbow. This aim is the most prominent aim of this proposal because, 1) it will help us to evaluate the

reported mechanical properties of the CT-SDEA; 2) it will give us the flexibility to measure the specific mechanical properties that are needed for our application; 3) it will result in an artificial muscle for the other aims of this proposal; and 4) it will provide the necessary data relationships for developing the control feedback systems for aims that follow.

Hypothesis 2.1: The tested soft actuator has reliable stress responses and its mechanical properties including stress, electro-mechanical delay, length-tension curve, stress response hysteresis, axial Young's modulus, longitudinal strain, strain-rate, and power to mass ratio, and efficiency are comparable to those of human skeletal muscle.

Hypothesis 2.2: The configured artificial muscle, consisting of series and parallel arrangement of the chosen soft actuator, will produce stress and strain sufficient to provide support and movement of a tensile load equivalent to that of a 2-year-old boy, during both unloaded and loaded conditions.

Aim 3: To develop a feedback controlled length modulation mechanism for the configured artificial muscle.

Purpose: This aim will create a proprioceptive artificial muscle with length modulation controllability. This feedback control mechanism will be the basis for controlling elbow flexion of a phantom model in Aim 4.

Hypothesis 3.1: Similar to the function of muscle spindles of biologic muscle, the electrical characteristics of the artificial muscle may be used to provide "proprioceptive" information of actuator length without using sophisticated external sensors.

Hypothesis 3.2: The proprioceptive artificial muscle will autonomously change length and rate of length change, within its nominal range of operation, following a sigmoidal trajectory characterized by the operator.

Aim 4: To demonstrate the capability of the proprioceptive artificial muscle in muscle-like actuation of a prototype pediatric exoskeleton's elbow joint.

Purpose: This aim will assess the capability of the CT-SDEA in forming artificial muscles for actuating exoskeletons. A prototype of an upper extremity pediatric exoskeleton will be developed that is actuated by the configured proprioceptive artificial muscle to control its elbow flexion.

Hypothesis 4.1: The artificial muscles actuating the exoskeleton will produce maximum elbow flexion velocity and acceleration comparable to commercial upper extremity rehabilitation exoskeletons (e.g. ARMin – angular velocity 91 º/s; acceleration 116 º/s2) over the designed 36º range of elbow flexion in the sagittal plane while bearing a load in excess of the weight of the 2-year-old boy's forearm and hand.

Hypothesis 4.2: The powered exoskeleton will reach any desired degree of elbow flexion, within its active range of motion, 36º, following a sigmoidal joint angle trajectory characterized by the operator, with maximum velocity and acceleration comparable to commercial upper extremity rehabilitation exoskeletons (e.g. ARMin – angular velocity 91 º/s; acceleration 116 º/s2).

Chapter 2

ASSESSING THE STATE OF SOFT ACTUATOR TECHNOLOGY FOR USE AS ARTIFICIAL MUSCLES IN PEDIATRIC EXOSKELETAL REHABILITATION DEVICES

2.1 Abstract

Due to variety in soft actuator technology, choosing the suitable actuator for a specific application is nontrivial. To the best of our knowledge, there are no recent studies that compared the capabilities of existing soft actuators in powering exoskeletons. Therefore, we compared five soft actuator candidates that can be deployed in exoskeleton applications. The inclusion criteria were softness, acoustically noiseless operation, and demonstrated ability to lift a tensile load equal or greater than the weight of a two-year old boy forearm+hand, 3.38 N, in the literature. Accordingly, two thermally driven actuators, Coiled Nylon Fiber (CNF) and Ethanol-Based Phase-Change (EPC); and three electro-active polymer actuators, Plasticized Poly Vinyl Chloride (PVC) gel, Stacked Dielectric Elastomer (DE) and Hydraulically Amplified Self-Healing Electrostatic (HASEL), were chosen for the comparison. These actuators were compared in their stress, unidirectional strain, strain-rate, power-to-mass ratio, and efficiency. The Stacked DE actuator with reported force of 32 N, unidirectional strain of 18%, strain-rate of 500%/s, and efficiency of ~28%, showed the closest resemblance to mammalian skeletal muscle. Thus, a commercially available stacked DE actuator was chosen as the most applicable soft actuators technology for pediatric rehabilitation robots.

2.2 Introduction

Soft actuators, i.e., actuators having Young's modulus in the range of soft biological material (10^4-10^9 Pa) such as muscle and tendon (Figure 2.1), are highly desirable in assistive robots because, they increase the safety of the device and adapt more readily to various objects.[37] When natural feel combines with acoustically noiselessness operation, the resultant actuator may substantially increase the acceptability of the assistive robots that include them. These features may even more significant in pediatric population. Additionally, a soft contractile linear actuator can closely follow any complex origin and insertion point of a target muscle, e.g., a supinator muscle, to augment its complex motion while occupying more minimal space. Such continuously deformable muscle like actuators can be configured to actuate virtually unlimited types of degrees of freedom in contrast to their hard-bodied counterparts[37,42]. Among all proposed soft linear actuators, only a few of them have shown to be capable of generating comparable force to human skeletal muscle. In this proposal, we call this group of soft actuators artificial skeletal muscle.

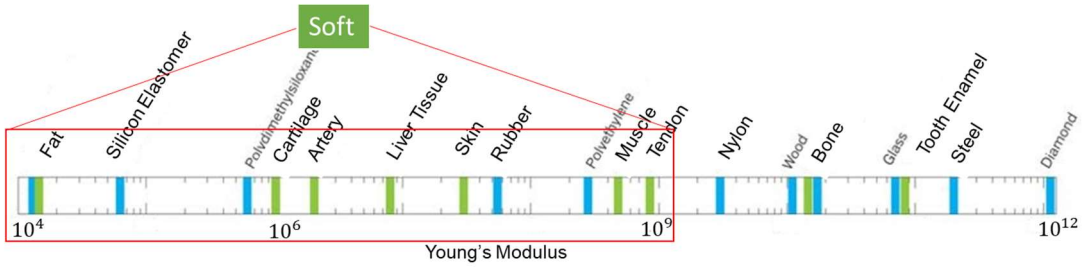

Figure 2.1 Softness in comparison to biologuical tissue[37]. The Young's modulus of biological tissues and non-bilogical materials are depected in green and blue, respectively.

A variety of electronic, ionic, thermally, and photo activated soft actuators with interesting muscle-like characteristics have been developed[39,51,52]. Due to their

scalability, manufacturing and structural complexity, however, a few of them have shown promise as artificial skeletal muscle. Recently, polymer based actuators have attracted great attention due to their unique mechanical characteristics, which can be tailor made for the targeted applications[40]. Many electro-active polymer (EAP) and thermally driven polymer actuators have shown promising capability to act as artificial skeletal muscle.

Thermally activated actuators usually have large strain and high force generation capability, which surpass human skeletal muscle.[44,45,53] The most studied and commercially available actuators of this kind are Shape memory alloys (SMAs)[62], which due to their Young's modulus 2×10^{10}Pa, are not considered soft based on aforementioned definition. Although usually in the soft range, shape memory polymers (SMPs) have limited force generation capability[47]. Conversely, thermally driven polymer fibers, e.g., Coiled Nylon Fiber (CNF) actuators[44], and phase-change actuators, e.g., the Ethanol-Based Phase–Change (EPC)[46], are soft and have linear operation. Their large strain and power to weight ratios make them potentially versatile artificial skeletal muscles. Similar to most thermally driven actuators, despite high power-to-mass generation capability, CNF and EPC have limited response times, actuation frequency, and efficiency.

Activation mechanism is a prominent criterion in choosing a suitable actuator for any applications. For active exoskeletons, light[63] and magnetically[64] activated actuators are less interesting because their source of activation decreases their power to mass ratio and complicates their structural design. Electrical stimulation, however, is considered the most promising activation mechanism, because of its speed, availability, advances, and control systems[50]. Thus even thermally driven actuators use electro-

thermal activation[44,46]. Furthermore, since natural muscle use electro-chemical signal to activate the muscle, for biomimetic applications and artificial muscles, electrical activation may be more preferable.

Electro-active polymer (EAP) actuators is an emerging class of electro-mechanical transducers that show unique combination of functional and structural properties that have no equals among alternative actuation technologies, such as large active strains, high power density, high mechanical compliance, scalability, no acoustic noise, and, in most cases, low cost[51]. EAPs are commonly classified into two major families: ionic EAPs, and electronic EAPs. Ionic EAP actuation mechanisms are mostly based on ion commute between two electrodes thus they usually need to operate either in a gel or a wet state electrolyte[52]. The performance of the latter, e.g. conductive polymers, CNT and Ionic Polymeric Metallic/Composites (IPMC), is adversely affected by their low efficiency, short lifespan, and high response time [45,52]. Additionally, their need for a wet state electrolyte, limits their operating temperature, increases their structural and packaging complexity. Plasticized Poly Vinyl Chloride (PVC) gel actuators are inexpensive ionic EAP actuators, with strain, efficiency, and power to mass ratio surpassing many artificial skeletal muscles alternatives[53,54].

As opposed to charge or mass transport of ionic, electronic EAPs (AKA, 'dry' EAPs or field-activated EAPs) are polymers that respond to an applied electric field by either reorientation of their internal structure (AKA, electrostrictive polymers) or electrostatic interaction of opposite charges, i.e., Maxwell pressure. Maxwell pressure is the electrostatic pressure between the charged electrodes of a capacitor. Although electronic EAPs need high activation electrical field (~150 MV/m), some of their prominent properties include large strains and stresses, fast response times, high strain-

rate, and long lifetime [50,52]. Despite these outstanding features, currently there are not many electronic EAPs suitable to act as artificial skeletal muscle. Ferroelectric polymers are mechanically rigid[53]. Liquid crystal elastomers, which are capable of producing large strain (up to the order of %100), have limited response time and stress generation capablity[51] The existing CNT aero gels have low force generation capability[51].

Alternatively, DE actuators are soft, acoustically noiseless, and lightweight actuators with outstanding muscle like features, which make them one of the most anticipated and studied soft actuators[34,42,52,56,65]. High power to mass ratios that can surpass human skeletal muscles, length self-sensing, and energy recuperation capability are among their unique features[42,56]. Their high driving voltage, however, limits the availability of compatible electrical components that can be used with them in a design. DE actuators consist of a thin elastomer film, which is coated on both sides with mechanically compliant electrodes forming a capacitor. When a high DC voltage is applied to this compliant capacitor, the electrodes squeeze the elastomeric dielectric in the thickness direction. DE actuators have already shown some promise as artificial skeletal muscles for orthotic and prosthetic devices[34]. These actuators have been formed into cylindrical rolls that have strain, shape, and performance similar to natural skeletal muscles[58]. One such actuator was configured to be a similar shape to a biceps muscle and to act on a life-size skeletal arm[55]. Although showing great potential, a few proposed DE actuator configurations can generate enough force to be deployed in an assistive upper extremity exoskeleton. For example Hydraulically Amplified Self-Healing Electrostatic (HASEL) actuators proposed by Acome's group[59] combined the power of hydraulic actuators and muscle-like behavior of DE actuators. The HASEL actuators showed interesting capabilities such as, high force and tensile actuation generation.

Stacked DE actuators proposed by Kovacs et al.[60] is a powerful versatile DE actuator configuration that shows the most similarity to human skeletal muscle compared with other soft actuators. Kovacs group stacked multiple layers of thin enhanced DE actuators to create this novel actuator. In this configuration, each layer can be considered as sarcomere within a myofibril. These capabilities led these actuators to become the first and only commercially available DE actuator that can be deployed as artificial skeletal muscle[61].

Despite many efforts to compare alternative actuators[39,40,51,52], to the best of our knowledge, **this chapter is the first one that specifically focused on comparing the soft, noiseless, actuators with demonstrated comparable force and linear displacement to human skeletal muscle.** In this chapter, the aforementioned thermally driven actuators (i.e., CNF and EPC actuators) and electro-active polymer actuators (i.e, PVC gel, HASEL and Stacked DE) were compared in their capabilities to deploy as artificial skeletal muscles. Thereby, the most suitable one for further investigation was chosen.

2.3 Method

2.3.1 Inclusion Criteria

Three major criteria will be used to include an actuator for comparison in this aim; 1) Softness, which defines as having a Young's modulus in the range of soft biological materials (10^4-10^9 Pa); 2) Demonstrated ability to lift a tensile load equal or greater than the weight of a two-year old boy forearm+hand, i.e., 3.38 N. The weight of the forearm and hand was estimated by using WHO child growth standard[66] and Winter's anthropometric data[67]; 3) acoustically noiseless operation.

2.3.2 Comparison Measures

For each of the following measures the terms High, Moderate, and Low will be used in comparison to that of human skeletal muscle (Table 1.1). The measures will be considered High when they are equal or higher than those of human skeletal muscle; will be considered Moderate when they are within one order of magnitude smaller than those of human skeletal muscle; and will be considered Low when they are more than one order of magnitude smaller than that of human skeletal muscle (Table 2.1). In this study, an actuator is called comparable to skeletal muscle in a specific measure when the measure is in High or Moderate range. Note that, if the typical value of a measure is reported in Table 1.1 for human skeletal muscle, it will be used in the comparison; otherwise, the maximum value from the table will be used.

Stress is the amount of maximum generated force by an actuator divided by the its cross section area. For this measure, High, Moderate and Low were defined >=100 kPa, >=10 kPa, and < 10 kPa, respectively.

Unidirectional strain is defined as the ratio of unidirectional displacement to the initial length of the actuator. For this major, High, Moderate, and Low were defined >=20%, >=2%, and < 2%, respectively.

Power to mass ratio is used to compare the maximum power of different actuators by normalizing the maximum generated power to the actuator's mass. For this major, High, Moderate, and Low were defined >=50 W/kg, >=5 W/kg, and < 5 W/kg, respectively.

Strain-rate is a measure of actuation speed, and is defined as the maximum changes in strain per unit of time. For this major, High, Moderate, and Low were defined >=500 %/s, >=50 %/s, and < 50 %/s, respectively. Unlike skeletal muscle, actuation frequency is reported as a measure of contrition speed for most of the compared

actuators in this study. Therefore, by assuming the actuation and recovery phase in a complete cycle have equal speed, we can drive a rough estimation of the strain–rate, for the sake of comparison. This assumption may not be correct for many cases especially thermally driven actuators, where heating speed, i.e., actuation phase, can be higher than cooling speed, i.e. recovery phase.

Efficiency or electro-mechanical efficiency is ratio of the mechanical (output) energy to the electrical (input) energy expended during a complete cycle of actuation. For this major, High, Moderate, and Low were defined >=40%, >=4%, < 4%.

Table 2.1: High, Moderate and Low range for the comparison measures.

	Skeletal Muscle		Soft Actuator (SA)		
Property	**Typical**	**Max**	**High**	**Moderate**	**Low**
Strain (%)	20	>40	>=20	20>SA>2	2=<
Stress (kPa)	100	350	>=100	100>SA>10	10=<
Strain-rate (%/s)		500	>=500	500>SA>50	50=<
Power to mass (W/kg)	50	200	>=50	50>SA>5	5=<
Efficiency (%)		40	>=40	40>SA>4	4=<

2.4 Results

Five groups of actuators were chosen for the comparison in this aim; 1) CNF actuators; 2) EPC actuators; 3) PVC Gel actuators; 4) Stacked DE actuators; and 5) HASEL actuators. Although manufacturing cost and complexity were not part of the inclusion criteria, all of the compared actuators were moderately simple and inexpensive to make. Note that, power to mass ratio, strain-rate, and efficiency were not reported for all of the actuators.

2.4.1 Coiled Nylon Fiber (CNF) actuators

Table 2.2: The contraction of the coiled nylon 6.6 fiber caused by increase in temperature. By coiling nylon thread, the longitudinal strain can be magnified substantially[44]. The column on the right shows the pros and cons of these actuators, in summary.

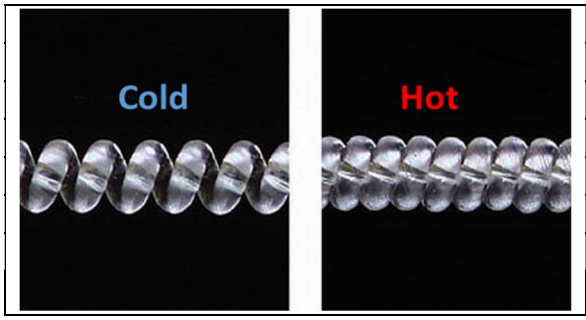

Pros
High stress
High strain
Thin diameter
Cons
Low strain-rate
Low efficiency
High driving temperature

These thermally driven actuators are made by coiling inexpensive high-strength, nylon threads. Heating the straight, i.e., uncoiled, nylon threads result in reversible thermal longitudinal contraction. For example, a straight nylon 6.6 thread with 127 µm diameter, will contract 4% longitudinally when heated from 20º to 240º C, which is similar to contractions achieved by commercially available NiTi shape memory wires[44]. Because the longitudinal contraction is accompanied by radial expansion, these threads also function as torsional actuators. Thereby, the contraction can be amplified by twisting the thread to create coils (Table 2.2). The coiled actuator is made by twisting the thread while it is under tensile load and then thermally annealed to strengthen it. The amount of tensile load used in coiling process is important, because it dictates the spring index of the coil -that is the ratio between the wire diameter and outer diameter of a coil or spring. The larger the spring index the smaller the strain and the larger the stress generation capabilities. After coiling, Haines et al[44]. showed that the thermal longitudinal contraction of nylon 6.6 increased from 4% (straight thread) to 34% (coiled

thread) when heated from 20º to 240º C. Additionally, by changing the direction of coiling, the resultant actuator fiber can either expand or contract by heating. When heated from 20º to 120º C, the CNF, with spring index of 1.7 (340 µm outer diameter) showed 21% unidirectional contraction and 22 MPa optimal load (for each fiber maximum stress was realized under a specific load called optimal load), while the one with 1.1 indices (265 µm) showed 9.3% contraction and 50 MPa optimal load[44]. Interestingly, the coiled nylon thread with 1.1 spring index had 2.1 kW/kg averaged power to mass ratio, which is 42 times the typical power to mass ratio of human skeletal muscle (Table 2.1). Since this actuator has a very small diameter, it can be used in textiles; twelve CNF actuators were woven in parallel into a textile and could lift a 3 kg tensile load[45]. The cycle life of a CNF was tested under 22 MPa of tensile load and 1 Hz of actuation for 1.2 M cycles and no significant change in unidirectional strain was observed[44]. This actuation required 30V/cm voltage, which decreases the efficiency dramatically. When operating in air, the reported efficiency of these fibers was 1.08%[44], even less than the NiTi shape memory wire. Although 5 and 7.5 Hz actuation frequency were reported for in water and in helium actuation respectively, the actuation frequency in open air was only 1 Hz (roughly 2%/s strain-rate) for the CNF[44]. Table 2.2 summarizes the pros and cons of these actuators.

2.4.2 Ethanol-Based Phase-Change (EPC) actuators

These phase-change actuators use the extreme volume change in liquid to vapor transition of ethanol and elastic properties of a silicone elastomer. By entrapping ethanol in the elastomeric matrix, silicone, and heating the material to ethanol boiling temperature, 78.4º C, the elastomer expands substantially due to the extreme volume change of ethanol's liquid to gas transition (Table 2.3). Miriyev et al.[46] reported High

force and strain generation capabilities for these actuators, i.e., 120N (1.3 MPa stress) to 0 N force for 0% to %140 unidirectional expansion respectively, for a 2 g actuator. The reported strain-rate and efficiency, however, was dramatically Low 2.5 %/s and 0.2% respectively[46]. A muscle-like configuration of these actuators was tested as a biceps muscle on a skeleton (without any control for the weight of the forearm) and could flex the arm to 90 degrees (the initial elbow angle was not reported), however, the power used for this motion was substantial, 45 W.[46] Finally, the entrapped ethanol gradually escaped the elastomeric matrix through vaporization and the elastomer dried out, which decreases the cycle life of these actuators substantially. This ethanol escape issue can be resolved by special packaging to prevent evaporation. The pros and cons of this group of actuators can be seen in Table 2.3.

Table 2.3: Structure and principle of operation of the EPC actuators. By increasing the temperature the entrapped ethanol evaporates inside the elastomeric matrix and creates expansion[46]. Pros and cons of these actuators are summarized in the right column.

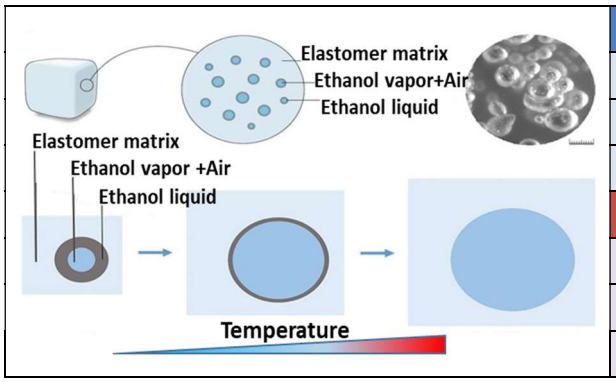

Pros
High Stress
High Strain
3D printable
Cons
Low strain-rate
Low efficiency
High Power consumption

2.4.3 PVC Gel Actuators

Table 2.4: Pros, cons, and the actuation mechanism of a stacked PVC Gel actuator. When an electrical field is applied, PVC Gel creeps into the air gap around the anode under Maxwell stress[53].

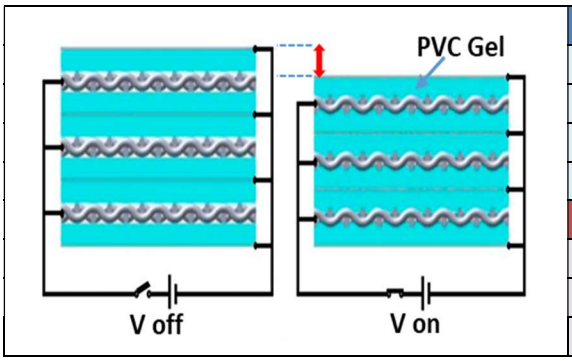

Pros
Moderate stress
Moderate strain
Moderate strain-rate
Power consumption
Cons
Low power to mass ratio
Pushing force
Bulky and rigid packaging

These are gel-based ionic EAP actuators. When placed between anode and cathode and electric field is applied, they contract due to Maxwell pressure, and return to its initial length (i.e., recovery phase) when electric field is off, due to its elasticity (Table 2.4). It was shown that the recovery stress, pushing force, is significantly higher than the Maxwell pressure, pulling force[53]. Therefore, the recovery stress was used as the main source of actuation. An actuator of 50×10×6 mm generated 39 N (78 kPa) and %12 unidirectional contraction under 400 V driving voltage[53]. The same size actuator showed peak power to mass ratio of 3 W/kg and 9Hz bandwidth (roughly 240%/s) [53]. The 14.4 mW, power consumption, under constant DC voltage of 400 V, makes this group of actuators a potential candidate for wearable rehabilitation devices. PVC Gel was tested as a lower extremity exoskeleton to assist quadriceps muscle contraction[54]. Cycle life testing, however, showed 64% reduction in contraction after about 170 K cycles, the performance stayed the same afterward to the end of the testing, 5.4 M cycles[53]. Additionally, most of the proposed packaging for these actuators were rigid

and bulky. The summery of the pros and cons of these actuators are presented in the Table 2.4.

2.4.4 Stacked DE Actuators

Table 2.5: Longitudinal contraction of Stacked DE actuator under Maxwell stress. Stacked DE actuators consist of multiple layers of compliant capacitors. Pros and cons of these actuators are summarized in the right column.

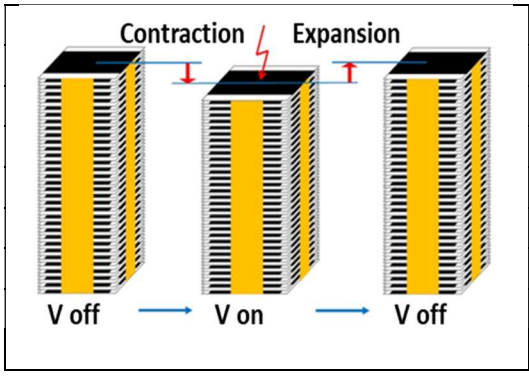

Pros
High stress
Moderate strain
High strain-rate
Moderate efficiency
Commercially available
Length self-sensing
Cons
High Driving voltage

This group of actuators are electronic EAPs, which use Maxwell pressure and capacitor structure to create unidirectional contractions. Stacked DE actuators consist of multiple layers of thin elastomers (~40 µm) coated with mechanically compliant electrodes, i.e., multiple layers of compliant capacitors. When DC voltage is applied, the resultant Maxwell pressure between the electrodes squeeze the thin dielectric elastomer in between, and the actuator contracts longitudinally (Table 2.5). The reported maximum force and unidirectional strain value for an actuator of 25 mm length and 20 mm of diameter were 32 N (i.e., 102 kPa) and 18% respectively under 4.2 kV driving voltage[60]. Among the investigated actuators in this aim, the Stacked DEAs were the only ones commercially available. Kovacs et al. tested these actuators for one year under 500 repetitive actuation per day. The result was a life of 182 k cycles, with no observed

fatigue. The reported strain-rate for this actuator was about 500%/s; and the typical reported efficiency for different DE actuators, without incorporating their energy recuperation capability, was 25%-30%[39,46]. Additionally, as a unique feature of DE actuator technology, this group of actuators has length-sensing capability, which may be exploited to implement position control without requiring additional components for sensing, thus reducing the mechanical complexity of the actuator. The driving voltage of these actuators, which is usually above, 1 kV, limit the available electronic components that can be used for driving and controlling these actuators. Pros and cons of these actuators are summarized in Table 2.5.

2.4.5 HASEL Actuators

This group of actuators combines the versatility of soft fluid actuators and muscle like properties of DE actuators. HASEL actuators are capacitors with a liquid dielectric. Under an electrical field, the resultant Maxwell pressure between electrodes, cause the liquid dielectric under the electrodes to displace to the adjacent surrounding volume. As voltage increases Maxwell pressure increases; after reaching a specific threshold voltage the electrodes abruptly approximate (AKA snap-through transition), which results in substantial hydraulic force (Table 2.6). Note that, by using the liquid elastomer the maximum driving voltage was increased to 40 kV without creating any permanent electrical breakdown -that is when current flowing through an electrical insulator after reaching a specific voltage[59]. This driving voltage is more than ten times the driving voltage of aforementioned stacked DE actuators, which substantially limits the electrical components available to be used with these actuators, especially in wearable applications. The higher the voltage, however, the higher the Maxwell pressure, which substantially increases the stress and strain generation capabilities show the relationship

between voltage and Maxwell pressure, where $\varepsilon_{0\ and}\ \varepsilon_r$ are the permittivity of free space and relative permittivity of the dielectric material respectively, V is the applied voltage, and d is the distance between to the two electrodes. Under 14.5 kV driving voltage and actuation frequency of 2.4 Hz a two-unit uniplanar configuration of HASEL actuator was capable of lifting 7 N of tensile load (114 kPa stress) with 124% (roughly 600 %/s) unidirectional expansion; the peak power to mass ratio of this actuator was Moderate,164 W/kg[59]. Efficiency of the actuator was 21% for the donut configuration with maximum actuation frequency of 20 Hz[59]. Under 1 kg of tensile load and 3.8 Hz of actuation, the cycle life of a uniplanar single-unit HASEL actuator was 158 k cycles[59].

Table 2.6: Pros, cons, and actuation mechanism of the HASEL actuator. When voltage pass the snap-through threshold, the liquid abruptly move in to the surrounding area and create substantial hydraulic force[59].

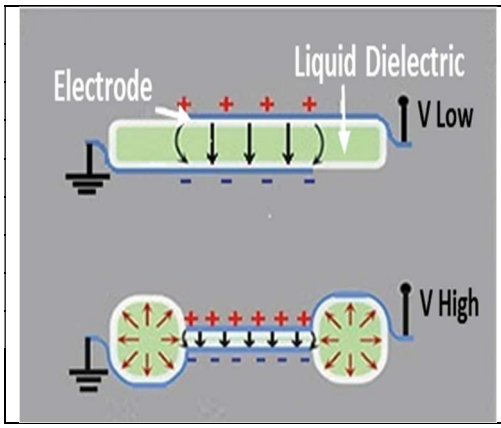

Pros
High stress
High strain
High strain-rate
Moderate power to mass ratio
Moderate efficiency
Length self-sensing
Cons
Very high Driving voltage
Risk of leakage

$$P = \varepsilon_0 \varepsilon_r (\frac{V}{d})^2 \quad (1)$$

2.5 Discussion

Mechanical properties of five groups of soft actuators (CNF, EPC, PVC Gel, Stacked DE, and HASEL) were compared (Table 2.7). Stacked DEAs showed High stress-rate, Moderate maximum strain and stress, which made this group of actuators a potential alternative for rehabilitation robotics. Their high driving voltage, however, limits the available electrical components for wearable applications.

Table 2.7: Summary of comparison between Coiled Nylon Fiber (CNF), Ethanol-Based Phase-Change (EPC), Poly Vinyl Chloride (PVC) Gel, Stacked Dielectric Elastomer (DE) and Hydraulically Amplified Self-Healing Electrostatic (HASEL) actuators.

	CNF	**EPC**	**PVC Gel**	**Stacked DE**	**HASEL**
Stress	High	High	Moderate	High	High
Strain	High	High	Moderate	Moderate	High
Strain-rate	Low	Low	Moderate	High	High
Efficiency	Low	Low		Moderate	Moderate

Although the compared thermally driven actuators, i.e., CNF and EPC, are powerful with High stress and unidirectional strain, however, the Low stain-rate are their major drawbacks for rehabilitation application. The contraction time-the time from neural signal to force- a human skeletal muscle is relatively short, e.g., the contraction time of soleus and digitorum longus muscles is as low as 36 ms and 12.5 ms respectively[68]. Because the time delay between generating a command and applying the activation signal to the actuator is usually very small in electrical systems, the contraction time is highly affected by the strain-rate. Therefore, an actuator deployed for use in an assistive device requires fast strain-rates. Furthermore, the higher the actuation frequency the higher the controllability. Additionally, the Low efficiency of these actuators further limit their capabilities in wearable applications, where low

energy consumption is vital.Although comparable to biological muscle (in the Moderate or High range) in most of the comparison measures, the aforementioned electro-active polymer actuators generated less unidirectional strain and stress in comparison to thermally driven actuators. Their strain-rate and efficiency, however, were usually much higher than thermally driven actuators. For example, the efficiency for CNF, and EPC are 1.08%[44] and 0.2%[46] respectively, where Stacked DEAs and HASEL actuators showed 30%[60] and 21%[59] efficiency respectively.

Long cycle life is another major concern in active assistive devices, where many actuations are needed per day to assist a motion in activities of daily living. For example most major muscles that contributes during gait activate at least once during a gait cycle [69], i.e., two consecutive steps. Thus, to assist a certain muscle during 5000 steps a day for a year, as an example, about 1 M cycle life is required for the actuation mechanism. In our study, the only group of actuators that showed such a cycle life was CNF, 1.2 M cycles[44]. The reported cycle life of the electro-active polymer actuators in this study where in the range of 158 k, 170 k, 182 k cycles for HASEL, PVC and Stacked DE actuators, respectively[53,59,60].

Note that the reported cycle life for the Stacked DE actuator was ambiguous in the literature. We assumed that the actuators underwent 182 k cycles based upon our interpretation of the sentence "After 1 year in operation and approximately 500 repetitive activations no failure due to fatigue has been reported to date"[60]. We assumed the writer meant 500 repetitive cycles per day for one year.

Among the compared electro-active polymers, PVC Gel showed Moderate stress and unidirectional strain. The Low power to mass ratio, 3 w/kg[53], short cycle life ,170 k cycles[53], are their major draw backs in rehabilitation robotics. Additionally, generating

pushing force complicated the packaging design of these actuators (Figure 2.2) and increased their bulk.

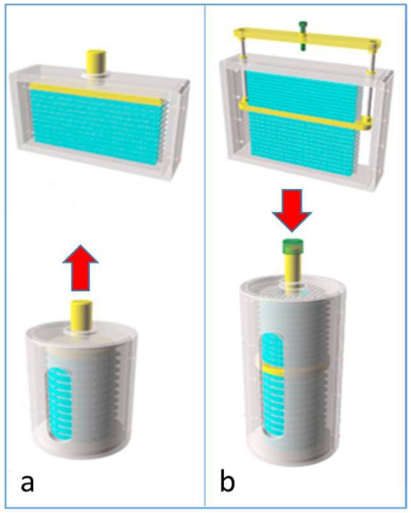

Figure 2.2: Pushing actuator (a) vs. pulling actuator (b). The proposed packagings for the pushing PVC actuators is substantially bulkier than that of pulling PVC Gel actuators.

HASEL and Stacked DE actuators on the other hand showed the most promising properties for rehabilitation applications in the literatures, including High stress, High strain-rate, and Moderate efficiency, despite their short cycle life of 158 k and 182 k cycles respectively[59,60]. Furthermore, both of these groups of actuators have a unique self-sensing feature, which is comparable to proprioception in biological muscle. This feature can decrease hardware complexity and manufacturing cost of the rehabilitation robots, through eliminating the need for additional displacement sensors. By having High stress, unidirectional strain, and power to mass ratio; and Moderate efficiency, HASEL actuators surpassed all the other four groups of actuators in the comparison measures. When compared with Stacked DE actuators, they showed substantially higher unidirectional strain, up to 124%[59](in the High range) vs 18%[60] (in the Moderate range).

The higher driving voltage (up to 10 times), shorter cycle life, risk of leakage, and snap through transition of HASEL actuators, however, made the Stacked DE actuators the strongest candidate, overall. The snap-through transition of the HASEL actuators is an all or none type of actuation, which complicates control mechanism if continuous length modulation is needed.

2.5.1 Chosen Actuator

Table 2.8: Reported properties of the commercially available Stacked DE actuator, CT-SDEA[61].

Reported properties in the manual	
Max Force/Stress	10 N/34.6 kN/m^2
Max strain	5%
Cycle life	70 M cycles
Actuation frequency	<100 Hz
Long term stability	>5 years
Max driving voltage	1200 kV

The Stacked DE actuators was the chosen group of actuators mainly due to Moderate unidirectional strain, 18%; and reported High stress and strain-rate value, 102 kPa and >500%/s respectively[60]. Also, the reported efficiency for DE actuators are typically Moderate, 25%-30%[39,46], which is higher than all of the investigated actuators. Being commercially available, CTsystems' Stacked DE actuator (CT-SDEA)[61], was an additional advantage over the other investigated actuators in this study. These

outstanding properties in addition to its soft, noiseless, and unidirectional contraction make the Stacked DE actuators a versatile group of actuators for rehabilitation applications.

Note that although CT-SDEA is produced based on the aforementioned Stacked DE actuators[60], the reported maximum force and unidirectional strain values are lower (Table 2.8). This difference is mainly because of the required long cycle life for commercial applications. CTsystems decreased the recommended activation voltage from 4.2 kV to 1.2 kV, which reduce the chance of electrical breakdown and increased the cycle life to more than 70 M cycles. This cycle life is much longer than those of reported for the compared actuators in this study, 1.2 M[44], 170 k[53] and 158 k cycles[59].

2.6 Conclusion

Stress, unidirectional strain, power to mass ratio, strain-rate, and efficiency of five groups of soft actuators (CNF, EPC, PVC gel, Stacked DE actuator, and HASEL) were compared. Stacked DE actuators showed High stress-rate, Moderate maximum strain and stress, which made them ideal for rehabilitation robotic applications. Their long cycle life is one of their most outstanding features, which makes them an ideal group of soft actuators where thousands of actuations is needed per day. They were the only commercially available actuators within the compared actuators. The reliability of the reported electro-mechanical properties and additional measure, such as hysteresis and length tension curve, must be assessed for this commercially available group of actuators. These assessments are valuable for comprehending limitations and capabilities of Stacked DEAs in wearable robotics.

Chapter 3

ASSESSING THE CAPABILITY OF A STACKED DIELECTRIC ELASTOMER ACTUATOR TO LIFT THE FOREARM OF A 2-YEAR-OLD BOY

3.1 Abstract

Recent commercial availability of a stacked dielectric elastomer actuator (SDEA) has opened up possibilities of their use as "artificial muscles" for rehabilitation robots and powered exoskeleton devices. Made by CTsystems, this actuator (CT_SDEA) is made from soft materials, and offers a lightweight and acoustically noiseless alternative to DC motor actuators used in conventional rehabilitation robotic systems. The purpose of the present work was to benchmark the electromechanical properties of CT-SDEAs to assess its capabilities and limitations for powering rehabilitation robots.

The electro-mechanical properties of the CT-SDEA that were benchmarked included the: stress response, electro-mechanical delay, Young's modulus, longitudinal strain, strain-rate, power-to-mass ratio, and current consumption. The observed properties were then compared with the reported values for mammalian skeletal muscle. Finally, CT-SDEA performance metrics, such as its length-tension properties and force generation hysteresis were assessed.

The CT-SDEAs tested in this study showed 21 ms electromechanical delay, and their calculated strain-rate was 660 %/s. They were able to generate 21.74 N of force

and have a 426 W/kg power-to-mass ratio. Their longitudinal strain was measured at 3.3%. Additionally, their steady state current consumption was 39 μA.

CT-SDEAs' fast response, short electromechanical delay and high strain-rate, make them highly suitable for closed-loop control. Additionally, their force generation capability, fast response, high power-to-mass ratio, and low steady state power consumption make them strong candidates for exoskeleton applications. Its longitudinal strain (3.3%) however, was less than that of skeletal muscle (20%). Depending on the application, their use may require the addition of mechanical linkages, for force to displacement conversion.

Finally, eight artificial muscles with various in-series and parallel CT-SDAEs were configured; and their longitudinal contraction and maximum force were measured. Thereby, we concluded that an artificial skeletal muscle consisting a bundle of three artificial myofibrils, each of which contains five CT-SDEAs in-series, has sufficient force, 60 N, to lift a 3.30 N tensile load 6.6 mm off the ground.

3.2 Introduction

To improve the acceptability and performance of rehabilitation robots, development of actuator technology with natural feel is highly desirable. Softness, i.e., having Young's modulus in the range of biological tissues, may improve degrees of freedom, safety and natural feel of the device [37]. If softness combines with noiseless and linear operation, the resultant muscle-like actuator will be a versatile alternative for rehabilitation purposes, especially exoskeletons, where the actuator is functioning in close proximity to human-limbs. Linear actuation of alternative actuators allows them to be placed along the skeletal system, like skeletal muscle, and reduce the overall bulk of the exoskeletal system. A reduction in bulk is achieved because rotational actuators

require gears to convert rotation to linear motion, lower actuation speeds and increase torque. Furthermore, linear actuation, when combined with softness, can follow complex geometries and result in multiple degrees of freedom using a single actuator [43]. For exoskeleton applications, it is desirable for the actuator to have force and displacement generation comparable to that of mammalian skeletal muscle. We call an actuator that is soft, noiseless, has linear actuation, and produces comparable force and displacement to skeletal muscle, an artificial skeletal muscle.

The prospective artificial skeletal muscle candidates mostly fall into two categories, thermally driven or electro-active polymers. Thermally driven polymer actuators are usually more powerful than electro-active actuators, especially in their strain capacity. For example, a 2 g ethanol-based phase-change actuator, proposed by Miriyev's group, could produce up to 120 N force and 140% strain[46]. Unlike electro-active polymers, however, these actuators have low actuation velocities (2.5 %/s strain-rate) and more importantly, low efficiencies (0.2%)[46]. These are major limitations in exoskeleton applications where fast and repetitive longitudinal displacement (contractions) are needed.

Soft electro-active polymer actuators, such as dielectric elastomer actuators (DEAs), are fast, efficient and offer a lightweight and acoustically noiseless alternative to DC motor actuators used in conventional rehabilitation robotic systems. DEAs have outstanding muscle-like behavior, which make them one of the most anticipated and studied soft actuators. Comparatively, central nervous system also use electrical commands to activate the skeletal muscles, which also consist of contractile polymers. Dielectric elastomer actuators consist of a compliant capacitor, an elastic dielectric sandwiched between two mechanically compliant electrodes (Figure 3.1). When a DC

voltage is applied to the electrodes, the resultant Maxwell pressure, the pressure between to oppositely charged plates due to electrostatic force, squeeze the dielectric in thickness direction. Equation 3.1, shows the parabolic relation of the Maxwell pressure and voltage, where $\mathcal{E}_r$ and $\mathcal{E}_0$ are polymer and void permittivity respectively, V is the applied voltage between electrodes, and d is the thickness.

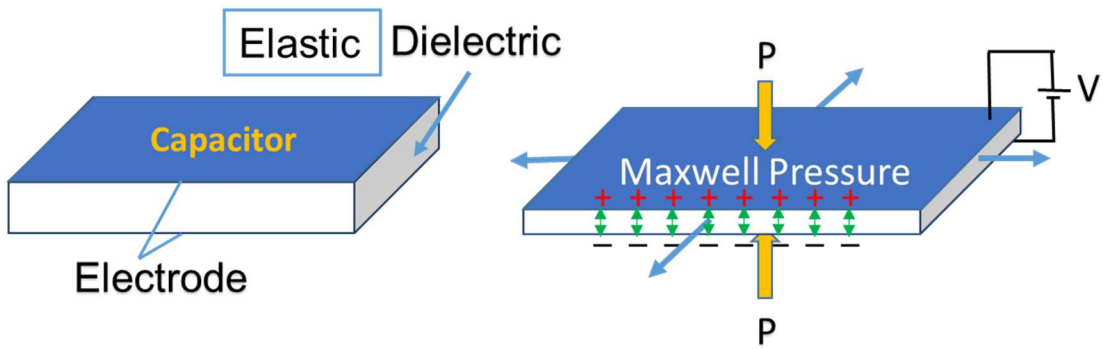

Figure 3.1 Maxwell pressure and the resultant compression or contraction of the elastic dielectric in a DEA compliant capacitor.

$$P = \varepsilon_r \varepsilon_0 (\frac{V}{d})^2 \tag{3.1}$$

High power to mass ratios that can surpass human skeletal muscles, fast response, length self-sensing, and energy recuperation capability are among DEAs unique features [42,56]. These actuators are also highly efficient. When a capacitor is fully charged, i.e., DEA is fully contracted, very small dielectric leakage currents (in the range of μA) are the only causes of current consumption [70]. The high driving voltage (>1 kV), however, can be disadvantageous in some applications, because, it limits the available electrical components that can be used within the system, and more importantly, create safety concerns. Their low power (usually in the range of few watts), which is due to their low current needed for operation, however, keeps them in the non-

hazardous range, and if appropriate insulating precautions are used. Additionally, under constant DC voltage, the applied electrical current dictates how fast a capacitance charges, and consequently, the speed of DEA's contraction. Depending on the desirable actuation velocity, the current can be limited non-hazardous values, e.g., by connecting a resistors in series with a DEA. Equation 3.2 shows the relationship between charge Q and instantaneous current i. The discharge rate of the DEA also needs to be taken into account in safety analysis. Zhang et al. simulated the electrical circuitry of their system and showed the safety of their DEA as a glove-like force feedback device[71], in accordance to IEC TS 60479-2 specifications[72].

$$Q = \int_{-\infty}^{\infty} i dt \tag{3.2}$$

DEAs have already shown some promise as artificial skeletal muscles for orthotic and prosthetic devices. In a novel approach, Carpi et al. showed the feasibility of using the multilayer DEA to actuate a hand orthosis[57]. Furthermore, DEAs have been formed into cylindrical rolls that have strain, shape, and performance similar to natural skeletal muscles[58]. One such actuator was configured to be a similar shape to a biceps muscle and to act on a life-size skeletal arm[55].

There are two main DEA configurations: 1) freestanding DEAs; and 2) DEAs with rigid frames. The rigid frames may not be ideal where soft actuators are preferable. Additionally, they are often heavier and bulkier than the freestanding designs due to their rigid frame. One of the most promising DEAs having a rigid frame configuration is the DE membrane actuator by Hodgin et al.[73]. Hau et al. stacked multiple such actuators and showed 72 N of force production, which is substantially higher than that of most proposed free-standing DEAs[74]. The cross-section of this actuator (85×85×35 mm), however, was bulkier than most other proposed linear DEAs. Pei et al. proposed

the more compact spring-rolled DEA which could generate 15 N force and 23% strain with a 60 mm cylindrical actuator[75]. Table 3.1 shows the mechanical properties of these designs. Despite these versatility, the cycle life of the rigid-frames DEAs may be limited due to unpredictable mechanical failure[76].

Table 3.1 The properties of DEA configurations. The strain column are the values reported under no load conditions. The reported weight in the stroke column is the load that was used measurement. The forces column reports the isometric (blocked) force. In the dimension column, the value in parenthesis represents the active length, i.e., the portion of the total length that was sandwiched between electrodes.

Configuration	Stroke mm	Strain	Force	Dimension (mm)	Voltage	Weight
Spring roll[58]	8 mm 0.5 kg	23%	15 N	(60 active) 20 layers	6000 V	8 g
Membrane[74]	2.25 mm 7.5 kg		72 N	85×85×35	2400 V	
Tubular[77]	1.25 mm No load	3%		100 (60 active)	2700 V	105 g
Helical[78]		8%	~0.65 N	80×13	~1200 V	
Folded[79]		5%	~3 N	85×25	~1000 V	
Stacked[60]	2.5 2.0 kg	18%	32 N	25×20	4200 V	4 g

In artificial skeletal muscle applications, the free-standing configurations offer more natural feel to the design. Various free-standing configurations are proposed such as, core-free rolled [76], helical [78], folded [79], and stacked DEAs [60] (Table 3.1). Figure 3.2 shows the aforementioned DEA configurations. Stacked DEAs proposed by Kovacs et al.[60] are powerful versatile DEA configurations that shows the most similarity to human skeletal muscle compared with other linear DEA configurations. Kovacs et al. stacked multiple layers of thin enhanced DEAs to create this novel actuator[60]. In this configuration, each layer can be considered as sarcomere within a myofibril of skeletal

muscle. This group of inexpensive tensile actuators were capable of producing 32N of isometric force and 15% strain while lifting a 1.1 kg tensile load [60]. These capabilities led these actuators to become the first and only commercially available Stacked DEA, which is manufactured by a company called CTsystems [61].

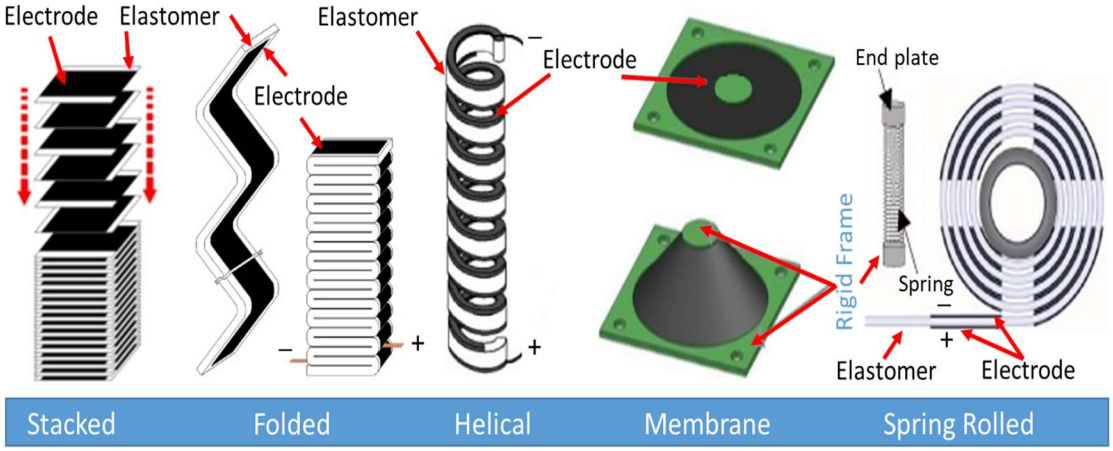

Figure 3.2 Various configuration of DEA. Stacked[60], Folded[80], Helical[78], Membrane[74], and Spring roll[58]. The black area in each configuration is the compliant electrode and the lighter area shows the elastomer.

To evaluate the reported properties and measure additional mechanical properties needed for our application, a stacked DEA by CTsystems (CT25.0-15-15-71, Compliant Transducer Systems, Dubendorf, Switzerland), which we call CT-SDEA, was benchmarked. The CTsystems' reported properties for this actuator is presented in Table 3.2. In the second phase, these actuators were configured in series and parallel in multiple configurations to form DEA-based artificial skeletal muscles and the force and shortening of these configurations were measured. This phase was accomplished to test the additive behavior of these actuators in series and parallel. Finally, by combining phases 1 and 2, we could choose the best available option for our application, which

was to develop an exoskeleton capable of actively assisting the elbow joint of a 2-year-old boy.

Table 3.2 The reported mechanical property of CTsystems' CT25.0-15-15-71, which we call CT-SDAE in this study[61].

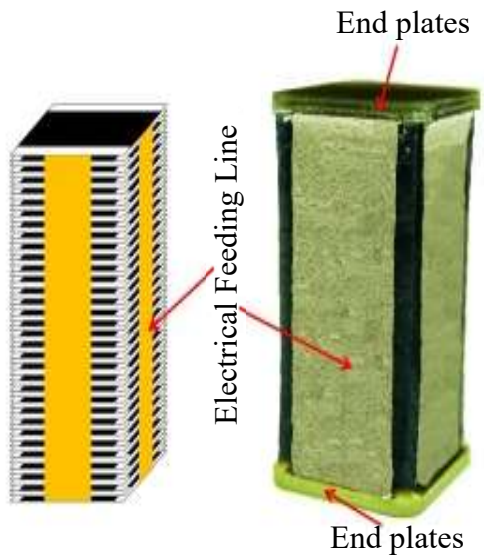

Max Force	10 N
Max strain	5%
Shortening	1.17 mm
Elastic Modulus	1.4 MPa
Cycle life	50 M cycles
Long term stability	>5 years
Actuation frequency	<100 Hz
Dimension	39×17×17 mm
Weight	11.3 g
Layer thickness	25 µm
Max driving voltage	1200 kV
Charge time	<5ms at 100 mA

3.3 Method

3.3.1 Testing Procedure

Thirteen CT-SDEAs were tested under isometric and isotonic contraction conditions. Under each condition, the CT-SDEAs were activated by three main waveforms; 1) triangular: an isosceles triangle shape waveform with period of 10 s and amplitude of 1230 V; 2) linear: a right triangle waveform with amplitude of 1230 V and period of 5 s; 3) square: a square waveform with amplitude of 1230 V and period of 5

s. The square waveform was proceeded and followed by a period of 5 s at 0 V. Note that the maximum recommended driving voltage of the CT-SDEA is 1200 V and its maximum tolerable driving voltage is 1400 V. While CT-SDEAs were receiving the activation waveforms, the generated force and/or longitudinal displacement (contraction) was recorded.

3.3.1.1 Isometric Condition

The length of the CT-SDEAs was held constant at its rest length, i.e., 39 mm, under no compression or extension, throughout the trials. The generated force under each activation waveform was recorded. To this end, the CT-SDEAs was screwed to a rigid frame from one end and to the load-cell from the other end in a vertical position. Using the data collected during the isometric condition, the following measures were calculated;

1. ***Force generation response*** was analyzed by superimposing the generated force of thirteen CT-SDEAs to the square waveform. Then, the similarity in response profile and maximum force generation, were compared between samples.

2. ***Maximum stress*** was calculated, using the aforementioned force generation dataset, by dividing the averaged maximum force, reported as mean and one standard deviation (mean ±SD), of the thirteen CT-SDEAs, divided by the area of the CT-SDEA's end-plate, 289 mm^2.

3. ***Electromechanical delay*** was calculated using the square activation waveform. This measure was defined as the time difference between the onset of the square waveform, and the onset of force generated by the CT-SDEAs. The onset of both force and voltage was calculated as follow: 1) the mean and standard deviation (SD) of the baseline, i.e., the first 4 s of each signal without activation, was calculated; 2) the onset threshold was set at mean of the baseline + 4SD; 3) the first value equal or higher than the threshold value was considered the onset of the signal.

4. ***Current consumption*** was reported as the peak transient current, its time constant and its steady state value using the square activation waveform.

5. ***Length-tension curve**:* to determine this curve the maximum force of a representative CT-SDEA generated by the square activation waveform was measured while it was at its rest length, nine compressed lengths (nine different lengths from 99.5% to 95.5% of its rest length), and ten extended lengths (ten different lengths from 100.5% to 105% of its rest length). The passive force at each length is defined as the pulling, (negative) or pushing (positive) elastic force exerted by the CT-SDEA at the baseline, i.e., under 0 V activation voltage. Active force at each length was defined as the total force generated by the CT-SDEA minus the baseline. This graph provides crucial information in applications where agonist/antagonist pairs of artificial skeletal muscles are needed at a joint.

6. ***Force generation hysteresis*** was determined by activating a representative CT-SDEA, using the triangular waveform, and plotting the force generated by the CT-SDEA against the HV amplifier's output voltage, i.e., 0 to 1230 V. To report the hysteresis quantitatively, the force generated in the ramp-up phase was subtracted from the force generated in the ramp-down phase at a certain activation voltage; then, the maximum of these differences was reported as the hysteresis, both as the absolute value, and the percentage of the maximum generated force. Additionally, another triangular waveform was used with shorter period, 1 s, to show the effect of speed of contraction on the hysteresis.

7. ***Axial Young's modulus*** was calculated using Equation 3.3, where F is force, L_0 is the initial length, ΔL is the length change and A is the CT-SDEA's end-plate area. The data collected for length-tension curve was used to calculate this measure.

$$Y = \frac{F \times L_0}{A \times \Delta L} \text{ (i.e., } \frac{Stress}{Strain}\text{)}, \tag{3.3}$$

3.3.1.2 Isotonic condition

For the isotonic condition, the CT-SDAEs were hung from the load-cell and a set of tensile loads were attached to them using 3D printed couplers. Then, the contraction for each loaded conditions were measured under the activation waveforms. The following measures were calculated using the isotonic contraction data.

1. ***Displacement generation hysteresis*** was measured similar to force generation hysteresis. The displacement of the actuator was measured,

instead of force, during the ramp-up and ramp-down of the triangular waveforms with 10s and 1s periods.

2. ***Maximum longitudinal strain*** was calculated by dividing the averaged maximum longitudinal contraction, reported as mean (SD), of thirteen CT-SDEAs to their normal length, 39 mm, using the linear activation waveform and 0.80 N of tensile load (g=10 m/s^2).

3. ***Strain-rate***, as measure of contraction speed, was calculated using the reported charge time and measured maximum longitudinal strain. Because the CT-SDEA is essentially a capacitance, its charge time is the same as its actuation time. This is also observable in the reported actuation frequency (100 Hz). To assess the possibility of evaluating the calculated strain-rate, the maximum rate of voltage increase in the square activation waveform was measured to calculate the maximum generated current, as a measure of charge time, using Equation 3.4. Where *C* is the CT-SDEA's capacitance.

$$i = C\frac{dV}{dt} \tag{3.4}$$

4. ***Power to mass ratio*** was calculated using a 0.40 N tensile load (g=10 m/s^2) under the square activation waveform, during sharpest rise of the contraction, onset to %88.5 of maximum contraction, i.e., two time constant (τ). The onset detection methodology was the same as the aforementioned electro-mechanical delay measure. The maximum power was calculated using Equation 3.5, where *m* is the mass of the tensile load *v(t)* is the speed of the contraction and *a(t)* is its acceleration. Then the calculated maximum power was normalized to the weight of the actuator, 11.3 g.

$$P(t) = \frac{d(\frac{1}{2}mv(t)^2)}{dt} + \frac{d(mgy(t))}{dt} = mv(t)[a(t) + g], \tag{3.5}$$

3.3.2 Artificial Skeletal Muscle Configurations

Eight different artificial skeletal muscles were configured and tested by connecting different number of CT-SDEAs in series and parallel. Series configurations included 1×2 (i.e., an artificial myofibril of two CT-SDEAs in series), 1×3,1×4, and 1×5 combinations. Parallel configurations included 2×1, 2×2 (i.e., two parallel artificial myofibrils of two CT-SDEAs in series), 3×1, and 3×4 combinations. Then, to assess the

configured artificial skeletal muscles lifting capabilities, the maximum force and shortening of each configuration were tested under 0.4 N (no-load condition), 3.3 g, and 6.8 N tensile loads (g=10 m/s^2). Based on Winter's anthropometric data[67] and WHO child growth standard[66], the weight of 2-year-old boy's forearm+hand was calculated at 338 g, i.e., 3.38 N. Thus, the 6.8 N load was picked to emulate a loaded limb condition, more than twice the weight of a 2-year-old boy's forearm+hand . The presented 1×1 configuration was the averaged value of thirteen CT-SDEAs for each measures. To connect the CT-SDEAs series and in parallel and to the test-rig, a set of specialized couplers were designed and 3D printed for each of these configurations.

3.3.3 Testing Setup

To benchmark the CT-SDEAs under isometric and isotonic contractions, a test-rig was designed and implemented (Figure 3.3). The main components of this test-rig were: 1) a laser displacement sensor (ILD 1420-25, Micro-Epsilon, Ortenburg, Germany) to measure longitudinal contraction displacement, with 1 µm precision; 2) a load-cell (LSB302, 25 lb, FUTEK Advanced Sensor Technology, Inc., Imine, CA, USA) to measure active and passive force; 3) a precision translational stage (Newport Corporation, Irvine, CA, USA), with 10 µm graduation and 102 N axial load capacity, to fine tune the load-cell position; 4) a high voltage (HV) amplifier (RC250-1.5P, Matsusada Precision Inc., Shiga, Japan) with 1500 V and 165 mA maximum output voltage and current respectively, to provide the necessary driving voltage, 0-1230 V, for the CT-SDEAs; 5) a CompactDAQ data acquisition system (CDAQ) (CDAQ-9174, National Instrument, Austin, TX, USA) containing an analog input module (NI 9215), an analog output module (NI 9263), a digital input and output module (NI 9375), and a H-bridge input module (NI 9237) for recording the load cell data; 6) two laser levels

(GLL2,Robert Bosch GmbH, Stuttgart, Germany) to align the CT-SDEAs vertically for isometric contraction conditions; 7) a software developed in LabVIEW (National Instrument, Austin, TX, USA), to record the data from the sensors, and monitor and control the HV amplifier.

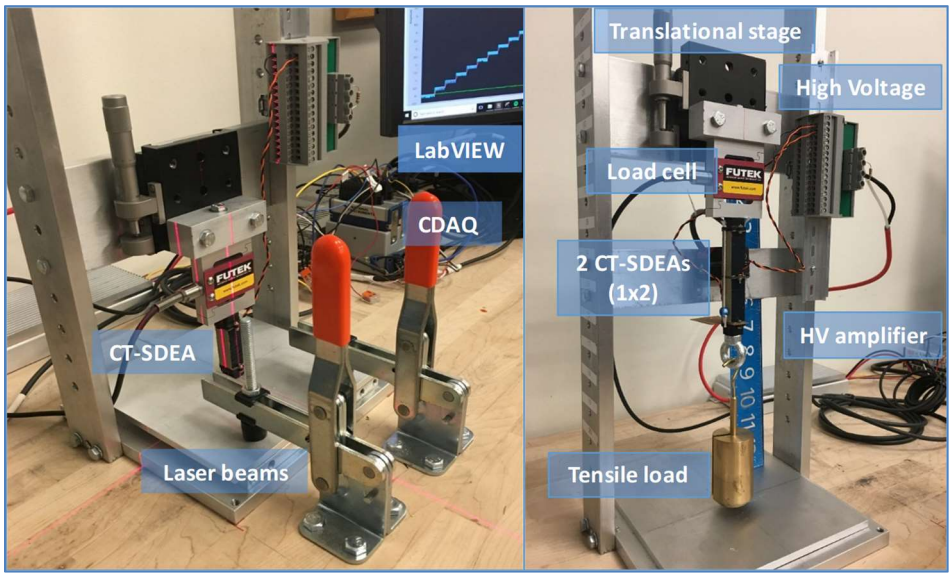

Figure 3.3 The test-rig in isometric (left panel) and isotonic contraction (right panel) conditions.

Figure 3.4 shows the electrical circuitry of the HV amplifier, V_{DC}, discharge resistance, R_{dis}, and CT-DEA. The CT-SDEA is modeled as a parallel variable capacitor, C, and resistor, R_L, in series with two electrode resistors, R_E. R_L model the non-ideal leakage current through the dielectric. The variability in the C, R_L, and R_E is due to the length modulation of the CT-SDEA, and consequently, changes in the electrical characteristics of the compliant capacitor. Electrode resistance of each CT-SDEA's layers was reported at 50 kΩ. Considering 1600 parallel layers of the CT-SDEA, the total electrode resistance, R_E, was as small as, 31.25 Ω. A 1 MΩ discharge resistor was

connected in parallel to increase the rate of discharging the CT-SDEA, and thereby, increase the pace of recovery, i.e., returning to initial state.

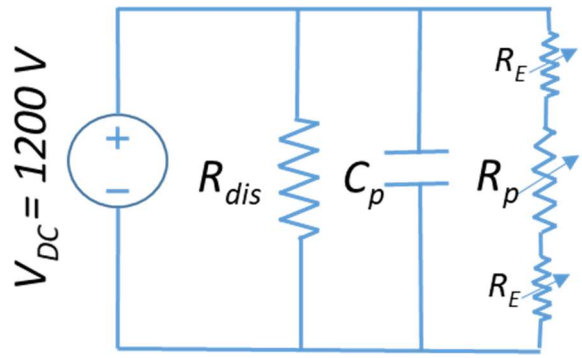

Figure 3.4 The electrical circuitry of HV amplifier, V_{DC}, a discharge resistance, R_{dis}, and CT-SDEA, in parallel with each other. CT-SDEA is modeled as a variable capacitance, C, and leakage resistor, R_L.

Preliminary results of our triangular waveform showed lack of symmetry between the ramp-up and ramp-down portion of the waveform using the Matsusada HV amplifier, due to its low slew-rate- that is the maximum rate at which an amplifier can respond to an abrupt change of input level. Therefore, for both force and displacement hysteresis, a faster HV amplifier was used (HA51U-1.6P10-3, hivolt.de, Hamburg, Germany), with 80 V/µs slew-rate. A 10 MΩ (recommended by CTsystems) discharge resistor was used for the hysteresis tests.

3.3.4 LabVIEW Code

To generate and monitor the activation waveforms and record the data from the sensors, a LabVIEW code was developed. The LabVIEW code generated a set of command signals, similar to activation waveforms in period and profile, to be amplified by the HV amplifier. The sampling rate of the command signal was 1 kS/s via analog output of the CDAQ. While applying the command waveform, the LabVIEW code

simultaneously recorded the input signals via the analog input modules of the CDAQ. The LabVIEW code collected data from load-cell and displacement sensors while monitoring the output current and voltage of the HV amplifier (Figure 3.5). Force (load-cell signal) and the monitoring signals (i.e., output current and voltage of the HV amplifier) were collected via CDAQ, synchronously, having negligible time differences between them. The laser displacement signal, however, was collected via a USB port and was synchronized as close as possible with other input signals via our designed software.

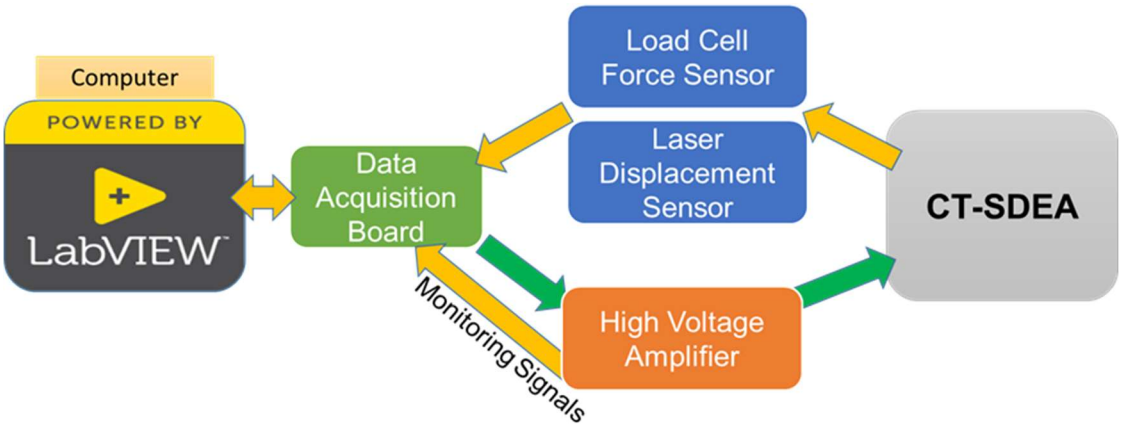

Figure 3.5 The block diagram of the testing setup.

3.4 Results

3.4.1 Benchmark Testing of CT-SDEAs

On average, the 13 CT-SDEAs generated 10.01 ±0.2 N, i.e., 35 kPa stress, and 1.30 ±0.8 mm of shortening. The amount of shortening was slightly higher than that of reported by CT-SDEAs (Table 3.2).

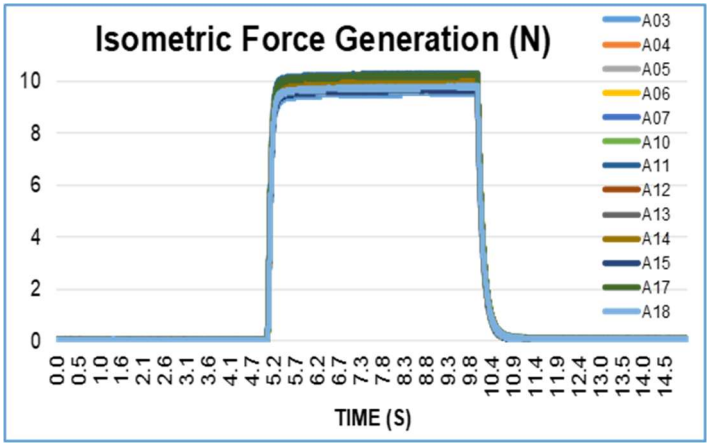

Figure 3.6 The force generation response of thirteen CT-SDEAs in generating force under the square activation waveform superimposed on top of each other. A01 to A13 are each of thirteen actuators tested for this measure.

The force generation profile of the thirteen actuators were identical, however, the maximum force variation between CT-SDEAs ranged 9.74 N to 10.34 N (Figure 3.6). Additionally, the CT-SDEAs had fast response times, with electromechanical delay shorter than that of mammalian skeletal muscle, 21 ms (Table 3.3). Similar to most mechanical properties of the CT-SDEA, its axial Young's modulus, 0.87 MPa had lower value in comparison with mammalian skeletal muscle (Table 3.3). Power-to-mass ratio and electromechanical delay of the CT-SDEA were higher than that of skeletal muscle (Table 3.3). Using 3.3% measured longitudinal strain (Table 3.3) and charge time, 5 ms (Table 3.2), the strain-rate was measured at 660 %/s. Using Equation 3.2, the measured maximum transient current, and CT-SDEA's capacitance the $\frac{dV}{dt}$, i.e., slew-rate, was measured 9×10^7 V/s, which was substantially lower than the needed slew-rate, 4.2×10^8V/s, to produce 100 mA needed for 5 ms of charge time.

Table 3.3 CT-SDEA electromechanical properties in comparison to properties of mammalian skeletal muscle.

Property	Typical	Max	CT-SDEA
Strain (%)	20[48]*	>40[39]	3.3
Stress (MPa)	0.1[39]	0.35[39]	0.037
Strain-rate (%/s)		500[39]	660
Power to mass (W/kg)	50[39]	200[39]	429.1
Cycle life (M Cycle)		1000[39]	>50[61]**
Axial Young Modulus (MPa)	10-60[39]		0.87
Electromechanical delay (ms)	54[49]		21

*** This is reported by the CTsystems[61].*
** The reported value for biceps[48].*

The CT-SDEA showed 22.77 mA maximum transient current with 35.8 ms time constant, and a steady state current of 39 µA. Consequently, R_L was calculated at 35.1 MΩ. The CT-SDEA capacitance, C, was measured 237 nF.

The Length-Tension curve (Figure 3.7) shows active and passive force generation capability of the CT-SDEA under different levels of extension/compression. Although small, the more extended the CT-SDEA, the less force it could generate. The active force ranged from 11.01 N to 8.98 N for 4.5% compression and 5.0% extension, respectively. The CT-SDEA showed a substantial passive force under compression and extension due to the elasticity of the dielectric layer, i.e., silicone elastomer (Figure. 3.7, grey trace). The passive force ranged from -12.54 N to 12.76 N for 4.5% compression and 5.0% extension respectively. Thus, the maximum total force was 21.74 N.

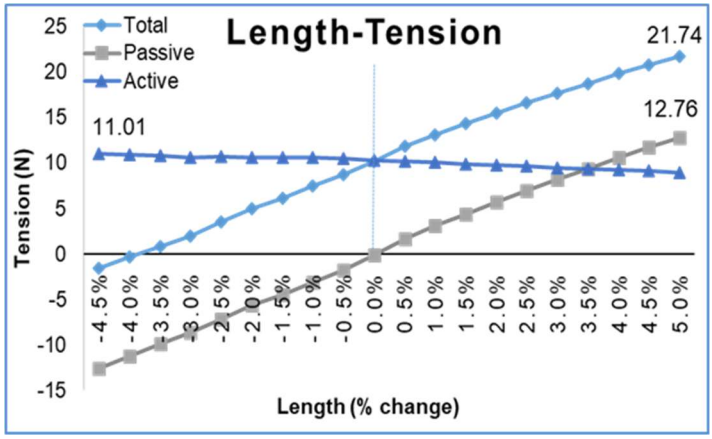

Figure 3.7 The active and passive force generation of a representative CT-SDEA under different levels of compression and extension. The 0.0% is the normal length of the actuator. Positive and negative percentages are extension and compression respectively

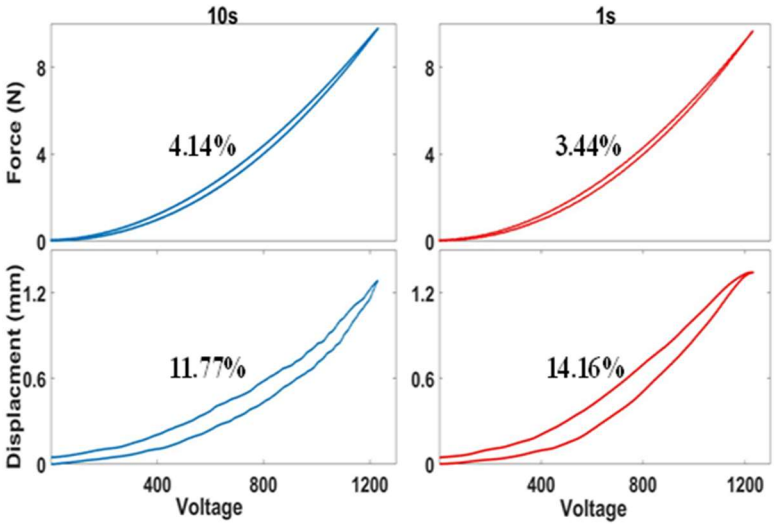

Figure 3.8 The force and displacement hysteresis of a representative CT-SDEA.

Figure 3.8 shows the low force generation hysteresis of the CT-SDEAs for both 10 s and 1 s triangular waveforms (upper panels), at 0.41 N (4.14%) and 0.33 N (3.44%), respectively. The shape of this graph shows the parabolic relationship between Maxwell pressure and applied voltage (Equation 3.1). In comparison with force, the displacement hysteresis is much higher, 0.15 mm (11.77%) and 0.19 mm (14.16%) for the 10s and 1s

triangular waveforms respectively. The hysteresis graph is important for assessing the complexity of the needed control mechanism.

The maximum longitudinal contractions of the thirteen CT-SDEAs under eleven different tensile loads, from 0.8 N to 1.08 N (g=10 m/s^2), were averaged and depicted in Figure 3.9. As tensile load increased, the maximum reachable contraction decreased.

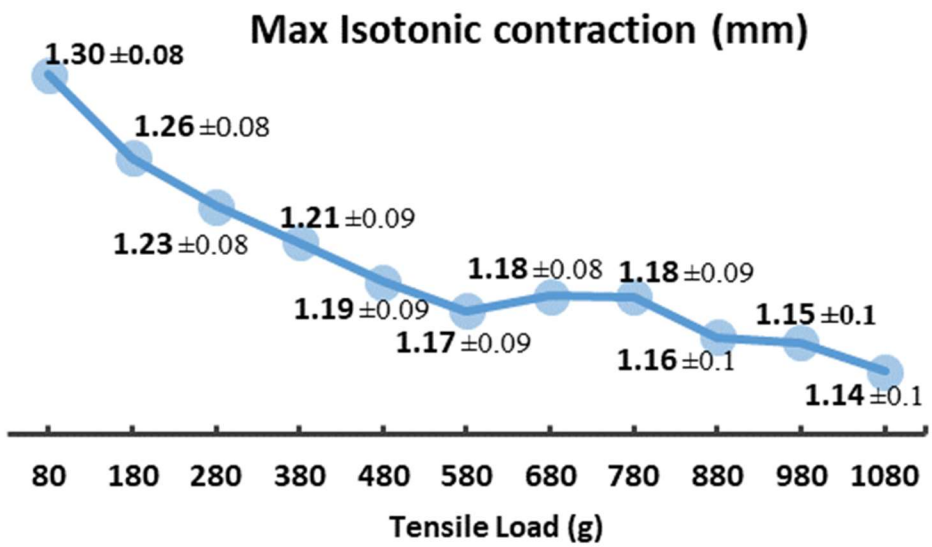

Figure 3.9 Averaged maximum (Max) longitudinal contraction of 13 CT-SDAEs, under 11 tensile load.

3.4.2 Artificial Muscle Configurations

The different configurations of the artificial skeletal muscle showed linear additive behavior of force and displacement when the CT-SDEAs were configured in parallel and in series. When CT-SDEAs are added in parallel, the maximum force generated is multiplied by the number of actuators used (contraction displacement remains the same), while when added in series, contraction displacement multiplied by the number of actuators used (force generation remains the same). For example, as

expected, by adding the CT-SDEAs in series, 1×1 to 1×5, the force generation stayed the same at ~10 N of maximum force (Figure 3.10). The configurations with two CT-SDEA's myofibrils in parallel (2×1 and 2×2) and three CT-SDEAs myofibrils in parallel (3×1 and 3×4) showed ~20 N and ~30 N of maximum force respectively (Figure 3.10), with 6.8% linearity error. By increasing the number of CT-SDEAs in the myofibril, the artificial skeletal muscles' maximum shortening increased almost linearly, with 6.9% linearity error. For example, under 0.4N of tensile load a single CT-SDEAs showed 1.3 mm of maximum shortening and a myofibril of 5 CT-SDEAs in series showed 6.53, i.e., 5 × 1.3 (Figure 3.11). This linearity, however, decreased by increasing the tensile load, and thereby, extending the CT-SDEAs when they were at their rest state. Because each 1×5 myofibril approximately produced a maximum of 20 N of total force based on the length-tension curve (~10 N of active and ~10 N of passive, Figure 3.7) and 6.5 mm of longitudinal contraction (Figure 3.11), we assumed that the 3×5 artificial muscle could produce up to ~60 N of total force and 6.5 mm of shortening.

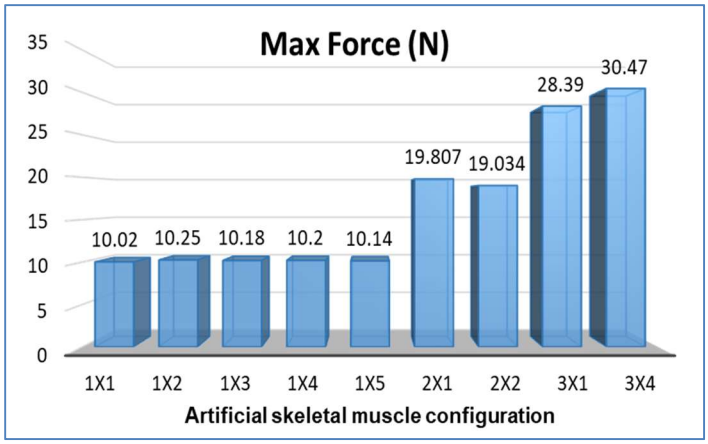

Figure 3.10 Maximum (Max) force generation of eight configured artificial skeletal muscles and 1×1 configuration, which is the averaged max force generation of thirteen CT-SDEAs. By increasing the number of CT-SDEA myofibrils in parallel the max force generation of the artificial muscles increased almost linearly.

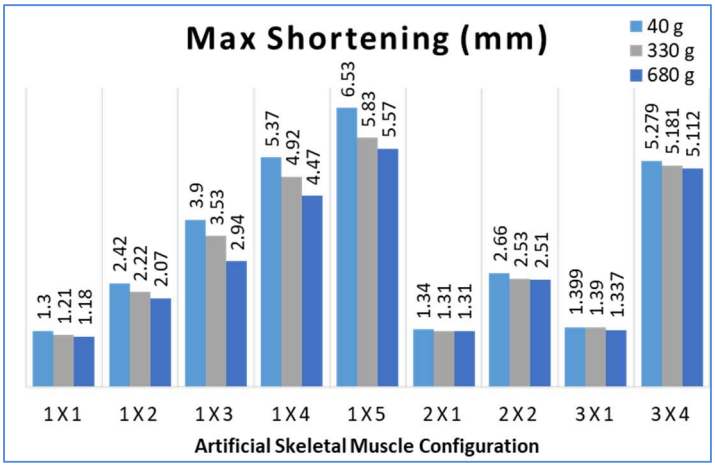

Figure 3.11 Maximum (Max) shortening, of the eight configured artificial skeletal muscles and 1×1 configuration, which is the averaged max contraction of thirteen CT-SDEAs. By increasing the number CT-SDEAs in a bundle the maximum contraction increased almost linearly.

3.5 Discussion

The mechanical properties of the CT_SDEA, a commercially available stacked DEA, were measured. Aside from substantial force generation, noiseless operation, and

high power to mass ratio, in comparison to other alternative actuators, the CT-SDEAs' high cycle life, reported by CTsystems, and low energy consumption are outstanding. The results were compared with CTsystems reported values, and that of the mammalian skeletal muscle. When compared with the CTsystems reported values, CT-SDEAs showed similar force generation capability, however, the measured shortening was slightly higher. The calculated Young's modulus was smaller than the reported value. Almost all measured properties were comparable to those of skeletal muscle, except strain and cycle life.

CT-DEAs showed substantially higher power-to-mass ratio and electro-mechanical delay, 429 W/kg and 21 ms respectively, in comparison with skeletal muscle, 200 W/kg and 54 ms respectively. The former is mostly the result of their light weight, 11.3 g, high strain-rate and substantial force generation. The low electro-mechanical delay, i.e., fast response-time, in combination with short actuation time, i.e., strain-rate, will help the design of a fast and effective closed-loop control mechanism. This is highly desirable in rehabilitation robotics.

One of the outstanding feature of CT-SDEAs in comparison to other alternative soft actuators, such as Hydraulically Amplified Self-Healing Electrostatic (HASEL)[59], polymer fiber and Plasticized Poly Vinyl Chloride (PVC) gel[53], are their high cycle life, >50 M cycles. Recently, >70 M cycle is reported for the new models. In comparison, PVC gel performance decreased by 60% after only 170 k cycles[53] and the reported cycle life for HASEL is 158 k cycles[59]. Although smaller than skeletal muscle, this feature makes CT-SDEAs a desirable alternative for active exoskeletons, where many contractions are needed per day to assist an individual with an impaired musculoskeletal system.

As expected from a capacitor, steady state current consumption, i.e., the dielectric leakage current of the CT-SDAE, was very low, less than 39 μA. Ideally, once a capacitor is charged the current consumption must be zero, however, in reality there is always a small leakage through the dielectric material. This is due to the very high, but not infinite, resistance of the dielectric, 31.5 MΩ in CT-SDEA. This low power consumption, 0.047 W (39 μA × 1230 V), for holding the contraction is remarkable, whereas, the versatile soft ethanol-based phase-change actuators consume 45 W to flex the forearm of a skeleton[46]. To charge the CT-SDEA for full contraction, the transient current consumption of one actuator, however, reaches as high as 22.77 mA for a couple of milliseconds. For safety concerns, one can trade off the contraction velocity by limiting the current, (Equation 3.2). This can be done simply by connecting a resistor in-series with the actuator.

In active exoskeletons, where assisting motion is usually the main goal, the shortening, i.e., longitudinal displacement, of the artificial skeletal muscle must be large enough to allow for its contraction alongside the impaired muscle. The maximum strain of the CT-SDEAs (3.3%), however, was substantially lower than skeletal muscle (20%). In a study on 13 adults Pappas et al.[48] showed about 4 cm of shortening in maximum voluntary contraction of biceps muscle. The averaged upper-arm length of these participants were about 32 cm (~20 cm biceps length). Thus, if an artificial skeletal muscle contains eight CT-SDEAs in-series, total length of about 32 cm, its maximum shortening would be about 1.4 cm (each CT_SDEA producing 1.3 mm of shortening). This is equivalent to about one third of the shortening of an adults biceps muscle[48]). Therefore, assisting the biceps in its full range of motion (ROM) is quiet challenging. However, one can either leverage the substantial force of the SDEAs, 21.74 N total force

(Figure 3.7), to magnify the displacement using mechanical linkages; or assist the skeletal muscle's contraction in its partial ROM.

The difference in Young's modulus between our measurement and the reported value by CTsystems, may be due the limitations of our testing set up compared to that of the manufacturer. Similarly, the incapability in recreating the reported charge time, to reach the reported actuation frequency, and thereby, measuring the maximum strain-rate, was due to the slow slew-rate of the Matsusada HV amplifier and the maximum reachable transient current of the hivolt amplifier, 20 mA. The necessary transient current to replicate the reported charge time, i.e., actuation time, was 100 mA (Table 3.2), which was not reachable in activation of one CT-SDEA using the square waveform. The small range of extension/compression, 4.5% - 5%, that we used for calculating Young's modulus, may also be a contributing factor in the resultant smaller value.

3.6 Conclusion

To assess the capability of stacked DEAs for rehabilitation robotic applications, CT-SDEAs were benchmarked; and their mechanical properties were compared to the reported values for skeletal muscle. The CT-SDEA showed comparable properties to skeletal muscle in most features of interest, including response time, stress and power to mass ratio. Its cycle life, although shorter than skeletal muscle, appear sufficient for rehabilitation purposes and was substantially higher than other alternative soft actuators. Its strain, however, was substantially lower than those of human skeletal muscles, which may impose challenges in design.

Using these results, we concluded that a 3×5 artificial muscle can lift the weight equal to a 2-year-old boy forearm+hand, by 6.5 mm, and generates ~60 N of maximum

total (active + passive) force. Therefore, it may be a prospective actuator for use in pediatric exoskeletons, considering its fast response, high strain-rate, and cycle life in comparison to other soft alternatives.

Chapter 4

PROPRIOCEPTIVE ARTIFICIAL SKELETAL MUSCLE

4.1 Abstract

For a sensor-free closed-loop control of a commercially available stacked dielectric elastomer (SDEA), a self-sensing length modulation system was developed. This length modulation feedback will mimic the proprioception in human motor control. During actuation, the changes in the DEA capacitance, was used to sense the longitudinal contraction of the actuator.

First, a previously established length self-sensing technique was implemented on a CTsystems' stacked DEA (CT-SDEA). A low-pass filter was designed by connecting a resistor in series with a CT-SDEA. Then a high frequency signal was superimposed to the driving, low frequency, activation waveform. By measuring the amplitude of the output of this low-pass filter, the displacement of the CT-SDEA was inferred. Then, this length self-sensing technique was implemented to an artificial muscle consisting of three CT-SDEAs in series. To mimic the muscle spindle's function in mammalian skeletal muscle, the middle CT-SDEA was then sensed, while the artificial muscle was contracting. By fitting this self-sensing information to the displacement information of the muscle, measured by a laser displacement sensor, the capability of length self-sensation was validated. The self-sensing output signal was plotted against the measured displacement and polynomial curve was then fitted to this graph. The results showed that 2nd order polynomial fit better, 6% error, than a 1st order polynomial, 16% error.

4.2 Introduction

In active wearable technology e.g., active exoskeletons, where the device operates in close vicinity of human body, actuators that are soft, lightweight, compact, efficient, and acoustically noiseless are highly desirable. Dielectric elastomer actuators (DEAs) are one the most promising alternate that shows all of the aforementioned muscle–like characteristics[40,52,56]. DEA is an elastic dielectric sandwiched between two compliant electrodes. When high voltage is applied (usually in the range of 1-5 kV) the electrostatic force, i.e., Maxwell pressure, contracts the non-compressible, elastic, dielectric. The controllability of these actuators is demonstrated by Carpi et al[81]. They showed the feasibility of open-loop control of DEAs using biosignals, i.e., EMG, EEG, and ECG, for wearable technology[81]. In rehabilitation robotics, however, closed-loop controls are more preferable due to their reliability. In such applications, precise displacement feedback is often required for a robust closed-loop motion control. Interestingly, unlike conventional actuators, DEAs do not require an independent sensing device such as encoder or tachometer. Changes in DEAs electrical characteristic can be used to infer their length modulation[82,83]. When multiple degree of freedom is needed, in applications such as rehabilitation robotics, this feature may substantially reduce the cost and complexity, and improve the efficiency of the system.

Skeletal muscle use proprioception as a prominent feedback for controlling motion and balance. Proprioception is the awareness of the body in space. It is the use of joint position sense and joint motion sense to respond to stresses placed upon the body by alteration of posture and movement[84,85]. To do so, skeletal muscle use two types of sensors; 1) muscle spindles, i.e., displacement sensor, which are located in the muscle and their firing rate is proportional to muscle length; and 2) Golgi tendon organs, force sensors, which are located between muscle and tendon and sense the force generated by

skeletal muscle. Proprioceptive information are sent through fast-conducting Aα fibers to the central nervous system for proper balance and motor control. Therefore, in biomimetic rehabilitation robots a proprioceptive artificial skeletal muscle, which is capable of simultaneous actuation and sensation, is desirable. Such artificial muscle can be deployed in a closed-loop control of joint motion more readily. Similar to skeletal muscle, length modulation of DEAs can be inferred during actuation, via the changes in electrical characteristics of these compliant capacitors, with no need for sophisticated external sensors[86]. In this chapter, we will focus on the implementation of the length modulation sensation on a DEA-based artificial muscle. This capability is usually denoted "self-sensing"[70,82,87–89].

4.2.1 DEA Length Self-Sensing Theory

Due to its promising prospective, various length self-sensing techniques have been proposed in past decade. Jung et al.[82], Chuc et al.[83] and Hoffstadt et al.[70] superimposed a high frequency (usually in 50 -100 Hz range) sensing signal on top of the DEA's actuating DC voltage, and thereby, measured the changes in the sensing signal's amplitude for length self-sensation.

To develop the proprioceptive artificial skeletal muscle, we will re-evaluate Jung et al. self-sensing algorithm[73] on a commercially available Stacked DEA. The DEA self-sensing mechanism works by inferring longitudinal contraction information from changes in the electrical characteristics of the DEA (Figure 4.1). The impedance of the DEA, X_c, changes by its longitudinal contraction, which can measure by recording V_{output}, using Equation 4.1.DAE's impedance, X_c, is inversely proportional to the DEA's capacitance, C. By using Equation 4.2, and the known frequency of V_{input}, f, C

can be measured. Finally, by using Equation 4.3, the thickness of the DEA (d) can be calculated.

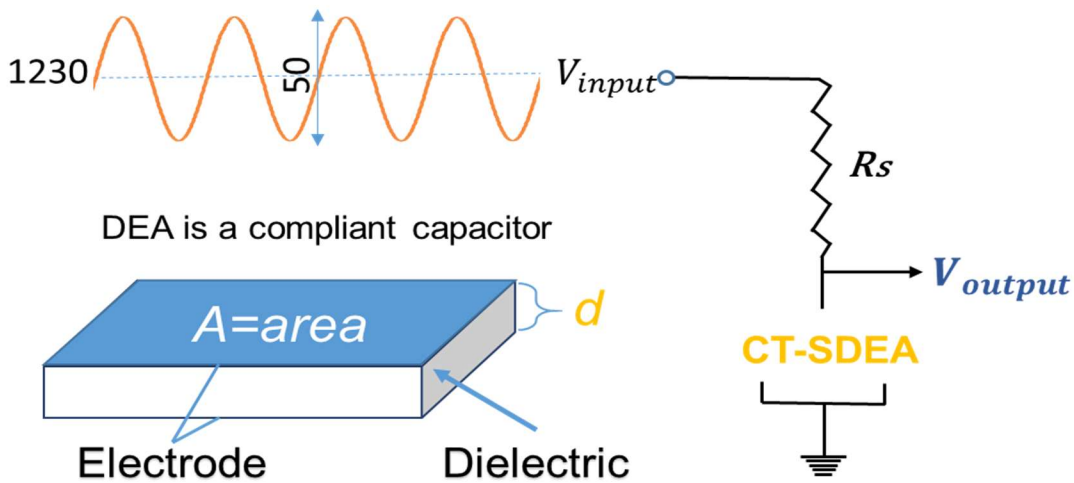

Figure 4.1 DEAs length self-sensing algorithm based on the changes in their electrical characteristics.

$$V_{output} = \frac{X_c}{R_s + X_c} V_{input} \tag{4.1}$$

$$X_c = \frac{1}{2\pi f C} \tag{4.2}$$

$$C = \varepsilon_0 \varepsilon_r \frac{A}{d} \tag{4.3}$$

As DEA in Figure 4.1 contracts longitudinally, i.e., d decreases, its capacitance increases (Equation 4.3), consequently, in frequency domain, the cut-off frequency, F_c decrease (Equation 4.4).

$$F_c = \frac{1}{2\pi R C} \tag{4.4}$$

Where R is the total resistor in the electrical circuitry including R_s.

In other words, when a DEA longitudinally contracts its capacitance increases, thus F_c decreases, consequently, the attenuation of input signal increases, which results in V_{output} decrease (Figure 4.2).

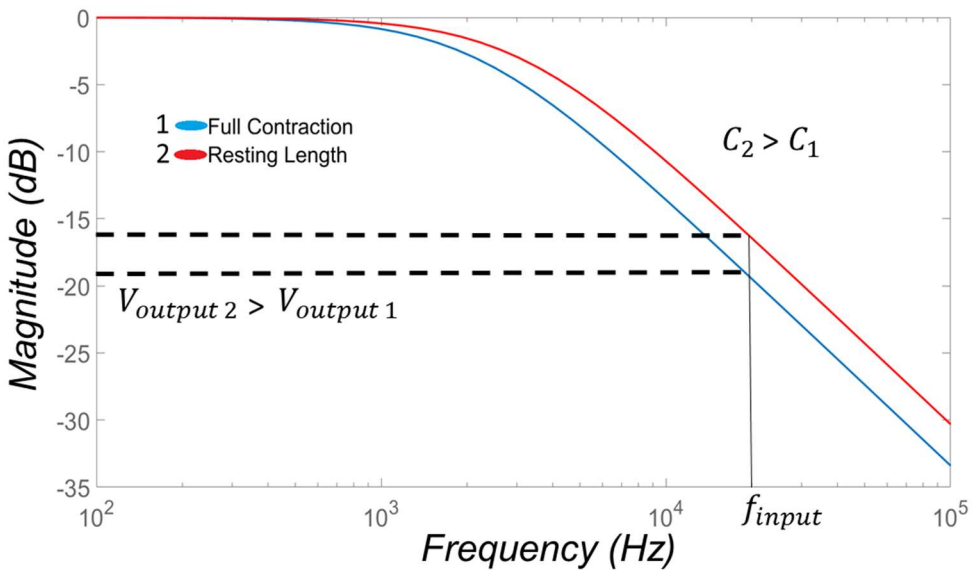

Figure 4.2 The magnitude of Bode digram of the self-sensing low pass filter. With a constant frequency (f_{input}), as the DEA's capacitance increases, due to longitudenal contraction, the cut-off frequency (frequency at -3dB) decreases, and therefore, the attenuation of input signal decreases, $V_{output\ 2} > V_{output\ 1}$.

There were several attempts to improve the length self-sensing in the DEAs. Ye et al. added artificial neural network to improve the error and nonlinearity of this technique[90]. For further improvement, adaptive modeling techniques such as least square[91] and recursive extended least square[86] and extended Kalman filter[87] were also used, in addition to this frequency domain self-sensing technique, for online identification of DEAs capacitance and resistance, whilst actuation. Outside of the laboratory, superimposition of a high frequency signal on a high actuation DC voltage

is nontrivial if not impossible for a portable application. To eliminate the need for a high frequency signal, Gisby et al. proposed two time domain techniques, 1) using the actuator's discharge rate to measure its capacitance in a PWM driven DEA[92]; 2) using arbitrary oscillation in voltage instead of superimposing high frequency signal[88].

In this chapter the length self-sensing mechanism proposed by Jung et al. was added to a commercially available Stacked DEA by CTsystems (CT25.0-15-15-71, Compliant Transducer Systems, Dubendorf, Switzerland), which we call CT-SDEA. The comprehension and implementation of this self-sensing will help us in developing the robust PID controller that uses this proprioception as its feedback. Additionally, implementation of this well-established technique will be used as the gateway to implementation of more sophisticated aforementioned techniques.

4.3 Method

Figure 4.3 (a) shows the electrical model of a DEA, where C_P and R_P, are its variable capacitor and resistor, respectively, which are in series with two electrode resistors, R_E. R_P models the non-ideal leakage current through the dielectric. The variability in the C_P, R_P, and R_E is due to the length modulation of the CT-SDEA. In the low frequency range (e.g., 10-100 Hz), R_E can be neglected[70,83] (Figure 4.3 b).

Figure 4.3 Electrical model of a DEA. C_p and R_p are the polymer's capacitance and resistance, respectively, and R_E is the electrodes' resistance (a). In the lower frequency range one can ignore R_E[70] (b).Note that, the muscle spindle in the skeletal muscle, unlike the 1x3 artificial muscle, is connected in parallel to the muscle fibers.

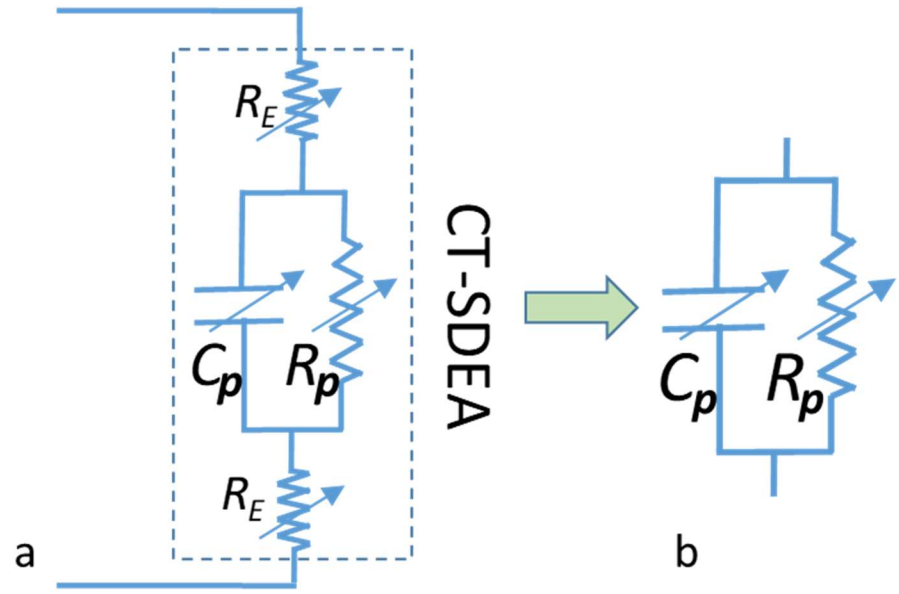

Figure 4.3 (a) The electrical model of a DEA. C_p and R_p are the polymners capacitanc and resistance, respectively, and R_E is the electrods' resistance. In the lower frequency range R_E can be ignored[70] (b).

4.3.1 Theoretical Analysis

Based on the electrical circuitry in Figure 4.3 (b), by using Laplace transformation the impedance of the CT-SDEA can be calculated through Equation 4.5.

$$X_c = \frac{R_p}{1+R_p C_p s} \tag{4.5}$$

By adding Equation 4.5 to Equation 4.1 the V_{output} to V_{input} (Figure 4.1) transfer function can be derived (Equation 4.6), which is a first order lag system, the low pass filter (Figure 4.2).

$$H(s) = \frac{R_p}{R_s R_p C_p s + R_p + R_s} \tag{4.6}$$

For a stacked DEA, C_p and R_p can be calculated using the slightly modified formulas introduced by Hoffstadt et al.[86], Equations 4.7 and 4.8, respectively. Where n is the number of stacked layers in the CT-SDEA; A_e is the active area of each layer (the

area covered by electrode); d_0 is the resting length of the actuator, CT-SDEA, excluding the thickness of its end plates; $\mathcal{E}_r$ and $\mathcal{E}_0$ are polymer's (silicone rubber for CT-SDEA) relative permittivity and void permittivity, respectively, V is activation voltage, and d is the length of the activated actuator. Table 4.1 shows the reported or measured values of these parameters.

$$C_p(d) = n^2\varepsilon_0\varepsilon_r \frac{A_e}{d0}(\frac{d_0}{d})^2 \text{ or } C_p(d) = C_{p0}(\frac{d_0}{d})^2 \tag{4.7}$$

$$R_p(d) = \frac{1}{n^2}\rho_0 \frac{d0}{A_e}(\frac{d}{d_0})^2 \text{ or } R_p(d) = R_{p0}(\frac{d}{d_0})^2 \tag{4.8}$$

Using Equations 4.7 and 4.6 the polymer's time constant, τ_p, can be calculated. Equation 4.9 shows that the actuator's time constant only depends on polymer's physical characteristics [83,86].

$$\tau_p = C_p R_p = \varepsilon_0\varepsilon_r\rho_0 \tag{4.9}$$

In Equation 4.9, ρ_0 is the resistivity of the dielectric material, i.e., silicone rubber in CT-SDEA.

Table 4.1 R_P and C_P Parameters' definition and their measured or reported values.

Parameter	Detention	Value
d_0	Resting length of the CT-SDEA	36.89 mm
A_e	Active are of the CT-SDEA	134.56×10^{-6} m
N	Number of layers	1600
C_{p0}	CT-SDEA's capacitance at resting length	237×10^{-9} F
$\mathcal{E}_r$	Silicone rubber relative permittivity	2.8
$\mathcal{E}_0$	Void permittivity	$8.854187187\times10^{-12}$
R_{p0}	CT-SDEA's resistance at resting length	191×10^{5} Ω
ρ_0	Dielectric resistivity	1.8264×10^{11} Ω.m

R_{p0} and ρ_0 were calculated experimentally. During an isometric contraction, the length of the CT-SDEAs was held constant at its rest length, 39 mm, under no compression or

extension, throughout the trials. After application of a square activation waveform, with amplitude of 1230 V and period of 5 s, the CT-SDEAs showed 38 ms time constant, during discharge period. Using Equation 4.8 and considering a 1 MΩ discharge resistance connected in parallel with the CT-SDEA, R_{p0} and ρ_0 were calculated at 191×10^5 Ω and 1.8264×10^{11} Ω.m, respectively.

The gain of a first order lag system, in time domain, K (Equation 4.10), for a sinusoidal input with frequency of f, is presented in Equation 4.11. This gain was calculated for different R_s and input frequencies, as the length of the CT-SDEA changed. The time constant, τ and A in H(s) (Equation 4.6) is shown in Equation 4.12 and 4.13, respectively.

$$\frac{A}{\tau s+1} \tag{4.10}$$

$$K = \frac{A}{\sqrt{(1+(2\pi f\tau)^2)}} \tag{4.11}$$

$$\tau = \frac{R_s\varepsilon_r\varepsilon_0\rho_0 d_0^2}{R_s d_0^2+R_0 d^2} \tag{4.12}$$

$$A = \frac{R_{P0}d^2}{R_s d_0^2+R_{p0}d^2} \tag{4.13}$$

4.3.2 Proof of Concept

To test the feasibility of this length self-sensing technique a CT-SDEA was screwed to a rigid frame from one end and to a load-cell, connected to a precision translational stage (Newport Corporation, Irvine, CA, USA) with 10 µm graduation, from the other end in a vertical position. The CT-SDEA then was passively compressed and extended to 5% of its resting length, 39 mm, using the precision stage. For each condition, i.e., compression and extension, a sensing signal, 10 Hz sinusoidal waveform

with 50 V amplitude, was generated by a high voltage (HV) amplifier (UltraVolt 5HVA24-BP1-F, Advanced Energy, Ronkonkoma, NY, USA) and applied to the actuator. A 10 MΩ resistor was connected in series with the CT-SDEAs and V_{output} (Figure 4.1) was recorded via a CompactDAQ data acquisition system (CDAQ) (CDAQ-9174, National Instrument, Austin, TX, USA) containing an analog input module (NI 9215), an analog output module (NI 9263), a digital input and output module (NI 9375). This CDAQ was also used to control and monitor the high voltage amplifier.

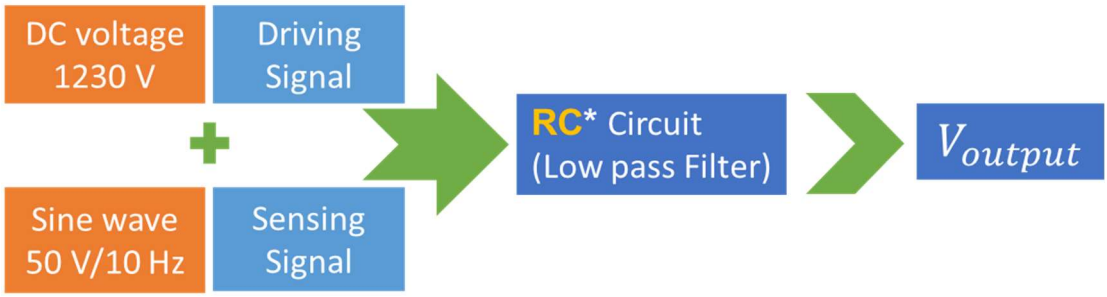

Figure 4.4 The block diagram of the testing setup.

4.3.3 Real-Time Length Self-Sensing

A command waveform was generated in LabVIEW (National Instrument, Austin, TX, USA) by superimposing a sinusoidal sensing signal, with 50 Hz and amplitude of 0.3125 V, on a linear waveform, i.e., a right triangle waveform with amplitude of 6.25 V and period of 1 s (Figure 4.5). This sensing signal, then, was amplified, 160 times, by a HV amplifier (HA51U-1.6P10-3, hivolt.de, Hamburg, Germany); resulting a sinusoidal sensing waveform with amplitude of 50 V superimposed on a driving, low frequency, linear waveform, 0 to 1000 V. The HV amplifier was capable of generating up to 1600 V output voltage, 20 mA dynamic current (<1 ms), 10 mA static current, with 70 kHz frequency. By connecting 220 Ω

resistor to a CT-SDEA in series, the amplitude of the sensing signal, V_{output}, was monitored. Then this value was mapped to the displacements measured by a laser sensor.

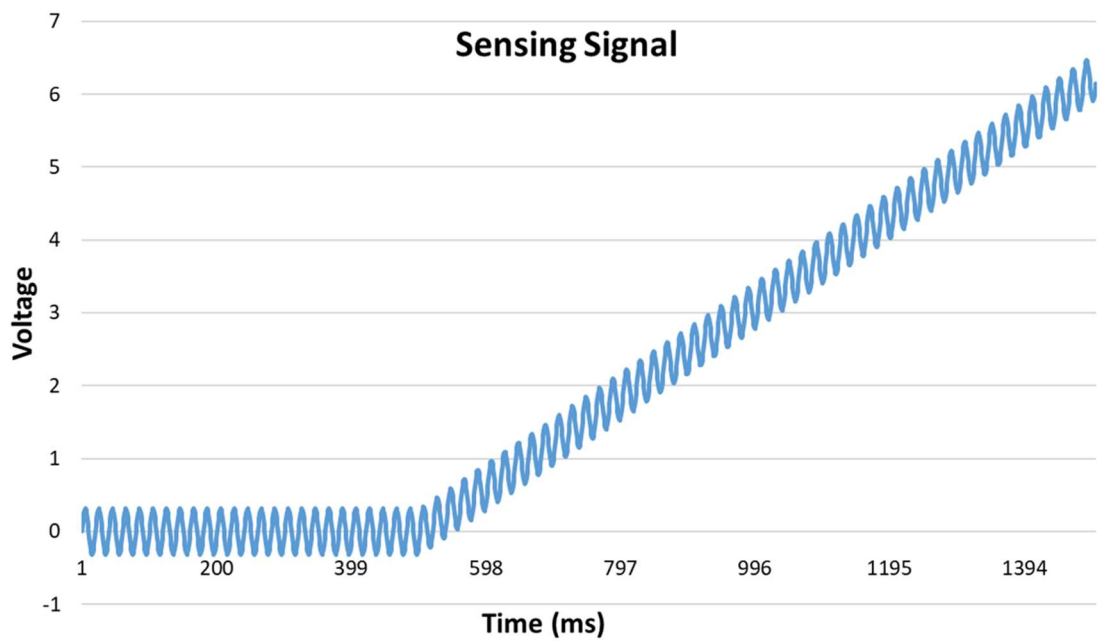

Figure 4.5 Pre-amplified sensing + actuating signal. 50 Hz sinusoid signal was supperimposed on top of a linear waveform.

The NI CDAQ, used in the proof of concept testing, controlled the amplifier and recorded, V_{output}, with 1 kHz sampling frequency. A laser sensor displacement (ILD 1420-25, Micro-Epsilon, Ortenburg, Germany) recorded the longitudinal contraction of the CT-SDEA with 250 Hz sampling frequency, simultaneously, to evaluate the length self-sensing property of the actuator. Both laser displacement and self-sensing data were streamed into a LabVIEW program for online signal processing. The laser displacement was connected to a personal computer via a USB port. V_{output} was plotted against the laser displacement sensor data to verify the accuracy of this technique. Then to be able

to infer the displacement from the reading the V_{output}, 1st and 2nd order polynomial curves were fitted to this graph.

To develop a proprioceptive artificial skeletal muscle this mechanism was added to a configured 1×3 artificial muscle consisting of CT-SDEAs in series. The period of the linear waveform used for activating this muscle was 8 s. The self-sensation was added to the middle CT-SDEAs. Similar to the single CT-SDEA's self-sensation, this CT-SDEA was connected in series to a resistor; and the voltage of this resistor were monitored. This voltage then was mapped to the configured artificial skeletal muscle's displacement, measured by the laser displacement sensor. A 1st order polynomial, then, was added to this data set. This CT-SDEA with length self-sensing capability, within the proprioceptive artificial muscle, resembles the role of muscle spindle of the mammalian skeletal muscle. Note that, the muscle spindle in the skeletal muscle, unlike the 1x3 artificial muscle, is connected in parallel to the muscle fibers.

4.4 Results

4.4.1 Theoretical Analysis

The changes in the time domain gain of the circuit in Figure 4.1, in respect to length modulation of the CT-SDEA, is depicted in Figure 4.6 for different input frequencies, f, when R_s was 220 Ω (a), and for different R_s values, when frequency was 50 Hz (b). The low pass behavior of the $H(s)$, Equation 4.6, is observable in this Figure. The gain of the circuit for f and R_s used in our experiment, 50 Hz and 220 Ω, respectively, is depicted in Figure 4.7 (a). As longitudinal contraction increases, the gain decreases, which is also observable in the recorded V_{output}. As the CT-SDEA contracted, the amplitude of the V_{output} decreased (Figure 4.7 (b)).

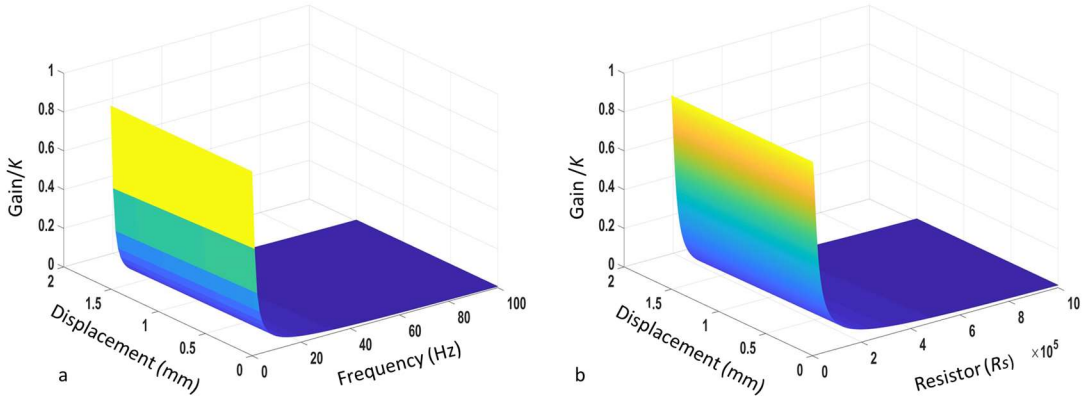

Figure 4.6 The gain, as theratio of peak-to-peak amplitude, of the self-sensing circuit for different input frequencies at constant R_s= 220 Ω and for different R_s values at 50 Hz input frequency.

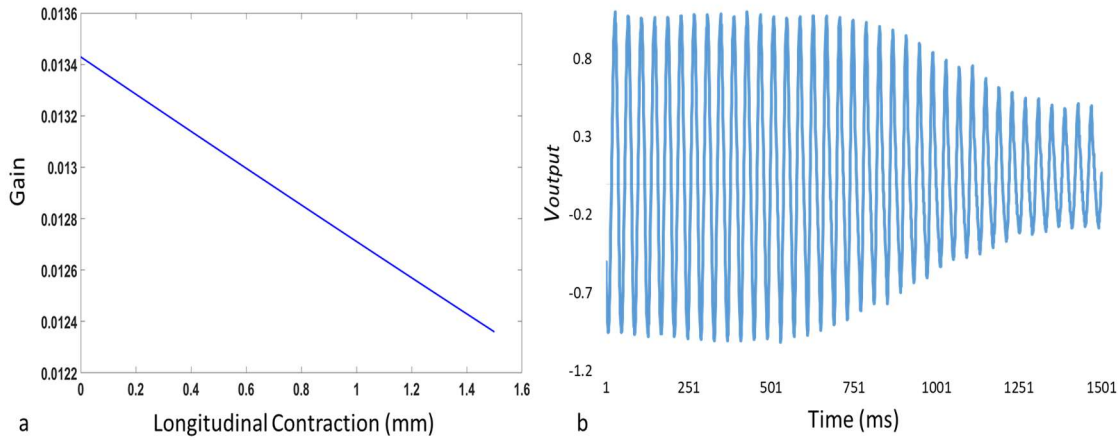

Figure 4.7 The gain of the self-seinsing cicuitry for Rs= 220 Ω and 50 Hz input frequency, f (a). As the CT-SDEA contracted the V_{output} intensity decreased (b).

4.4.2 Proof of Concept

The changes in the amplitude of the 10 Hz sinusoid signal at resting length (0%), 5% compression, and 5% extension, can be seen in Figure 4.8. As the CT-SDEA compressed the amplitude of the sensing signal decreased (Figure 4.8, blue trace) and as the actuator extended the signal's amplitude increased (Figure 4.8, red trace).

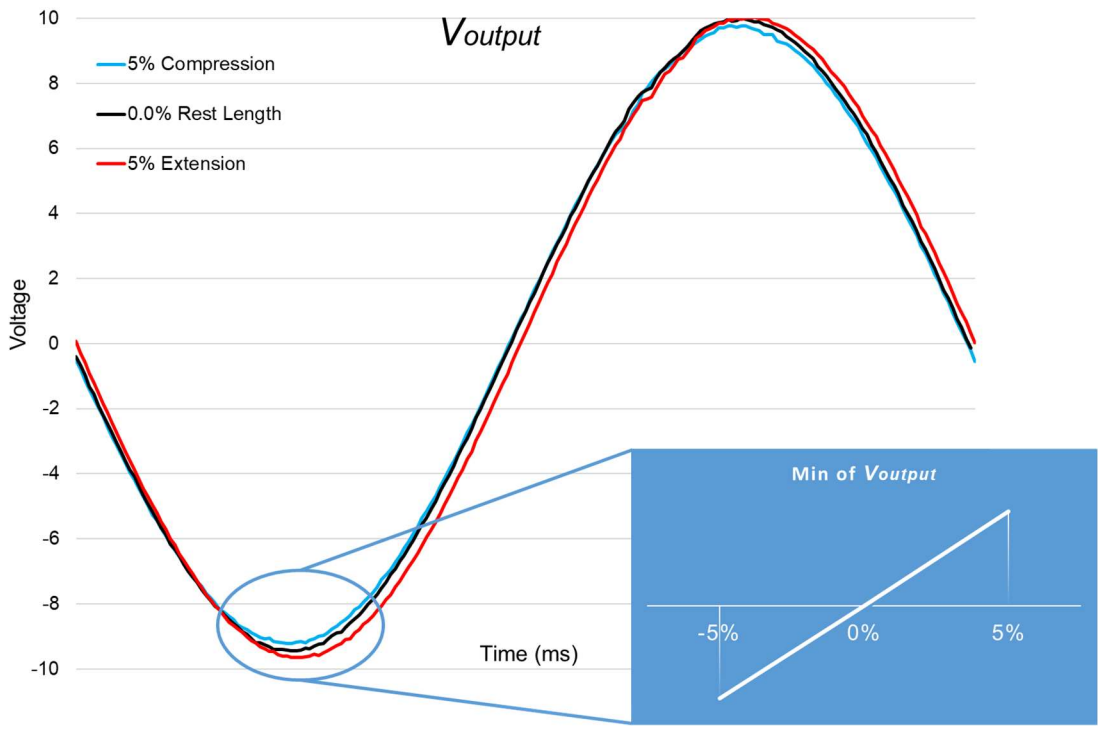

Figure 4.8 The recorded V_{output} at resting length, 0% (black trace), 5% extension (red trace) and 5% compression (blue trace). The insert shows the minimum (min) of each of the three V_{output} graphs connected with a line.

4.4.3 Real-Time Length Self-Sensing

The real-time length self-sensing of the CT-SDEA is depicted against displacement sensor (Figure 4.9). The self-sensing can be inferred from the changes in the V_{output}'s peak-to-peak (P-P) value (Equation 4.1 to 4.3), which is negated to follow the trend of the laser displacement sensor's output. Equation 4.14 is the fitted 2nd order curve, with 6 % fitting error, (Figure 4.9, red trace). Figure 4.10 shows changes in the V_{output}'s P-P value against displacement (blue trace), and 1st order fitted curve (red trace), with 15% linearity error. Equation 4.15 is the 1st order fitted curve.

The changes in V_{output} P-P value, while the 1x3 artificial muscle was contracting is depicted in Figure 4.11 (a). The data is negated to follow the laser displacement's output. In Figure 4.11 (b) the muscle's displacement, measured by the laser

displacement sensor, shows slight unsteadiness in the contraction of the muscle. These two graphs are plotted against each other in Figure 4.12 and a 1st order polynomial was fitted to the resultant graph. The linearity error is 25% due to the unsteadiness.

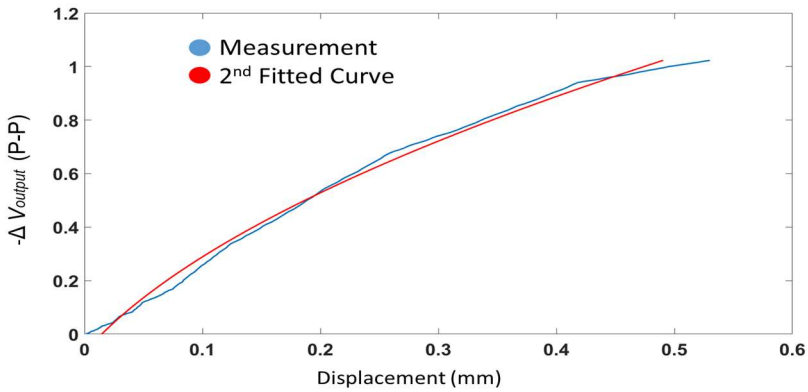

Figure 4.9 The peak-to-peak amplitude of the V_{out} was plotted against the measured displacement of a CT-SDEA (blue trace). A 2nd order polynomial was then fitted to this waveform (red trace). With 6% fitting error.

$$0.2307x^2 + 0.229x + 0.0147 \tag{4.14}$$

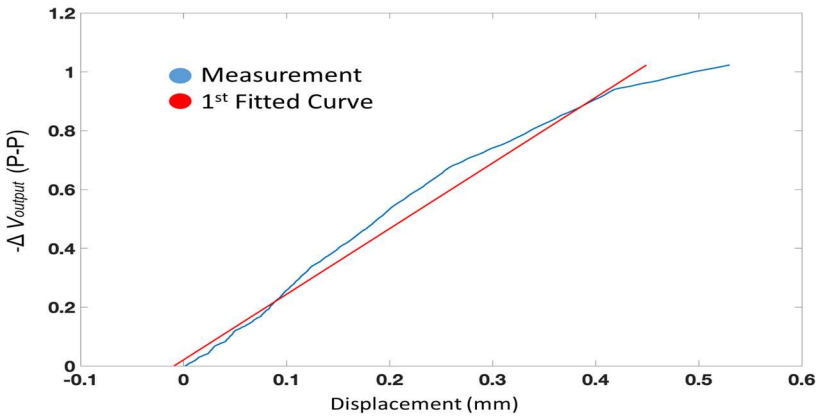

Figure 4.10 The peak-to-peak amplitude of the V_{output} was plotted against the measured displacement of a CT-SDEA (blue trace). A 1st order polynomial was then fitted to this waveform (red trace). The linearity error was 15%.

$$0.4482x - 0.0093 \tag{4.15}$$

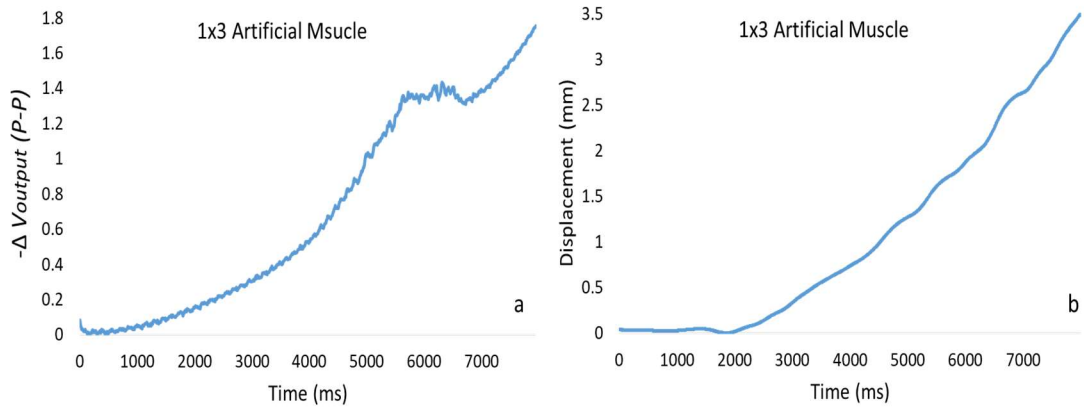

Figure 4.11 The changes in the peak to peak (P-P) value of V_{output} (a). This value was negated to follow laser diplacment measurements. The artificial muscle was contracting under a linear stimulation waveform with 8 s period. The recordered diplacment, using the laser sensor, during this contraction is depicted in (b).

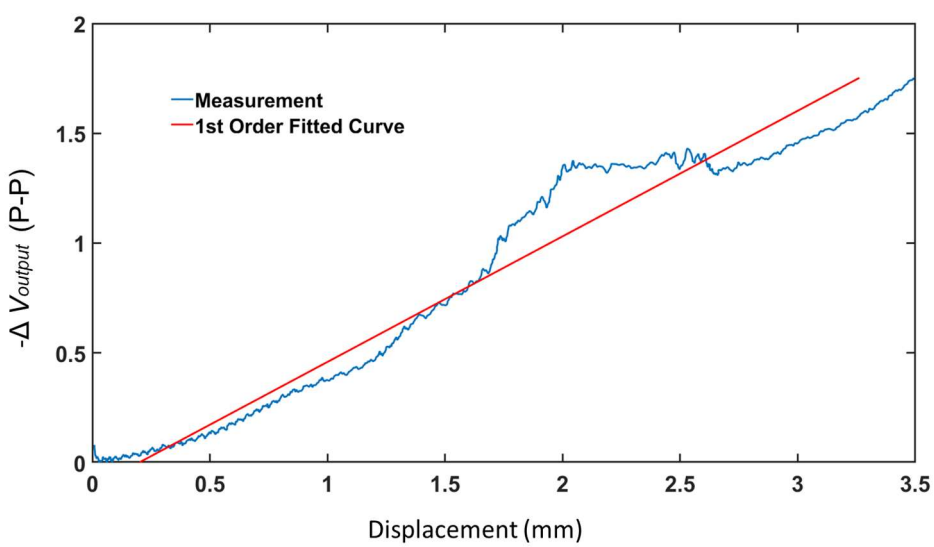

Figure 4.12 The negated changes in V_{output} 's P-P value was plotted against the measured displacement of the1×3 artificial msucle, by the laser sensor (blue trace). A 1st order polynomial was then fitted to this waveform (red trace).

4.5 Discussion

The capability of adding length self-sensing to the CT-SDEA was investigated in this study. To monitor the changes in the capacitance of CT-SDEA and the artificial muscle, A CT-SDEA was connected in series with a resistor and the actuators voltage were measured. The results linear relationship between the resistor's voltage and the displacement of the CT-SDEA for the large portion of the range, however, the 2nd order fitted polynomial showed lower fitting error in comparison with 1st order polynomial, 6% vs 15%, respectively, which was not in accordance with the theoretical analyses. . Using one CT-SDEA's self-sensation to infer the longitudinal contraction of the artificial muscle was similar to the role of the muscle spindle in the mammalian skeletal muscle. The muscle spindle however is in parallel with the muscle fibers in mammalian skeletal muscle, unlike the 1x3 artificial muscle we tested in this study. Unlike single CT-SDEA, the relationship between the muscle's longitudinal contraction and V_{output} was not as smooth as a single CT-SDEA, potentially due to slightly unsteady contraction that happened as the result of mechanical compliance of the muscle.

As can be seen in Figure 4.7 (a) the relationship between V_{output}'s peak and the displacement of the CT-SDEA was expected to be linear, however, the fitted 2nd order curve in Figure 4.9 showed a lower error in comparison to the 1st order curve (Figure 4.10). This could be the result of modeling the circuit with limited precision, especially ignoring variable electrode resistance, R_E, in Figure 4.3. A more precise transfer function proposed by Hoffstadt et al.[86], which includes $R_{E,}$ can be used for future investigations. More precise parameter identification using modeling techniques such as extended Kalman filter[87] least square[91] or recursive extended least square[86], may also improve the V_{output} vs. displacement relationship.

Using Maxwell pressure formula, Equation 4.14, the measured length modulation using the aforementioned length self-sensing technique can also be used to infer the force generated by the artificial muscle[93], where V is the applied voltage between electrodes, and d is each layer's thickness. The calculated Maxwell pressure can be converted to force by assuming the electrode area stays constant throughout contraction. Using this information, however, the external force applied to the actuator cannot be inferred.

$$P = \varepsilon_r \varepsilon_0 (\frac{V}{d})^2 \tag{4.14}$$

The result of adding proprioception to the artificial muscle showed smooth behavior at the beginning and end of the curve, however, as the low frequency fluctuations intensified during the artificial muscle contraction the voltage of the resistor behaved differently. This may be the result of non-uniform contraction of the artificial muscle due to its mechanical compliance. By confining such artificial muscles in a low friction and flexible shell, resembling muscle fascia, the motion of the artificial muscle can be restricted to a certain direction. This is also important when large displacement is a critical. Due to small strain of the CT-DEAs, 3.3%, any undesirable motion reduces the total displacement in the target direction.

Although popular, a limitation of this frequency domain self-sensing technique, i.e., superimposing a high frequency signal on the activation waveform, is its potential for wearable applications. Although producing high driving voltage, usually more than 1000 volt, for portable application has already been proposed using compact and portable electrical components such as EMCO DC to HV DC converters (XP Power, Sunnyvale, CA, USA), the superimposition of a high frequency signal on this voltage in lightweight and compact portable circuit is a nontrivial task. Therefore, to resolve

this, other techniques has been proposed[87,89]. The most promising one is measuring the time constant of the DEA during the discharge period, whilst using pulse width modulation (PMW) for driving the actutor[93]. The PWM can be generated using photo-diode, such as OC100HG (VOLTAGE MULTIPLIER, INC., Visalia, CA), or HV transistors, such as STN0214 (STMicroelectronics, Geneva, Switzerland).

4.6 Conclusion

To add proprioception to our artificial muscle a frequency domain length self-sensing technique was implemented on the commercially available stacked DEA, CT-SDEA. A resistor was connected in series with the CT-SDEA; the actuator's voltage was then monitored to measure its length modulation, which resulted in the capacitance variation, and thereby, change ion actuator's voltage.

The result of our study showed a 2nd order polynomial as the better fit to the relationship between the actuator length and the low pass filter output. Although linear in majority of the contraction, this 2nd order relationship was in contrary to the linear relationship calculated theoretically. More sophisticated system identification technique such as recursive extended least squares is needed to model the CT-SDEAs more accurately for robust closed-loop control of the CT-SDEA's length modulation.

To replicate the role of muscle spindle in the mammalian skeletal muscle, this proprioception was then added to the middle CT-SDEA in a 1×3 artificial muscle configuration, and then its length modulation was mapped to the length modulation of the whole muscle. Although the result showed close relationship between the measured muscle displacement and the middle CT-SDEA's proprioception, this relationship was not as smooth as that of a single CT-SDEA, mainly due to minor sway during the contraction of this soft CT-SDEA-based artificial muscle.

Chapter 5

A MECHANIZED ELBOW JOINT POWERED BY A DE-BASED ARTIFICIAL SKELETAL MUSCLE.

5.1 Abstract

To increase the acceptability of exoskeletons, there is a growing attention toward finding an alternative soft actuator that can safely perform at close vicinity of human body. In this study, we investigated the capability of the dielectric elastomer actuators, a highly anticipated soft actuator, in muscle-like actuation of rehabilitation robots. The elbow joint of an upper extremity phantom model was actuated by an artificial skeletal muscle consisting of commercially available stacked DEAs, in series and parallel. Three different muscle configurations, 1×4 (an artificial myofibril consist of four CT-SDAE in series), 3×4, and 3×5 were tested under various tensile loads, 1 N to 4.5 N, placed at the center of mass of the forearm+hand of the phantom model. The active range of motion, angular velocity, and angular acceleration of the phantom model's tip of the hand were measured using motion capture system.

The 3×5 artificial muscle produced 22º of elbow flexion with 224 º/s angular velocity in the sagittal plane, under a 1 N tensile load. With gradual increase in the driving voltage, using a linear activation waveform, this muscle could smoothly contract throughout its active range of motion. This precise contraction response to gradual changes in driving voltage, in combination with the high-speed contraction, is highly desirable for rehabilitation robots. The active range of motion, however, was

substantially reduced as the tensile loads increased, which limits the capability of these muscles in upper extremity exoskeletons

5.2 Introduction

Modern concepts of rehabilitation support the use of intensive, repetitive, and task-oriented approaches aimed at restoring upper extremity disability[94]. Intense repetitions of coordinated motor activities, however, constitute a significant burden for the therapists, assisting patients. Therefore, mass practice is difficult to achieve during a typical therapy session. To counteract this, prevailing research studies present a wide variety of rehabilitation devices[24]. Assistive robots with the ability to perform repetitive tasks with patients are among these technically advanced devices. The more automated an assistive robot, the less supervision is needed. While increasing the independence of the user in performance of activities of daily living (ADLs), an assistive robot will potentially increase the dosage of interaction that consequently may result in more cognitive, social and motor development. In addition, it is expected that the potential kinematic and kinetic measurement derived from close-loop systems in such robots will contribute to the understanding of how different treatment variables (dosage, amount, type of assistance provided) influence motor learning and recovery in children. Another advantage is the ability to provide more motivating training context, by means of a computer gaming environment with quantitative feedback to motivate practice[95]. Thus, these robots are getting more and more attention in rehabilitation engineering.

Exoskeleton such as ARMin[27,96–101], MIME[102], T-WREX[30,31,103], and MIT-Manus[104,105] already showed promising motor rehabilitation results, which resulted in commercial product such as Armeo Power, and Armeo Spring (Hacoma AG, Switzerland), the commercial replica of ARMin and T-WREX, respectively (Figure 5.1,

(a) and (b)). These commercially available devices are not practical for at home use and their size and cost limits their practicality for widespread utilization[16]. Furthermore, due to their complexity, a supervisor is required to operate these exoskeletons, which limits the intensity and duration of the training. Considering the healthcare delivery shifting away from clinical facilities and into the community, there is a growing need and attention for technologies for at home interventions and devices to assist ADLs[106]. Such exoskeletons are called assistive exoskeletons.

T-WREX[30,31,103] originally designed for such purposes and its pediatric version P-WREX, although smaller and simpler to use in comparison with their powered counterparts, cannot generate motion, thus, are limited in their capabilities[13]. MyoPro (Myomo, Cambridge, MA, USA), an electromyography-triggered active elbow brace [107], on the other hand, is one of the only commercially available powered exoskeletons; which showed efficacy for at home rehabilitation in controlled pilot studies[16,106] (Figure 5.1, c).

Figure 5.1 Example of comercially availbale exoskeltons (a) Aremo Spring.(b) Armeo Power.(c) Myomo. The Armoe devices, although versatile, are bulky, expensive and complex.

Most assistive exoskeletons that have been developed, as a group of highly promising rehabilitation robots, also suffer from lack of natural feel, that is their heavy, bulky, noisy, and rigid structure[16,106]. This usually leads to dissatisfaction, unacceptance, and finally abandonment of the device, especially in pediatric population. Therefore, innovations in the development of the next-generation rehabilitation robots can lead to significant benefits[108]. The conventional actuators used in most of these exoskeletons are designed for industrial applications, not interacting with human body, and therefore, result in these structural drawbacks. An effective orthosis must, in general, be silent, light weight, compliant, and portable[109,110]. Also because of their structural rigidity, the existing exoskeletons present challenges for safe interactions with humans. In contrast, an approach using softer materials has the potential to exhibit greater adaptation, sensitivity and agility. Softness and body compliance are salient features often exploited by biological systems, which tend to seek simplicity and show reduced complexity in their interactions with their environment[111]. Additionally unlike most conventional exoskeletons, by using soft sensors, actuators, and structures the user's natural degrees of freedom would be less constrained[112].

To advance the design of wearable assistive rehabilitation robots, the use of smaller and lighter skeletal muscle-like actuators are highly desirable to enable reductions in cost, labor, and to increase the dosage of training and motivation while maintaining precision of movement. The ideal candidate actuators for exoskeletons should closely mimic the prominent properties of skeletal muscle in, Young's modulus, linear actuation, acoustically noiseless operation, stress and strain, strain-rate, efficiency, cycle life, and actuation frequency. To this end, a variety of novel actuators, with different activation and actuation mechanisms and mechanical characteristics have

been proposed[44–46,53,59,62,63,113]. Among all, due to the capacity of polymer engineering in customization of various mechanical property based on the target application, there is a growing attention toward electro-active polymer actuators (EPA)[40].

With dielectric elastomer actuators, one of the most studied group of EPAs[58], it is possible to design mechanical systems with a soft feel and an external envelope (size and shape) approximating that of a natural limb[114]. The requirement for a "natural" look and feel is important to the goal of making the artificial or assisted limb feel integrated with the body. DEAs have been known for their unique properties, including large electrically-induced area strains (120-380%), large electrically-induced stresses (up to about 3 MPa) and low response times (1ms or even lower with low-losses elastomers)[113,115–118], which exceed the characteristics of natural muscle. Fundamentally, both DEAs and natural muscles consist of soft viscoelastic matter that can generate forces in response to electrical stimuli[56]. The force and strain of DEAs can be electrically modulated to control their stiffness[119]. Inherently compliant (soft) DEAs can mimic the agonist/antagonist muscle pairs found in nature, so that concentric contraction of one artificial skeletal muscle is taken up by eccentric contraction in the other[120]. This property is applicable in modulating joint stiffness over ranges wider than those possible with a single actuator[114]. Finally, human motor control uses sensory feedback from muscle spindles and Golgi tendon organs within the muscles. By combining proprioception with actuation, natural muscle is multi-functional[88]. Likewise, in DEAs elastomer deformations are inextricably linked to changes in electrical parameters that include capacitance and resistance, so the state of strain can be inferred by sensing these changes, enabling closed-loop control without any additional sensor setup. In contrast, commonly used actuators in robotics need

independent sensing devices for closed loop control, which increase the size and complexity of the system with higher number of actuators. All of these unique properties make DEAs particularly suitable for developing light, soft and inconspicuous mechanical systems with noise free actuation. DEAs are an area of immediate interest for driving orthoses and prostheses.

DEAs are fabricated from conformable elastomers, and thereby, they can be shaped into many actuator configurations and over a wide range of dimensions. Folded[79], helical[78] and rolled[77] DEAs are some of the proposed configurations for linear actuation. From the perspective of artificial skeletal muscle designs, one of the most interesting DEA configuration is the stacked actuator. The hierarchic structure of human skeletal muscles is considered a useful analogous actuator model of numerous sarcomeres in series [42]. Similarly, stacked DAEs (SDEAs) are capable of effectively coupling the deformations of individual DE layers to provide linear actuation. As with sarcomeres, employing a large number of DEA layers amplifies linear displacement. The novel and highly reliable SDEA invented by Dr. Kovacs et al.[60], CEO of CTsystems, represents the most appropriate DEA design when noiseless and linear contractions of a soft actuator are required in close proximity to humans. CTsystems, the first and only mass production manufacturer of commercial DEAs having a stacked muscle-like configuration.

In this study, we actuated an elbow joint of an upper extremity phantom model using multiple CTsystems' SDEAs (CT-SDEAs) connected in series and parallel arrangements. Carpi et al. previously showed the possibility of using Dielectric elastomers in orthoses design[57,121,122]. This study was the first that assessed the capability of CT-SDEAs to act as an artificial biceps muscle. These novel and reliable

actuators, have only recently become available, thus opening the way for the development of novel rehabilitation robotic devices that take advantage of the touted characteristics DEAs have over conventional actuators used in robotic applications. Thereby, CT-SDEAs may revolutionized the field of rehabilitation robotics.

5.3 Method

5.3.1 Configuring Artificial Skeletal Muscle

As one of the very first group that used CT-SDEA, a bundle of these new generation actuators was configured to form an artificial skeletal muscle. These muscles were the first artificial skeletal muscle that will have artificial sarcomeres (each DE layer in the CT-SDEA), motor units (each CT-SDEA), myofibrils (the CT-SDEAs connected in series), muscle fibers (the bundle of parallel artificial myofibrils), and importantly, proprioception, i.e., the length self-sensing capability, in a single mechanical structure. This unique structural and functional similarity to human skeletal muscle gives this artificial skeletal muscle the flexibility to 1) configure different number of artificial muscle sarcomeres (i.e., the number of layers within the CT-SDEA) and artificial motor units (CT-SDEAs) and myofibrils (CT-SDEAs in series) to modulate force and displacement generation capability of the resultant muscle; 2) control the amount of force generation of the muscle using the number of activated motor units and myofibrils by modulating their driving voltage; 3) create complex actuation by activating specific motor units in the artificial muscle myofibrils, and thereby, creating multiple degrees of freedom using one artificial skeletal muscle; 4) controlling length modulation of the artificial skeletal muscle using proprioception as

the feedback; and 5) controlling the stiffness of the muscle when eccentric contractions are needed.

Three artificial skeletal muscle configurations were used in this study 1×4, i.e., one artificial myofibril consisting of four CT-SDEAs in series, 3×4, and 3×5, i.e., three artificial myofibrils in parallel each consisting of five CT-SDEAs in series.

Table 5.1 CT-SDEA specifications.

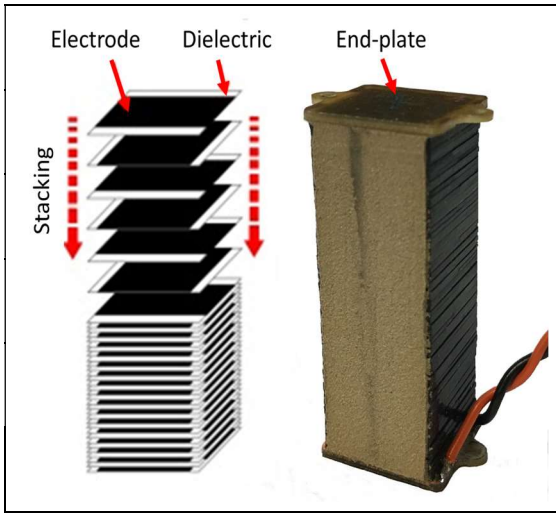	Max Force	10.1 N
	Max strain	3.3%
	Shortening	1.3 mm
	Dimension	39×17×17 mm
	Weight	11.3 g
	Max driving voltage	1200 kV

5.3.2 Testing Procedure

The steps to investigate the exoskeleton design include:

1. Implementing an upper extremity phantom model as the exoskeleton's testing platform.
2. Biomechanical analysis.
3. Mounting the artificial skeletal muscles and mechanical designs directly on the phantom model.
4. Mapping the length modulation of the artificial skeletal muscles to the degree of elbow flexion of the phantom model.

5. Designing an exoskeleton powered by the artificial skeletal muscle.

5.3.2.1 Implementing an Upper Extremity Phantom Model as the Exoskeleton Testing Platform

To simulate the motion, length, and weight of a 2-year-old upper extremity, a phantom model was developed. This model had a weight mount at the calculated center of mass (COM) of a 2-year-old boy's forearm. The COM location from forearm's center of rotation, 16.28 cm, was calculated based on the 2-year-old boy standard height, 94 cm[66], and Winter's anthropometric data[67]. Thereby, we could simulate the weight of a 2-year-old forearm+hand, and during different loading conditions.

5.3.2.2 Biomechanical Analysis.

Before testing the artificial skeletal muscle in flexing an elbow joint experimentally, the capability of the configured 3×5 artificial skeletal muscle in creating 15 cm, 36º, range of motion (ROM) at of the tip of the hand of a 2-year-old boy was assessed theoretically.

5.3.2.3 Mounting the Artificial Skeletal Muscle and the Mechanical Structure Directly on the Phantom Model

For empirical measurement of the maximum achievable active range of elbow flexion by the artificial skeletal muscles, they were mounted directly on the phantom model. This step helped us to avoid the complication of designing the exoskeleton before testing the artificial skeletal muscle's capabilities in creating elbow flexion. The 3D instrumented motion capture (MoCap) was used to measure ROM, angular velocity and acceleration, of the elbow flexion, in the sagittal plane under different loads. To test the capability of the artificial skeletal muscles in actuating the elbow joint, different levels of tensile load, 1 N (the weight of the phantom's model forearm) to 4 N (g=10

m/s^2), were attached on the COM of the forearm+hand, which was calculated at the previous step. The weight of the forarm+hand of a 2-year-old boy, calculated at 330 g (3.3 N, g=10 m/s^2) using standard weight for a 2-year-old boy, 15.4 kg[66], and Winter's anthropometric data[67]. The goal was to reach 36º of elbow flexion with 91º/s velocity and maximum acceleration of 116º/s^2. The chosen velocity and acceleration were used in the design of ARMin upper extremity exoskeleton[27]. To measure these parameter the muscles were under 1 N of tensile load, i.e., the load of the forearm of the phantom model, and a square activation waveform, with 1230 V amplitude, 5 s period, and 50% duty cycle activated the muscles.

5.3.2.4 Mapping the Length Modulation of the Artificial Skeletal Muscle to the Degree of Elbow Flexion of the Phantom Model

Using the MoCap data, the applied voltage to the muscle was mapped to the degree of elbow flexion. Thereby, we will be able to reach the desire degree of elbow flexion by controlling the artificial skeletal muscle's activation voltage. A linear activation waveform, i.e., a right triangle waveform with amplitude of 1230 V and period of 5 s, was applied to the 3×5 artificial muscle and the resultant elbow flexion was plotted against the applied voltage.

5.3.2.5 Designing an exoskeleton powered by the artificial skeletal muscle.

Using the results of the previous steps, an exoskeleton was designed in SOLIDWORKS (Dassault Systèmes, Vélizy-Villacoublay, France), which is powered by 4×5 artificial muscle.

5.3.3 MoCap

ROM, angular velocity, and angular acceleration was calculated using kinematic data collected by MoCap (Motion Analysis Corp, Santa Rosa, CA, USA) with 128 Hz sampling frequency. Reflective markers were attached to the tip of the hand, shoulder piece, forearm, and upper arm, and center of rotation on the elbow piece, of the phantom model. The data were analyzed offline in Visual 3D (C-motion Inc, Germantown, MD, USA).

5.3.4 Control and Monitoring System

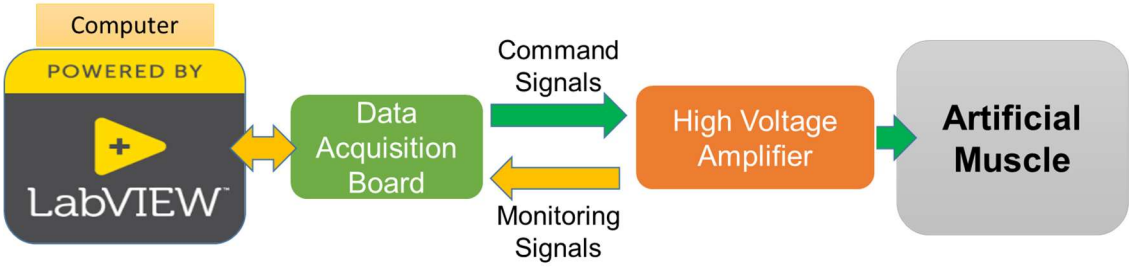

Figure 5.2 The block digram of the control and monitoring system for driving the artificial muscles.

The main components of the control and monitoring system were: 1) a high voltage (HV) amplifier (RC250-1.5P, Matsusada Precision Inc., Shiga, Japan) with 1500 V and 165 mA maximum output voltage and current, respectively, to provide the necessary driving voltage, 0-1230 V, for the CT-SDEAs; 2) a CompactDAQ data acquisition system (CDAQ) (CDAQ-9174, National Instrument, Austin, TX, USA), containing an analog output module (NI 9263) and analog input module (NI 9215), for generating the command signal to control the HV amplifier and monitoring its output voltage and current, respectively; 3) software developed in LabVIEW

(National Instrument, Austin, TX, USA), to control the CDAQ. Figure 5.2 illustrates the block diagram of this system.

5.4 Results

5.4.1 Upper Extremity Phantom Model

A phantom model was designed and 3D printed (Figure 5.3). The model had a weight mount, which is located about 16 cm from the center of rotation of the forearm.

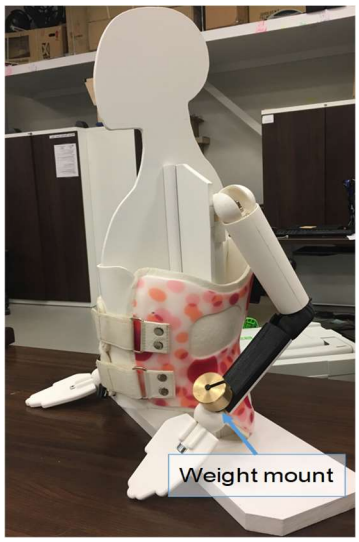

Figure 5.3 The designed and 3D printed upper extremity phantom model.

5.4.2 Biomechanics Analysis

The capability of the 3×5 artificial muscle with, 60 N force and 6.5 mm longitudinal contraction, in creating elbow flexion was theoretically calculated.

First, the insertion point of the artificial skeletal muscle for creating 15 cm ROM, CĆ (Figure 5.4), at the tip of the hand of a 2-year-old by, with 94 cm height and 15.4 kg of weight[66], was calculated. By using Winter's anthropometric data[67], the length of

the forearm+hand of a 2-year-old boy was measured 23.876 cm. Then, considering 6.5 mm of maximum contraction, BB́, and using the Thales theory (Equation 5.1), the insertion point of the muscle, B, was calculated at 1.034 cm from the center of rotation, A (Figure 5.4).

$$\frac{AB}{AC} = \frac{BB'}{CC'} \tag{5.1}$$

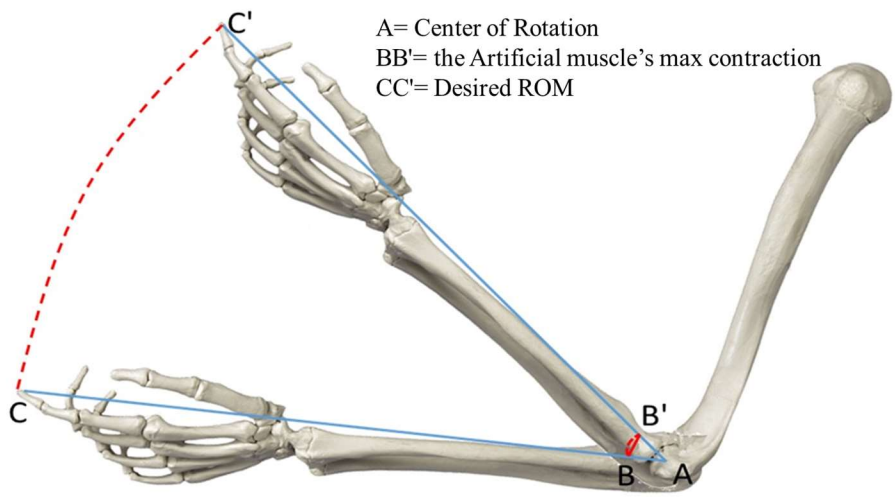

Figure 5.4 Artificial muscle's insertion point calculation. Using Thales theorem and 15 cm desire value at the tip of the hand the insertion point was calculated at about 1 cm from the center of rotation.

To assess if the torque generated by the artificial skeletal muscle at its insertion point is enough to create motion at the forearm, it was compared with gravity torque at the COM (Figure 5.5). COM was calculated at 16.2834 cm from the center of rotation, A, using Winter's anthropometric data[67]. Having the maximum force generation of the 3×5 artificial muscle (60 N) and its lever arm, AB=1.034 cm, it was theoretically shown that the maximum torque that the muscle is capable of generating at the insertion point, 62.04 Ncm, is higher than the gravity torque at the COM, 55.168 Ncm, for unloaded

condition (Figure 5.5). For loaded condition, however, a mechanical system should be designed to magnify the torque of the artificial skeletal muscle.

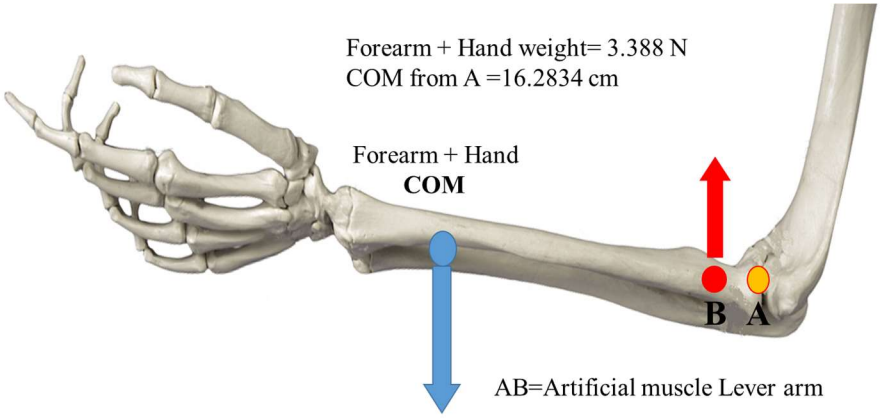

Figure 5.5 The torque generated by the artificial skeletal muscle at its insertion point (red) and the torque generated by the gravity at the COM (blue). The higher torque generated by the artificial skeletal muscle shows capability to create forearm motion.

5.4.3 Testing the Artificial Skeletal Muscle Powered Elbow Joint

To investigate the capability of the CT-SDEA-based artificial muscle in flexing the elbow, three muscle configurations were tested. The artificial skeletal muscles were connected to the forearm of the phantom model through a coated wire rope, with 1.6 diameter. To magnify the displacement of the 1×4 muscle, a cam-shaped pulley system was 3D printed and mounted on the elbow piece of the phantom model (Figure 5.6). To be able to adjust the tension of this cable and detach the muscle from the forearm easily, a connector was designed for this cable wire, using a Wago connector (WAGO Kontakttechnik GmbH & Co. KG, Minden, Germany). Figure 5.6 shows this connector and its 3D printed casing for the attachment to CT-SDEA's end-plate. Using the proposed design, the 1×4 was not capable of lifting the forearm+hand of the phantom

model, 145 g. The phantom model powered by the 1×4 and MoCap system is demonstrated in Figure 5.7. The CT-SDEA in the artificial skeletal muscle was connected to the power terminal in parallel and was driven by HV amplifier using the customized LabVIEW program. This muscle configuration was not capable of creating elbow flexion.

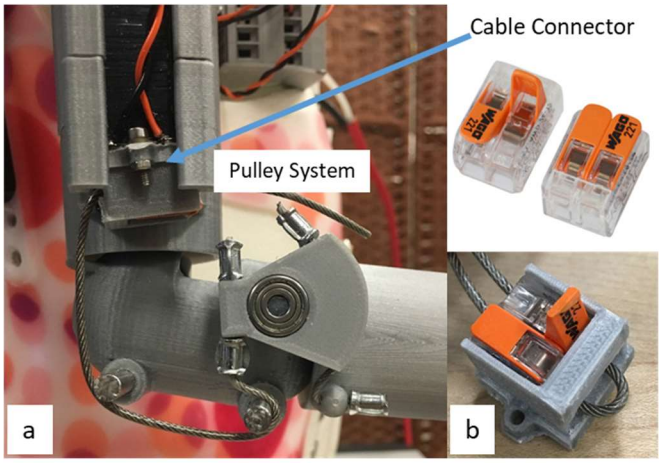

Figure 5.6 The cam-shaped pully system to magnify the displacement of the artifical msucles (a). The designed wire rope connector (b).

Figure 5.8 shows the elbow joint powered by the 3×4 artificial muscle. The muscle was directly attached to the elbow piece of the artificial skeletal muscle and no mechanical linkages were used in this design. An end-plate was 3D printed to connect three artificial myofibrils in parallel. This end-plate had casing for the Wago connector to connect the wire rope to the muscle. The CT-SDEAs in the artificial skeletal muscle were connected in parallel to the power terminal. The active ROM of the joint was 18º (Figure 5.9), and its angular velocity were measured at 138 º/s (Table 5.3).

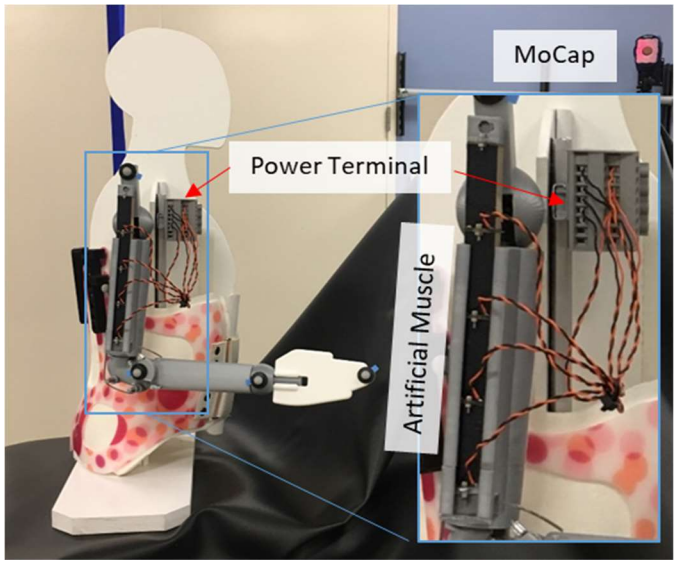

Figure 5.7 The elbow joint powred by a 1×4 artificial muscle. Muscles were connected in parallel to power terminal. Five reflective markers were attached to the arm and hand for MoCap kinemtic analysis

As calculated in the Biomechanical Analysis section, the capability of the 3×5 artificial muscle was tested in powering the elbow (Figure 5.10). The degrees of elbow flexion under different levels of tensile load are depicted in Figure 5.11. As the load at COM increased the degree of elbow flexion decrease. Table 5.2 shows 5° to 8° degree of supination of the elbow created while the artificial skeletal muscle was flexing the elbow. Under 100 g of load, the degree of elbow flexion was slightly more than the 3×4 muscle, 22° (Figure 5.11). Table 5.3 shows the angular velocity of the elbow flexion, 224 °/s.

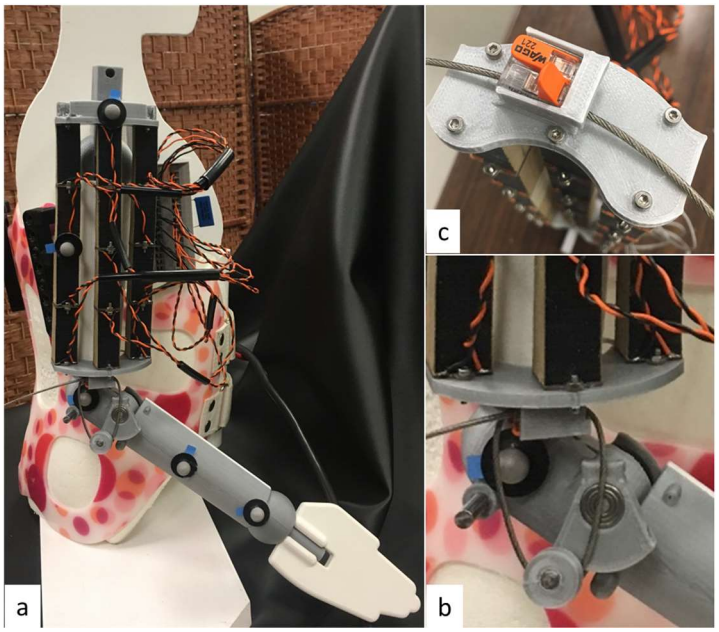

Figure 5.8 The elbow joint powered by the 3×4 artificial msucle (a). The puly system were not used in this design and the muscle was directly connected to the elbow piece of the phantom modle (b). (c) the 3D printed end-plate with Wago connector casing, to attach three artificial myofibrils in parallel.

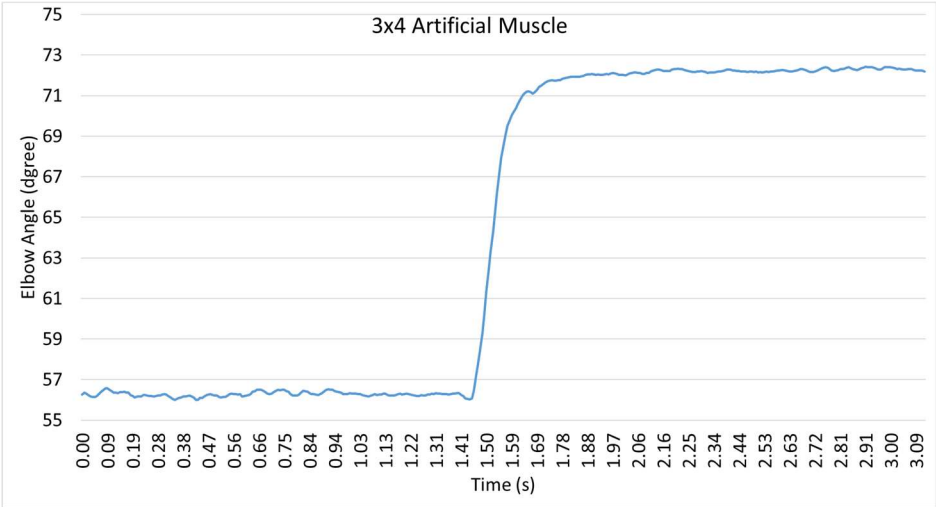

Figure 5.9 The elbow flexion angle of the phantom model's elbow joint, powered by the 3×4 artificial msucle. The sampling frequency was 128 Hz. 0° elbow flexion was the antomical neutral position of the elbow, full elbow extension.

Table 5.2 Forearm supination of the phantom model's elbow joint powered by 3×5 artificial muscle, under different tensile loads. g=10 m/s^2.

	1 N	1.5 N	2 N	2.5 N	3. N	3.5 N	4 N
Supination	5.5°	6.7°	7.2°	8.3°	8.0°	8.2°	5.0°

The parabolic relationship between elbow flexion and voltage is depicted in Figure 5.13 (a). This relationship is similar to the parabolic relationship of the CT-SDEA's longitudinal contraction and voltage (Figure 5.13 (b)).

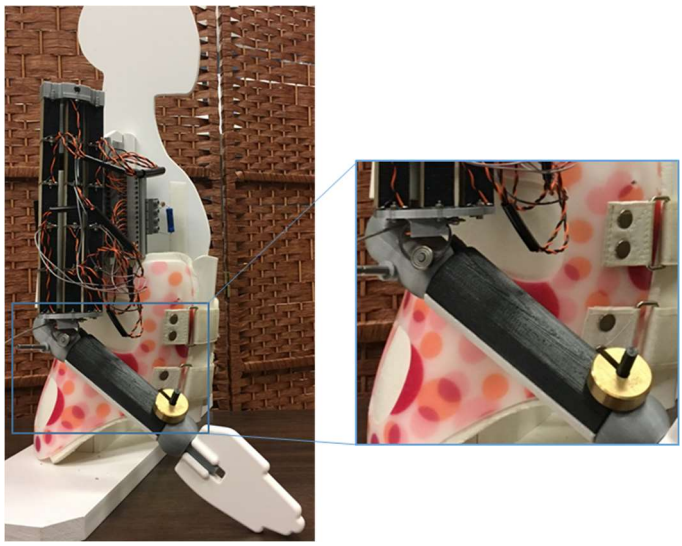

Figure 5.10 The 3×5 muscle directly attached to the forarm of the phantom model. Different loads were mounted on the COM of the forearm+hand, 16 cm from the center of rotation.

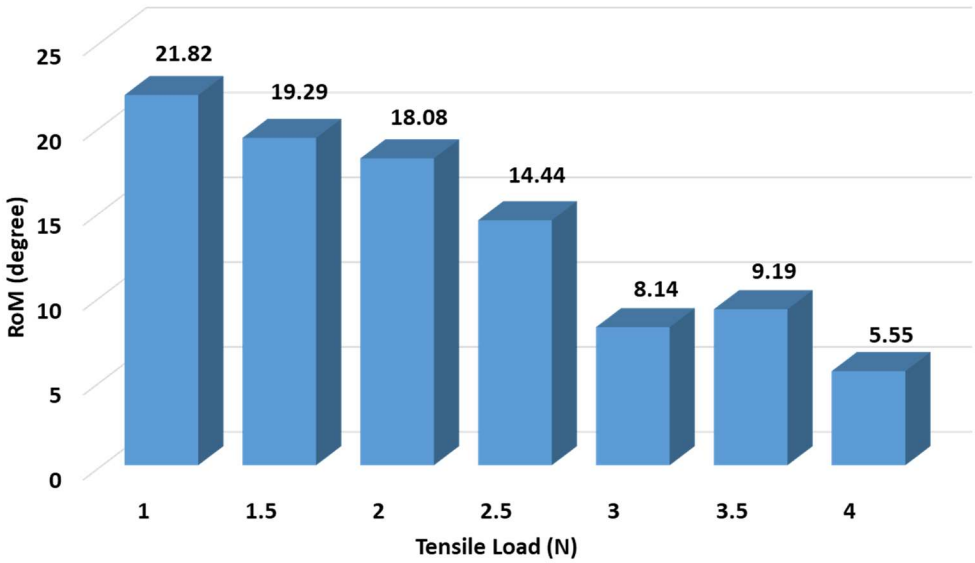

Figure 5.11 The active range of motion (ROM) of the phantom model's elbow joint, powered by 3×5 artificial muscle, under different levels of tensile load.

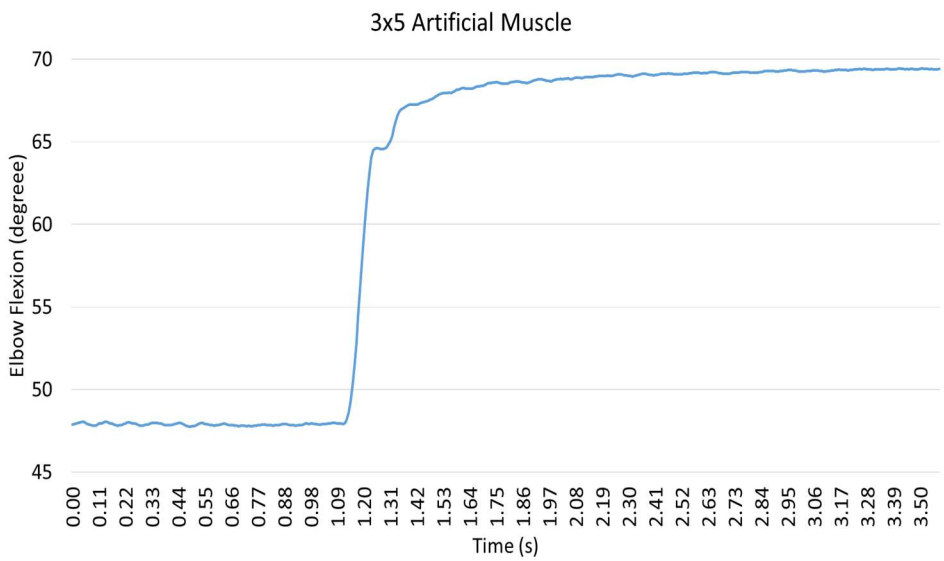

Figure 5.12 The elbow flexion angle of the phantom model's elbow joint, powered by the 3×5 artificial msucle. The sampling frequency was 128 Hz. 0° elbow flexion was the antomical neutral postion of the elbow, full elbow extension.

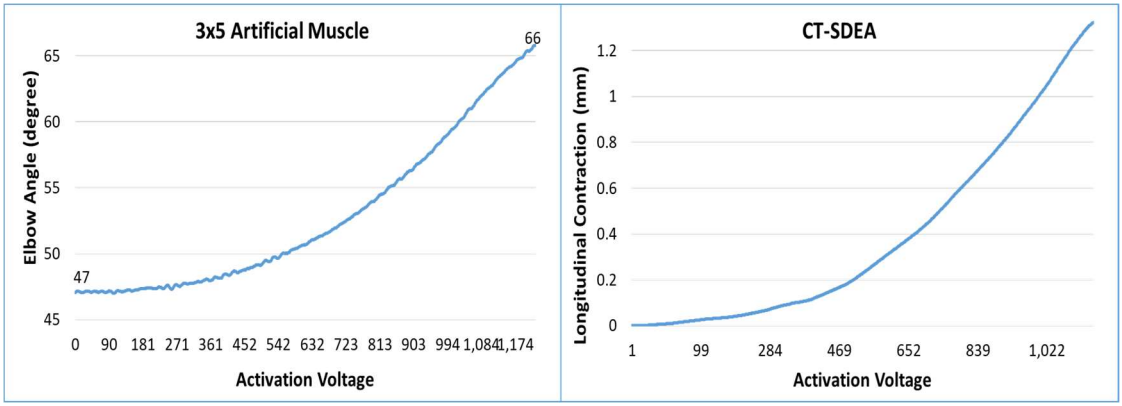

Figure 5.13 Using the linear activation waveform the degree of elbow flexion was mapped to the activation voltage (a). 0° elbow flexion was the antomical nutral postion of the elbow, full elbow extension. The parabolic relationship between voltage and elbow flexion is similar to the relation between a CT-SDEA's longitudenal contraction and its voltage (b).

Table 5.3 The measured ROM, angular velocity and angular acceleration for the exoskeletons powered by 1×4, 3×4 and 3×5 artificial muscles. The muscles were under 1 N of tensile load while contracting. The square activation waveform was applied to the muscles.

Exoskeletons design	ROM	Angular velocity	Angular acceleration
1×4 muscle with pulley	0º	0 º/s	0 º/s^2
3×4 muscle without pulley	18º	138 º/s	1280 º/s^2
3×5 muscle without pulley	22°	224 °/s	2824 º/s^2

5.4.4 Exoskeleton Design

Figure 5.14 demonstrate the proposed exoskeleton designs using the results of this study. The design is powered by 3×4 artificial muscle, which was chosen due to the limited length of a 2-year-old boy upper arm, 17.5 cm[67]. The design contains three brackets located around the end-plate of the CT-SDAEs to confine the undesirable motion of the artificial skeletal muscle and the bowing effect.

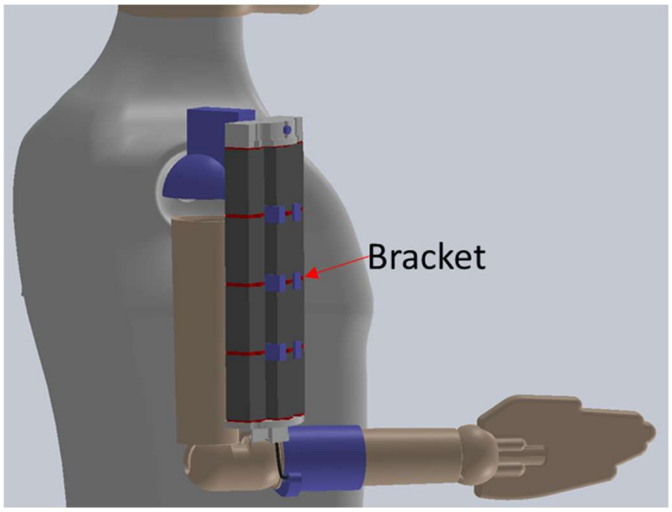

Figure 5.14 The CAD model of a potential exoskleton, powered by the 3×4 artificial msucle. Three brackets are located on the CT-SDEAs' endplates of the middle artificial myofibril.

5.5 Discussion

Three different muscle configurations were used to power an elbow joint of a phantom model. The 3×4 and 3×5 artificial muscles created 18° and 22° of elbow flexion, respectively, under 1 N tensile load, the weight of the phantom model's forearm. The high angular velocity of these contractions, 224° and 138°, for the 3x5 and 3x4 muscles respectively, is highly desirable in exoskeleton applications were fast and controlled contraction is needed. The reduction in elbow flexion contraction, at the presence of higher tensile loads, however, may be a substantial hurdle for such applications.

The discrepancy between the theoretical biomechanical analysis, showing the capability of artificial skeletal muscle in producing 36° of elbow flexion, and empirical results may be due to friction in the phantom model and the softness of the actuator and the cable pulley/cam mechanism. Due to the muscles' softness, undesirable deformity was observed during contraction, under tensile load. The generated supination (Table

5.2) shows the effect of these deformities and the undesirable motions. This may substantially affect the elbow joint's active ROM, considering the limited contraction of these artificial skeletal muscles, < 6.5 mm. One solution is to confine these artificial skeletal muscles in a low friction and flexible shell, similar to muscle fascia, and attach these muscles to a harder skeletal-like structure, to confine these soft actuators' motion to certain direction. In exoskeleton applications this can be done by highly flexible materials such as silicone films.

Adding a suitable mechanical transmission, may improve the artificial skeletal muscle powered elbow joint dynamics. A simple cam-shaped pulley system was tested with the 1×4 artificial muscle (Figure 5.6). This mechanical linkage was not capable of magnifying a displacement due to the mechanical loss of the cable driven system. A more sophisticated cable-driven transmission system may substantially improve the performance of the artificial skeletal muscles tested in this study. A magnification of displacement is specifically critical for exoskeleton applications. As an example, the reported value for displacement of the biceps muscle in adults is 4 cm[48], where active ROM of the elbow is about 160º, where the artificial skeletal muscle tested in this study had 0.66 cm displacement.

When activated by the linear activation waveform, the 3×5 artificial muscle showed smooth gradual increase in its degree of elbow flexion (Figure 5.10). The parabolic relationship between voltage and longitudinal contraction of the CT-SDEAs was also observable in the degree of elbow flexion of the elbow joint powered by the artificial skeletal muscle. Combination of this smooth high-resolution contraction, i.e., response to the slight increase of the driving voltage, and speed of contraction may simplify a proposed control mechanism.

As the tensile load increased, at the COM of the forearm+hand, from 1 N to 4 N ($g=10\ m/s^2$) the degree of elbow flexion was reduced substantially from 21.8° to 5.5°. This may improve by increasing the lever arm and trading off the ROM at the lighter loads. Due to the flexibility of the actuator, however, this may result in the bowing of the artificial skeletal muscle during contraction. Deploying push-pull cables in the design, instead of the wire rope, may also improve the ROM by reducing some of the existing slack in the cable.

Another limiting factor of the 3×5 artificial muscle is its length, 20 cm, which is longer than the upper arm of a 2-year-old, 17.5 cm. This population was proposed as a group that may benefit using an exoskeleton powered by CT-DEA-based artificial muscles. Due to mechanical compliance, however, these muscles could be bent over the shoulder to resolve this issue. Further experiments are needed to test this solution. Because the active ROM of the 3x4 artificial muscle, 18º , was close to that of generated by the 3×5 artificial muscle, 22º, it can be used, instead to resolve the length issue.

The proposed exoskeleton (Figure 5.14) is based on the phantom model morphology, however, a design is needed in the future that fits to a child real upper-extremity geometry. The complex dynamic of the elbow joint, e.g. instant center of rotation, however, will make this transition substantially challenging.

5.6 Conclusion

The capability of CT-DEA-based artificial muscle in actuating an elbow joint of a pediatric exoskeleton was investigated. Three different artificial skeletal muscle configurations, 1×4, 3×4 and 3×5, were tested. As expected, the 3×5 artificial muscle created the highest degree of elbow flexion. This muscle created high angular velocity about the elbow, which is desirable for exoskeleton applications. The ROM, however,

was limited, especially in the presence of a tensile load equal to or more than that of a 2-year-old forearm+hand. Additionally, the 3×5 artificial muscle required an upper arm length of about, 20 cm, which is higher than that of a 2-year-old boy, 17.5 cm.

The result of this study suggested that the degree of elbow flexion for an elbow joint actuated by CT-SDEA without proper transmission system is limited. Therefore, further improvement is necessary to add a suitable transmission system, to adjust the displacement of the muscle at its insertion point.

Chapter 6

CONCLUSION

In this dissertation, muscle-like stacked dielectric elastomer actuators (DEAs)[60,70,86,123] were used to form artificial skeletal muscles. Unlike conventional actuators (DC motors), these soft actuators create longitudinal contraction while having acoustically noiseless operation. These features will substantially improve the natural feel of rehabilitation robots, such as powered exoskeletons, which may improve user compliance. In addition, DE actuator's mechanical properties are comparable to those of skeletal muscle. Being soft, they can closely mimic the morphology of the skeletal muscle, thus reducing orthoses size while increasing the types of degrees of freedom. Their compact size and light weight will improve upon the heavy and conspicuous designs of existing powered exoskeletons.

In Aim 1 the state of soft actuator technology for use as artificial skeletal muscles in pediatric exoskeletal rehabilitation devices was assessed, and thereby, the Stacked DEA was chosen. The inclusion criteria for this aim were softness, linear actuation, acoustically noiseless operation, and demonstrated ability to lift a tensile load equal or greater than the weight of a two-year old boy's forearm+hand, 338 g. Accordingly, two thermally driven actuators, Coiled Nylon Fiber (CNF)[44] and Ethanol-Based Phase-Change (EPC)[46]; and three electro-active polymer actuators, Plasticized poly vinyl chloride (PVC) gel[53], Stacked dielectric elastomer (DE)[60] and hydraulically amplified self-healing electrostatic (HASEL)[59], were chosen for the comparison. These actuators were compared in their stress, unidirectional strain, strain-rate, power-to-mass ratio, and

efficiency. The result of our comparison showed that, within the group of aforementioned actuators, HASEL actuators and Stacked DEAs can satisfy Hypothesis 1.1-that is soft actuator technology has sufficiently progressed to allow muscle-like actuation of rehabilitation robots. The Stacked DEA, however, was the chosen due to its higher cycle life, gradual high-resolution contraction, unlike snap-through contraction of HASEL actuators, and its commercial availability. In addition to having High stress-rate, Moderate maximum strain and stress, their long cycle life is one of their most outstanding features, which makes them an ideal group of soft actuators where thousands of actuations are needed per day. Thus, a commercially available stacked DE actuator was chosen as the most applicable soft actuators technology for pediatric rehabilitation robots. CTsystems[61] is the one and only manufacturer of the commercially available Stacked DEAs, which we called CT-SDEA.

In Aim 2, a CT-SDAE-based artificial muscle, which is capable of lifting a tensile load equivalent to that of a 2-year-old boy's forearm and hand was configured. To do so, the electro-mechanical properties of the CT-SDEA were benchmarked. These properties included the: stress response, electro-mechanical delay, Young's modulus, longitudinal strain, strain-rate, power-to-mass ratio, and current consumption. The observed properties were then compared with the reported values for mammalian skeletal muscle[124]. Finally, CT-SDEA performance metrics, such as its length-tension properties and force generation hysteresis were assessed[124].

The CT-SDEAs tested in this study showed 21 ms electro-mechanical delay, and their calculated strain-rate was 660 %/s. They could generate 21.74 N of force and have a 426 W/kg power-to-mass ratio. Their longitudinal strain was measured at 3.3%. Additionally, their steady state current consumption was measured 39 μA. These results

contributed to confirming Hypotheses 2.1 - that is the tested soft actuator has reliable stress responses and its mechanical properties including stress, electro-mechanical delay, length-tension curve, stress response hysteresis, axial Young's modulus, longitudinal strain, strain-rate, and power to mass ratio, and efficiency are comparable to those of human skeletal muscle. CT-SDEA showed comparable characteristics to the human skeletal muscle, in Medium or High range: including response time, stress, and power to mass ratio. Its cycle life, although shorter than skeletal muscle, appear sufficient for rehabilitation purposes and was substantially higher than other alternative soft actuators. Its strain, however, was substantially lower than those of human skeletal muscles, which may impose challenges in design.

Finally, eight artificial muscles with various in-series and parallel CT-SDAEs were configured; and their longitudinal contraction and maximum force were measured. Thereby, we concluded that an artificial skeletal muscle consisting a bundle of three artificial myofibrils of five CT-SDEAs in-series, has sufficient force, 60 N, to lift 3.3 N and 6.8 N tensile load 6.6 mm and 5.8 mm, respectively, off the ground. These results satisfied Hypothesis 2.2 - that is the configured artificial muscle, consisting of series and parallel arrangement of the chosen soft actuator, will produce stress and strain sufficient to provide support and movement of a tensile load equivalent to that of a 2-year-old boy's forearm+hand, during both unloaded and loaded conditions. Therefore, CT-SDEA may be a prospective actuator for use in pediatric exoskeletons, considering its fast response, high strain-rate, and cycle life in comparison to other soft alternatives.

In Aim 3 a possibility of adding feedback controlled length modulation mechanism using length self-sensing property of the DEAs was evaluated. To this end, a previously established length self-sensing technique in frequency domain[82] was

implemented on a CT-SDEA. A low-pass filter was designed by connecting a resistor, 220 Ω, in series with a CT-SDEA. Then a high frequency signal, 50 Hz, was superimposed to the driving, low frequency, activation waveform. By measuring the amplitude of the output of this low-pass filter, the displacement of the CT-SDEA was inferred. The result was then tested against a laser displacement sensor. The linearity error of relationship between low pass filter output and the displacement was 15%, however, when a 2nd order polynomial was fitted the error reduced to 6%. This was not in accordance with our theoretic calculation.

To mimic the muscle spindle's function in mammalian skeletal muscle[84], a series of three CT-SDEAs was configured. Using the same self-sensing method, the length modulation of the middle actuator was then sensed, while the artificial muscle was contracting. The self-sensing information of the middle actuators was mapped to the length modulation of the whole muscle, measured by a laser displacement sensor. Although the result showed close relationship between the measured muscle displacement and the middle CT-SDEA's length self-sensing, this relationship was not as smooth as that of a single CT-SDEA, potentially due to minor sway during the contraction of this soft CT-SDEA-based artificial muscle. These results showed the capability of adding length self-sensing to the CT-SDEA by monitoring its capacity, which satisfied the Hypothesis 3.1 - that is, Similar to the function of muscle spindles of biologic muscle, the electrical characteristics of the artificial muscle may be used to provide "proprioceptive" information of actuator length without using sophisticated external sensors. The linear relationship between the low-pass filter's output and displacement can be used for an open-loop control of the proprioceptive artificial muscle, however, Hypothesis 3.2 needs further investigation.

In Aim 4 the capability of the proprioceptive artificial muscle in muscle-like actuation of the elbow joint of a pediatric upper extremity phantom model was demonstrated. The elbow joint was actuated by an artificial skeletal muscle consisting of CT-SDEAs, in series and parallel. Three different muscle configurations, 1×4, i.e, a myofibril of four CT-SDEAs in series, 3×4, and 3×5 were tested under various tensile load, 1 N to 4.50 N, at the center of mass of the forearm+hand of the phantom model. The 3×5 artificial muscle produced 22º of elbow flexion with 224 º/s angular velocity in the sagittal plane, under 1 N of tensile load. With gradual increase in the driving voltage using a linear activation waveform, this muscle could smoothly contracts throughout its active range of motion (ROM). The ROM, however, was substantially reduced as the tensile loads increased, which limits the capability of these muscles in upper extremity exoskeletons. Although the angular velocity and acceleration of the elbow joint powered by the artificial muscle surpassed the design criteria of the ARMin exoskeleton, using the proposed design, the muscle could not create a 36 º of elbow flexion. Thus, the results couldn't satisfy Hypothesis 4.1 - that is, the artificial muscles mechanizing the exoskeleton will produce maximum elbow flexion velocity and acceleration comparable to commercial upper extremity rehabilitation exoskeletons (e.g. ARMin – angular velocity 91 º/s; acceleration 116 º/s2) over the designed 36º range of elbow flexion in the sagittal plane while bearing a load in excess of the weight of the 2-year-old boy's forearm and hand.

The gradual contraction of the 3x5 artificial muscle under small incremental increase of the driving voltage, in addition to its fast response time, showed potential for a robust closed-loop position control of a joint. Further investigation is needed, however, to investigate the capability of closed-loop control of the elbow flexion to

satisfy Hypothesis 4.2. The closed-loop control of the elbow flexion can be potentially implemented using the evaluated length self-sensing as the feedback loop.

This dissertation investigated the capability of a commercially available stacked DEA, CT-SDEA, to form an artificial skeletal muscle. The benchmark testing results of this actuator[124] shed lights on its potential rehabilitation applications. Several mechanical properties of the CT-SDEA, are similar and/or comparable to mammalian skeletal muscle including: softness, acoustically noiseless and linear operation, high cycle life, and fast response. In addition, the configured **CT-SDEA-based artificial skeletal muscle was the first of its kind to mimic the hierarchical structure of skeletal muscle, including: muscle fiber, myofibril, motor units and sarcomere**. These structures may potentially help mimicking some of the control and activation strategies of the central nervous system in human body. Additionally, the artificial muscle's capability to add the proprioception may reduce the complexity of the robots deploying such technology by eliminating the need for external displacement sensors. All of these outstanding features may improve the performance and user compliance of exoskeletons deploying this technology, which results in enhanced mobility, and thereby, social, physical and cognitive improvement.

6.1 Future Direction

The results of this work demonstrated the capabilities and limitations of CT-SDEAs in rehabilitation applications, which promote further investigations. The limited shortening range of CT-SDEAs[124] and undesirable deformity are two of the challenges in designing powered exoskeletons using these actuators. The former challenge may be resolved using a biomimetic approach. The artificial muscle can be confined by a thin, flexible, and low friction shell, which resemble muscle fascia. Thereby, the muscle

would be kept aligned with its associated segment, and its motion would be confined to the desirable direction. To tackle the latter challenge, two strategies must be perused; 1) the design of a compact transmission system for force-to-displacement conversion; 2) application of the configured artificial muscles on alternate joints with lower ROM. For example, the elbow joint requires >100º ROM for activities of daily living[125], while the ankle requires~30º ROM[126].

Accordingly, as the continuation of this project, an ankle-foot powered exoskeleton will developed for children with cerebral palsy (CP), using a gait phase detection algorithm developed in our lab for CP population[127–129], as a finite state controller, and the configured artificial skeletal muscle in this dissertation, as the actuator. This project is supported by National Science Foundation (NSF), the University City Science Center and University of Delaware's Venture Development Center.

Additionally, further investigation is needed to fully develop a proprioceptive artificial muscle. More sophisticated system identification techniques such as recursive extended least squares[86] is needed to model the CT-SDEAs. Using techniques such as those proposed by Hoffstad et al.[70,86,87] and Rizzello et al.[91,130–133], to develop a comprehensive CT-SDEA model, and thereby, simulate its electrical behavior during contraction, will facilitate implementing proprioception in CT-SDEA-based artificial muscles.

Furthermore, to find a proper control strategy for precisely controlling the joint motion, various control algorithms must be investigated. Controllers such as mode-based PID[134] and adaptive sliding-mode[135] using length self-sensing as feedback might be suitable candidates. Additionally, to control the timing and intensity of contraction,

EMG activity can be used as the feedback for exoskeleton applications[81]. To further assure robust and reliable joint motion in the cable-driven exoskeletons actuated by such artificial muscles, the proposed control algorithm for cable-driven robots[136–138], such as the one used in Cable-Driven Arm Exoskeleton (CAREX)[139], must be assessed for future CT-SDEA-driven exoskeletons.

The proposed exoskeleton in this dissertation is based on a phantom model morphology, however, a design is needed in the future that fits to a real child's upper-extremity geometry. One strategy is mounting of the artificial skeletal muscles on a previously proposed passive exoskeleton, such as P-WREX[13].

REFERENCES

1. Lobo MA, Harbourne RT, Dusing SC, McCoy SW. Grounding early intervention: physical therapy cannot just be about motor skills anymore. *Phys Ther*. 2013;93(1):94-103. doi:10.2522/ptj.20120158 [doi]

2. Needham A, Barrett T, Peterman K. A pick-me-up for infants' exploratory skills: Early simulated experiences reaching for objects using 'sticky mittens' enhances young infants' object exploration skills. *Infant Behav Dev*. 2002;25(3):279-295.

3. Libertus K, Needham A. Teach to reach: the effects of active vs. passive reaching experiences on action and perception. *Vision Res*. 2010;50(24):2750-2757. doi:10.1016/j.visres.2010.09.001 [doi]

4. Lobo MA, Kokkoni E, Cunha AB, Galloway JC. Infants born preterm demonstrate impaired object exploration behaviors throughout infancy and toddlerhood. *Phys Ther*. 2015;95(1):51-64. doi:10.2522/ptj.20130584 [doi]

5. Lobo MA, Galloway JC. Postural and object-oriented experiences advance early reaching, object exploration, and means-end behavior. *Child Dev*. 2008;79(6):1869-1890. doi:10.1111/j.1467-8624.2008.01231.x [doi]

6. Lockman JJ. A perception--action perspective on tool use development. *Child Dev*. 2000;71(1):137-144.

7. Anderson KD. Targeting recovery: priorities of the spinal cord-injured population. *J Neurotrauma*. 2004;21(10):1371-1383.

8. Hanson RW, Franklin MR. Sexual loss in relation to other functional losses for spinal cord injured males. *Arch Phys Med Rehabil*. 1976;57(6):291-293.

9. Bamshad M, Van Heest AE, Pleasure D. Arthrogryposis: a review and update. *J bone Jt surgeryAmerican Vol*. 2009;91 Suppl 4:40-46. doi:10.2106/JBJS.I.00281 [doi]

10. Stearns GE, Burtner P, Keenan KM, Qualls C, Phillips J. Effects of constraint-induced movement therapy on hand skills and muscle recruitment of children with spastic hemiplegic cerebral palsy. *NeuroRehabilitation*. 2009;24(2):95-

108. doi:10.3233/NRE-2009-0459 [doi]

11. Sakzewski L, Ziviani J, Boyd R. Systematic review and meta-analysis of therapeutic management of upper-limb dysfunction in children with congenital hemiplegia. *Pediatrics*. 2009;123(6):e1111-22. doi:10.1542/peds.2008-3335 [doi]

12. Ceprnja AR, Jukica M, Vlak T. Pediatric rehabilitation in children with obstetrical injuries of the brachial plexus. *Paediatr Croat*. 2012;56:232-239.

13. Babik I, Kokkoni E, Cunha AB, Galloway JC, Rahman T, Lobo MA. Feasibility and Effectiveness of a Novel Exoskeleton for an Infant with Arm Movement Impairments. *Pediatr Phys Ther*. 2016;28(3):338-346. doi:10.1097/PEP.0000000000000271 [doi]

14. Keller U, van Hedel HJA, Klamroth-Marganska V, Riener R. ChARMin: The first actuated exoskeleton robot for pediatric arm rehabilitation. *IEEE/ASME Trans Mechatronics*. 2016;21(5):2201-2213.

15. Fasoli SE, Ladenheim B, Mast J, Krebs HI. New horizons for robot-assisted therapy in pediatrics. *Am J Phys Med Rehabil*. 2012;91(11 Suppl 3):S280-9. doi:10.1097/PHM.0b013e31826bcff4 [doi]

16. Page SJ, Hill V, White S. Portable upper extremity robotics is as efficacious as upper extremity rehabilitative therapy: A randomized controlled pilot trial. *Clin Rehabil*. 2013. doi:10.1177/0269215512464795

17. Platz T. Evidenzbasierte armrehabilitation: Eine systematische literaturübersicht. *Nervenarzt*. 2003;74:841-849.

18. Feys H, De Weerdt W, Verbeke G, et al. Early and repetitive stimulation of the arm can substantially improve the long-term outcome after stroke: a 5-year follow-up study of a randomized trial. *Stroke*. 2004;35(4):924-929. doi:10.1161/01.STR.0000121645.44752.f7 [doi]

19. Damiano DL. Activity, activity, activity: rethinking our physical therapy approach to cerebral palsy. *Phys Ther*. 2006;86(11):1534-1540.

20. Charles JR, Wolf SL, Schneider JA, Gordon AM. Efficacy of a child-friendly form of constraint-induced movement therapy in hemiplegic cerebral palsy: a randomized control trial. *Dev Med Child Neurol*. 2006;48(08):635-642.

21. Richards L, Hanson C, Wellborn M, Sethi A. Driving motor recovery after stroke. *Top Stroke Rehabil*. 2008;15(5):397-411.

22. van der Lee JH, Snels IA, Beckerman H, Lankhorst GJ, Wagenaar RC, Bouter LM. Exercise therapy for arm function in stroke patients: a systematic review of randomized controlled trials. *Clin Rehabil*. 2001;15(1):20-31.

23. Kwakkel G, Kollen BJ, Krebs HI. Effects of robot-assisted therapy on upper limb recovery after stroke: a systematic review. *Neurorehabil Neural Repair*. 2008;22(2):111-121. doi:1545968307305457 [pii]

24. Maciejasz P, Eschweiler J, Gerlach-Hahn K, Jansen-Troy A, Leonhardt S. A survey on robotic devices for upper limb rehabilitation. *J Neuroeng Rehabil*. 2014;11(1):1.

25. Dollar AM, Herr H. Lower extremity exoskeletons and active orthoses: challenges and state-of-the-art. *IEEE Trans Robot*. 2008;24(1):144-158.

26. Rabischong P. Robotics for the handicapped. In: *Control Aspects of Prosthetics and Orthotics*. Elsevier; 1983:163-171.

27. Nef T, Mihelj M, Kiefer G, Perndl C, Muller R, Riener R. ARMin-Exoskeleton for arm therapy in stroke patients. In: *Rehabilitation Robotics, 2007. ICORR 2007. IEEE 10th International Conference On*. IEEE; 2007:68-74.

28. Rocon E, Ruiz AF, Pons JL, Belda-Lois JM, Sánchez-Lacuesta JJ. Rehabilitation robotics: a wearable exo-skeleton for tremor assessment and suppression. In: *Robotics and Automation, 2005. ICRA 2005. Proceedings of the 2005 IEEE International Conference On*. IEEE; 2005:2271-2276.

29. Rahman T, Galloway C, Kokkoni E, Lobo M. Development and Testing of a Modular Upper Extremity Exoskeleton for Infants. In: *BIODEVICES*. ; 2014:316-319.

30. Rahman T, Sample W, Jayakumar S, et al. Passive exoskeletons for assisting limb movement. *J Rehabil Res Dev*. 2006;43(5):583-590.

31. Haumont T, Rahman T, Sample W, et al. Wilmington robotic exoskeleton: a novel device to maintain arm improvement in muscular disease. *J Pediatr Orthop*. 2011;31(5):e44-9. doi:10.1097/BPO.0b013e31821f50b5 [doi]

32. Rahman T, Sample W, Seliktar R, et al. Design and testing of a functional arm orthosis in patients with neuromuscular diseases. *IEEE Trans Neural Syst Rehabil Eng*. 2007;15(2):244-251.

33. Ragonesi D, Agrawal S, Sample W, Rahman T. Series elastic actuator control of a powered exoskeleton. In: *Engineering in Medicine and Biology Society,*

EMBC, 2011 Annual International Conference of the IEEE. IEEE; 2011:3515-3518.

34. Biddiss E, Chau T. Dielectric elastomers as actuators for upper limb prosthetics: challenges and opportunities. *Med Eng Phys*. 2008;30(4):403-418. doi:S1350-4533(07)00104-X [pii]

35. Sanchez RJ, Wolbrecht E, Smith R, et al. A pneumatic robot for re-training arm movement after stroke: Rationale and mechanical design. In: *Rehabilitation Robotics, 2005. ICORR 2005. 9th International Conference On*. IEEE; 2005:500-504.

36. Hall ML, Lobo MA. Design and development of the first exoskeletal garment to enhance arm mobility for children with movement impairments. *Assist Technol*. 2017:1-8.

37. Rus D, Tolley MT. Design, fabrication and control of soft robots. *Nature*. 2015;521(7553):467.

38. Parette P, Scherer M. Assistive technology use and stigma. *Educ Train Dev Disabil*. 2004:217-226.

39. Madden JDW, Vandesteeg NA, Anquetil PA, et al. Artificial muscle technology: physical principles and naval prospects. *IEEE J Ocean Eng*. 2004;29(3):706-728.

40. Mirfakhrai T, Madden JDW, Baughman RH. Polymer artificial muscles. *Mater today*. 2007;10(4):30-38.

41. Gopura R, Bandara DS V, Kiguchi K, Mann GKI. Developments in hardware systems of active upper-limb exoskeleton robots: A review. *Rob Auton Syst*. 2016;75:203-220.

42. Yoo IS, Reitelshöfer S, Landgraf M, Franke J. Artificial Muscles, Made of Dielectric Elastomer Actuators-A Promising Solution for Inherently Compliant Future Robots. In: *Soft Robotics*. Springer; 2015:33-41.

43. Verl A, Albu-Schäffer A, Brock O, Raatz A. *Soft Robotics*. Springer; 2015.

44. Haines CS, Lima MD, Li N, et al. Artificial muscles from fishing line and sewing thread. *Science*. 2014;343(6173):868-872. doi:10.1126/science.1246906 [doi]

45. Lima MD, Li N, Jung de Andrade M, et al. Electrically, chemically, and

photonically powered torsional and tensile actuation of hybrid carbon nanotube yarn muscles. *Science*. 2012;338(6109):928-932. doi:10.1126/science.1226762 [doi]

46. Miriyev A, Stack K, Lipson H. Soft material for soft actuators. *Nat Commun*. 2017;8(1):596.

47. Leng J, Lan X, Liu Y, Du S. Shape-memory polymers and their composites: stimulus methods and applications. *Prog Mater Sci*. 2011;56(7):1077-1135.

48. Pappas GP, Asakawa DS, Delp SL, Zajac FE, Drace JE. Nonuniform shortening in the biceps brachii during elbow flexion. *J Appl Physiol*. 2002. doi:10.1152/japplphysiol.00843.2001

49. Cavanagh PR, Komi P V. Electromechanical delay in human skeletal muscle under concentric and eccentric contractions. *Eur J Appl Physiol Occup Physiol*. 1979;42(3):159-163.

50. Kim ,Tadokoro, Satoshi., KJ. *Electroactive Polymers for Robotic Applications : Artificial Muscles and Sensors*. London: Springer; 2007.

51. Carpi F, Kornbluh R, Sommer-Larsen P, Alici G. Electroactive polymer actuators as artificial muscles: are they ready for bioinspired applications? *Bioinspir Biomim*. 2011;6(4):45006.

52. Bar-Cohen Y, Cardoso VF, Ribeiro C, Lanceros-Méndez S. Electroactive polymers as actuators. In: *Advanced Piezoelectric Materials (Second Edition)*. Elsevier; 2017:319-352.

53. Li Y, Hashimoto M. PVC gel based artificial muscles: Characterizations and actuation modular constructions. *Sensors Actuators A Phys*. 2015;233:246-258.

54. Li Y, Hashimoto M. Design and prototyping of a novel lightweight walking assist wear using PVC gel soft actuators. *Sensors Actuators A Phys*. 2016;239:26-44.

55. Ashley S. Artificial muscles. *Sci Am*. 2003;289(4):52-59.

56. Carpi F, De Rossi D, Kornbluh R, Pelrine RE, Sommer-Larsen P. *Dielectric Elastomers as Electromechanical Transducers: Fundamentals, Materials, Devices, Models and Applications of an Emerging Electroactive Polymer Technology*. Elsevier; 2011.

57. Carpi F, Frediani G, Gerboni C, Gemignani J, De Rossi D. Enabling variable-

stiffness hand rehabilitation orthoses with dielectric elastomer transducers. *Med Eng Phys*. 2014;36(2):205-211. doi:10.1016/j.medengphy.2013.10.015 [doi]

58. Pei Q, Pelrine R, Stanford S, et al. Multifunctional electroelastomer rolls and their application for biomimetic walking robots. In: *Synthetic Metals*. International Society for Optics and Photonics; 2003:246-253. doi:10.1016/S0379-6779(02)00535-0

59. Acome E, Mitchell SK, Morrissey TG, et al. Hydraulically amplified self-healing electrostatic actuators with muscle-like performance. *Science (80-)*. 2018;359(6371):61-65.

60. Kovacs G, Düring L, Michel S, Terrasi G. Stacked dielectric elastomer actuator for tensile force transmission. *Sensors Actuators A Phys*. 2009;155(2):299-307.

61. Dr. Gabor Kovacs LD. CTsystems, Swiss compliant transducer. http://www.ct-systems.ch/. Published 2016.

62. Mohd Jani J, Leary M, Subic A, Gibson MA. A review of shape memory alloy research, applications and opportunities. *Mater Des*. 2014;56:1078-1113. doi:10.1016/J.MATDES.2013.11.084

63. Iqbal D, Samiullah M, Iqbal D, Samiullah MH. Photo-Responsive Shape-Memory and Shape-Changing Liquid-Crystal Polymer Networks. *Materials (Basel)*. 2013;6(1):116-142. doi:10.3390/ma6010116

64. Kohl M, Brugger D, Ohtsuka M, Takagi T. A novel actuation mechanism on the basis of ferromagnetic SMA thin films. *Sensors Actuators A Phys*. 2004;114(2-3):445-450. doi:10.1016/J.SNA.2003.11.006

65. Carpi F, Bauer S, De Rossi D. Materials science. Stretching dielectric elastomer performance. *Science*. 2010;330(6012):1759-1761. doi:10.1126/science.1194773 [doi]

66. de Onis M, Onyango AW. WHO child growth standards. *Lancet (London, England)*. 2008;371(9608):202-204. doi:10.1016/S0140-6736(08)60131-2 [doi]

67. Winter DA. *Biomechanics and Motor Control of Human Movement*. John Wiley & Sons; 2009.

68. Close RI. Dynamic properties of mammalian skeletal muscles. *Physiol Rev*. 1972;52(1):129-197. doi:10.1152/physrev.1972.52.1.129

69. Whittle MW, Levine D, Richards J, Whittle MW. *Whittle's Gait Analysis*.

Elsevier Health Sciences; 2012.

70. Hoffstadt T, Griese M, Maas J. Online identification algorithms for integrated dielectric electroactive polymer sensors and self-sensing concepts. *Smart Mater Struct*. 2014;23(10):104007. doi:10.1088/0964-1726/23/10/104007

71. Zhang R, Kunz A, … PL-HI for, 2006 undefined. Dielectric elastomer spring roll actuators for a portable force feedback device. *ieeexplore.ieee.org*. https://ieeexplore.ieee.org/abstract/document/1627137/. Accessed January 20, 2019.

72. IEC T. 60479-2: 2007 Effects of current on human beings and livestock. *Part*.

73. Hodgins M, York A, Seelecke S. Modeling and experimental validation of a bi-stable out-of-plane DEAP actuator system. *Smart Mater Struct*. 2011. doi:10.1088/0964-1726/20/9/094012

74. Hau S, Rizzello G, Seelecke S. A novel dielectric elastomer membrane actuator concept for high-force applications. *Extrem Mech Lett*. 2018. doi:10.1016/j.eml.2018.07.002

75. Ha SM, Yuan W, Pei Q, Pelrine R, Stanford S. Interpenetrating Polymer Networks for High-Performance Electroelastomer Artificial Muscles. *Adv Mater*. 2006;18(7):887-891.

76. Kovacs G, Ha SM, Michel S, Pelrine R, Pei Q. Study on core free rolled actuator based on soft dielectric EAP. In: Bar-Cohen Y, ed. Vol 6927. International Society for Optics and Photonics; 2008:69270X. doi:10.1117/12.776787

77. Sarban R, Jones RWW, Mace BRR, Rustighi E. *A Tubular Dielectric Elastomer Actuator: Fabrication, Characterization and Active Vibration Isolation*. Vol 25. Academic Press; 2011:2879-2891. doi:10.1016/j.ymssp.2011.06.004

78. Carpi F, Migliore A, Serra G, De Rossi D. Helical dielectric elastomer actuators. *Smart Mater Struct*. 2005;14(6):1210.

79. Carpi F, Salaris C, De Rossi D. Folded dielectric elastomer actuators. *Smart Mater Struct*. 2007;16(2):S300.

80. Carpi F, De Rossi D. Contractile dielectric elastomer actuator with folded shape. In: *Smart Structures and Materials*. International Society for Optics and Photonics; 2006:61680D-61680D - 6.

81. Carpi F, Raspopovic S, Frediani G, De Rossi D. Real-time control of dielectric elastomer actuators via bioelectric and biomechanical signals. *Polym Int*. 2010. doi:10.1002/pi.2757

82. Jung K, Kim KJ, Choi HR. A self-sensing dielectric elastomer actuator. *Sensors Actuators A Phys*. 2008;143(2):343-351.

83. Chuc NH, Thuy DV, Park J, et al. A dielectric elastomer actuator with self-sensing capability. In: *The 15th International Symposium on: Smart Structures and Materials & Nondestructive Evaluation and Health Monitoring*. International Society for Optics and Photonics; 2008:69270V-69270V - 8.

84. Lephart S, Fu F. The role of proprioception in the treatment of sports injuries. *Sport Exerc Inj*. 1995.

85. Houglum P. *Therapeutic Exercise for Musculoskeletal Injuries 4th Edition*.; 2016. https://books.google.com/books?hl=en&lr=&id=WVcvDAAAQBAJ&oi=fnd&pg=PR1&dq=therapeutic+exercise+for+musculoskeletal+injuries&ots=XV79cAKnpg&sig=OvqbWfbsPGNY_gg5vTdlDxhxeb0. Accessed March 18, 2019.

86. Hoffstadt T, Maas J. Self-sensing Algorithms for Dielectric Elastomer Multilayer Stack-Transducers. *IFAC-PapersOnLine*. 2016. doi:10.1016/j.ifacol.2016.10.583

87. Hoffstadt T, Maas J. Model-based self-sensing algorithm for dielectric elastomer transducers based on an extended Kalman filter. *Mechatronics*. 2018;50:248-258. doi:10.1016/j.mechatronics.2017.09.013

88. Gisby TA, O'Brien BM, Anderson IA. Self sensing feedback for dielectric elastomer actuators. *Appl Phys Lett*. 2013;102(19):193703. doi:10.1063/1.4805352

89. Rosset S, O'Brien BM, Gisby T, Xu D, Shea HR, Anderson IA. Self-sensing dielectric elastomer actuators in closed-loop operation. *Smart Mater Struct*. 2013;22(10):104018. doi:10.1088/0964-1726/22/10/104018

90. Ye Z, Chen Z. Integrated sensing and actuation of dielectric elastomer actuator. In: Bar-Cohen Y, ed. ; 2017:101630C. doi:10.1117/12.2262358

91. Rizzello G, Naso D, York A, Seelecke S. Closed loop control of dielectric elastomer actuators based on self-sensing displacement feedback. *Smart Mater Struct*. 2016. doi:10.1088/0964-1726/25/3/035034

92. Gisby TA, O'Brien BM, Xie SQ, Calius EP, Anderson IA. Closed loop control of dielectric elastomer actuators. In: Bar-Cohen Y, Carpi F, eds. ; 2011:797620. doi:10.1117/12.880711

93. Gisby TA, Calius EP, Xie S, Anderson IA. An adaptive control method for dielectric elastomer devices. In: *The 15th International Symposium on: Smart Structures and Materials & Nondestructive Evaluation and Health Monitoring*. International Society for Optics and Photonics; 2008:69271C-69271C - 8.

94. Calabrò RS, Russo M, Naro A, et al. Who May Benefit From Armeo Power Treatment? A Neurophysiological Approach to Predict Neurorehabilitation Outcomes. *PM&R*. 2016;8(10):971-978. doi:10.1016/j.pmrj.2016.02.004

95. Reinkensmeyer DJ, Boninger ML. Technologies and combination therapies for enhancing movement training for people with a disability. *J Neuroeng Rehabil*. 2012;9(1):1.

96. Nef T, Mihelj M, … GC-P 2006 I, 2006 undefined. ARMin-robot for rehabilitation of the upper extremities. *ieeexplore.ieee.org*. https://ieeexplore.ieee.org/abstract/document/1642181/. Accessed March 9, 2019.

97. Nef T, on RR-9th IC, 2005 undefined. ARMin-design of a novel arm rehabilitation robot. *ieeexplore.ieee.org*. https://ieeexplore.ieee.org/abstract/document/1501051/. Accessed March 9, 2019.

98. Nef T, Guidali M, and RR-AB, 2009 undefined. ARMin III–arm therapy exoskeleton with an ergonomic shoulder actuation. *content.iospress.com*. https://content.iospress.com/articles/applied-bionics-and-biomechanics/abb384187. Accessed March 9, 2019.

99. Nef T, Mihelj M, Kiefer G, … CP-2007 I 10th, 2007 undefined. ARMin-Exoskeleton for arm therapy in stroke patients. *ieeexplore.ieee.org*. https://ieeexplore.ieee.org/abstract/document/4428408/. Accessed March 9, 2019.

100. Nef T, Mihelj M, Riener R. ARMin: a robot for patient-cooperative arm therapy. *Med Biol Eng Comput*. 2007;45(9):887-900. doi:10.1007/s11517-007-0226-6

101. Nef T, Guidali M, Klamroth-Marganska V, Riener R. ARMin - Exoskeleton Robot for Stroke Rehabilitation. In: ; 2009:127-130. doi:10.1007/978-3-642-03889-1_35

102. Lum P, … CB-J of, 2006 undefined. MIME robotic device for upper-limb neurorehabilitation in subacute stroke subjects: A follow-up study. *Dep Veterans Aff*. https://scholar.google.com/scholar?hl=en&as_sdt=0%2C8&q=.+Lum%2C+P.S.%2C+Burga%2C+C.G.%2C+Loos%2C+M.V.%2C+Sho%2C+P.C.%2C+Majmundar%2C+M.%2C+Yap%2C+R.%3A+MIME+robotic+device+for+upper-limb+neurorehabilitation+in+subacute+stroke+subjects%3A+A+follow-up+study.+J.+Rehabil.+Res.+Dev.+43%285%29%2C+631–642+%282006%29&btnG=. Accessed March 9, 2019.

103. Rahman T, Sample W, Seliktar R. 16 Design and Testing of WREX. In: *Advances in Rehabilitation Robotics*. Springer; 2004:243-250.

104. Hogan N, Krebs HI, Charnnarong J, Srikrishna P, Sharon A. MIT-MANUS: a workstation for manual therapy and training. I. In: *[1992] Proceedings IEEE International Workshop on Robot and Human Communication*. IEEE; :161-165. doi:10.1109/ROMAN.1992.253895

105. Krebs H, Ferraro M, Buerger SP, et al. Rehabilitation robotics: pilot trial of a spatial extension for MIT-Manus. *J Neuroeng Rehabil*. 2004;1(1):5. doi:10.1186/1743-0003-1-5

106. Kim GJ, Rivera L, Stein J. Combined Clinic-Home Approach for Upper Limb Robotic Therapy after Stroke: A Pilot Study. *Arch Phys Med Rehabil*. 2015. doi:10.1016/j.apmr.2015.06.019

107. Stein J, Narendran K, McBean J, … KK-A journal of, 2007 undefined. Electromyography-controlled exoskeletal upper-limb–powered orthosis for exercise training after stroke. *journals.lww.com*. https://journals.lww.com/ajpmr/FullText/2007/04000/Electromyography_Controlled_Exoskeletal.2.aspx. Accessed March 9, 2019.

108. Qian Z, Bi Z. Recent development of rehabilitation robots. *Adv Mech Eng*. 2015;7(2):563062.

109. Shorter KA, Xia J, Hsiao-Wecksler ET, Durfee WK, Kogler GF. Technologies for powered ankle-foot orthotic systems: Possibilities and challenges. *IEEE/ASME Trans mechatronics*. 2013;18(1):337-347.

110. Vallery H, Veneman J, Van Asseldonk E, Ekkelenkamp R, Buss M, Van Der Kooij H. Compliant actuation of rehabilitation robots. *IEEE Robot Autom Mag*. 2008;15(3).

111. Dickinson MH, Farley CT, Full RJ, Koehl MA, Kram R, Lehman S. How

animals move: an integrative view. *Science*. 2000;288(5463):100-106. doi:8425 [pii]

112. Matsumoto Y, Nishida Y, Motomura Y, Okawa Y. A concept of needs-oriented design and evaluation of assistive robots based on ICF. In: *Rehabilitation Robotics (ICORR), 2011 IEEE International Conference On*. IEEE; 2011:1-6.

113. Zrínyi M, Zrinyi M. Intelligent polymer gels controlled by magnetic fields. *Colloid Polym Sci Colloid Polym Sci Kolloid-Zeitschrift und Zeitschrift für Polym*. 2000;278(2):98-103.

114. Herr HM, Kornbluh RD. New horizons for orthotic and prosthetic technology: artificial muscle for ambulation. In: *Smart Structures and Materials*. International Society for Optics and Photonics; 2004:1-9.

115. Bar-Cohen Y, Breazeal C. Biologically inspired intelligent robots. In: *Smart Structures and Materials*. International Society for Optics and Photonics; 2003:14-20.

116. Gurunathan Murugan, A.Vadivel, Marimuthu, R, Mulik, U.P,Amalnerkar, D.P, K. Electrochemically synthesised conducting polymeric materials for applications towards technology in electronics, optoelectronics and energy storage devices. *Mater Chem Phys Mater Chem Phys*. 1999;61(3):173-191.

117. Bar-Cohen Y. Electroactive polymer (EAP) actuators as artificial muscles reality, potential, and challenges. http://public.eblib.com/choice/publicfullrecord.aspx?p=728484. Published 2004.

118. Ayre M. Biomimetics applied to space exploration. In: *Proc. of 2nd Int. Conf. Design&Nature, Rhodes, Greece*. ; 2004.

119. Kornbluh RD, Prahlad H, Pelrine R, Stanford S, Rosenthal MA, von Guggenberg PA. Rubber to rigid, clamped to undamped: toward composite materials with wide-range controllable stiffness and damping. In: *Smart Structures and Materials*. International Society for Optics and Photonics; 2004:372-386.

120. Chiba S. Dielectric Elastomers. In: *Soft Actuators*. Springer; 2014:183-195.

121. Tognetti A, Carpi F, Lorussi F, et al. Wearable sensory-motor orthoses for tele-rehabilitation. In: *Engineering in Medicine and Biology Society, 2003. Proceedings of the 25th Annual International Conference of the IEEE*. Vol 4. IEEE; 2003:3724-3727.

122. Carpi F, Mannini A, De Rossi D. Elastomeric contractile actuators for hand rehabilitation splints. In: *The 15th International Symposium on: Smart Structures and Materials & Nondestructive Evaluation and Health Monitoring*. International Society for Optics and Photonics; 2008:692705-692710.

123. Chuc NH, Park JK, Thuy DV, et al. Multi-stacked artificial muscle actuator based on synthetic elastomer. In: *Intelligent Robots and Systems, 2007. IROS 2007. IEEE/RSJ International Conference On*. IEEE; 2007:771-776.

124. Behboodi A, Lee SCKSCK. Benchmarking of a Commercially Available Stacked Dielectric Elastomer As an Alternative Actuator for Rehabilitation Robotic Exoskeletons. In: *IEEE 16th International Conference on Rehabilitation Robotics (ICORR)*. Toronto, Canada: IEEE; 2019:499-505. doi:10.1109/ICORR.2019.8779378

125. Petuskey K, Bagley A, Abdala E, James MA, Rab G. Upper extremity kinematics during functional activities: Three-dimensional studies in a normal pediatric population. *Gait Posture*. 2007;25(4):573-579. doi:10.1016/J.GAITPOST.2006.06.006

126. Perry J, Burnfield JM. Gait analysis: normal and pathological function. 1992.

127. Behboodi A, Zahradka N, Wright H, et al. Real-Time Detection of Seven Phases of Gait in Children with Cerebral Palsy Using Two Gyroscopes. *Sensors*. 2019;19(11):2517. doi:10.3390/s19112517

128. Behboodi A, Zahradka N, Alesi J, Wright H, Lee SCK. Use of a Novel Functional Electrical Stimulation Gait Training System in 2 Adolescents With Cerebral Palsy: A Case Series Exploring Neurotherapeutic Changes. *Phys Ther*. 2019;99(6):739-747. doi:10.1093/ptj/pzz040

129. Behboodi A, Wright H, Zahradka N, Lee SCKCK. Seven phases of gait detected in real-time using shank attached gyroscopes. In: *Conference Proceedings : ...Annual International Conference of the IEEE Engineering in Medicine and Biology Society.IEEE Engineering in Medicine and Biology Society.Annual Conference*. Vol 2015. United States: IEEE; 2015:5529-5532. doi:10.1109/EMBC.2015.7319644 [doi]

130. Hodgins M, Rizzello G, York A, Seelecke S. High-Frequency Dynamic Model of a Pre-Loaded Circular Dielectric Electro-Active Polymer Actuator. In: *ASME 2013 Conference on Smart Materials, Adaptive Structures and Intelligent Systems*. ; 2013. doi:10.1007/s00265-008-0584-6

131. Rizzello G, Naso D, … BT-IT on, 2016 undefined. Robust position control of

dielectric elastomer actuators based on LMI optimization. *ieeexplore.ieee.org*. https://ieeexplore.ieee.org/abstract/document/7407332/. Accessed July 16, 2019.

132. Hodgins M, Rizzello G, Naso D, York A, Seelecke S. An electro-mechanically coupled model for the dynamic behavior of a dielectric electro-active polymer actuator. *Smart Mater Struct*. 2014;23(10):104006. doi:10.1088/0964-1726/23/10/104006

133. Hau S, Rizzello G, Hodgins M, … AY-I, 2017 undefined. Design and control of a high-speed positioning system based on dielectric elastomer membrane actuators. *ieeexplore.ieee.org*. https://ieeexplore.ieee.org/abstract/document/7876720/. Accessed July 16, 2019.

134. Rizzello G, Naso D, York A, Volumes SS-IP, 2014 undefined. Model-based PID control of a dielectric electro-active polymer positioning system. *Elsevier*. https://www.sciencedirect.com/science/article/pii/S1474667016433513. Accessed July 16, 2019.

135. Hoffstadt T, Maas J. Adaptive Sliding-Mode Position Control for Dielectric Elastomer Actuators. *IEEE/ASME Trans Mechatronics*. 2017;22(5):2241-2251. doi:10.1109/TMECH.2017.2730589

136. Renda F, Giorelli M, Calisti M, Cianchetti M, Laschi C. Dynamic Model of a Multibending Soft Robot Arm Driven by Cables. *IEEE Trans Robot*. 2014;30(5):1109-1122. doi:10.1109/TRO.2014.2325992

137. Behboodi A, Salehi S. SDRE controller for motion design of cable-suspended robot with uncertainties and moving obstacles. In: *IOP Conference Series: Materials Science and Engineering*. Vol 248. ; 2017. doi:10.1088/1757-899X/248/1/012031

138. Brackbill EA, Ying Mao, Agrawal SK, Annapragada M, Dubey VN. Dynamics and control of a 4-dof wearable cable-driven upper arm exoskeleton. In: *2009 IEEE International Conference on Robotics and Automation*. IEEE; 2009:2300-2305. doi:10.1109/ROBOT.2009.5152545

139. Mao Y, Agrawal SK. Design of a Cable-Driven Arm Exoskeleton (CAREX) for Neural Rehabilitation. *IEEE Trans Robot*. 2012;28(4):922-931. doi:10.1109/TRO.2012.2189496

Appendix A

DISCLAIMER

A substantial part of the Chapter 3 (theoretical results and figures) has been previously published in 2019 IEEE 16th International Conference on Rehabilitation Robotics (ICORR)[124]. The IEEE does not require individuals working on a thesis to obtain a formal reuse license.

In reference to IEEE copyrighted material, which is used with permission in this thesis, the IEEE does not endorse any of the University of Delaware's products or services. Internal or personal use of this material is permitted. If interested in reprinting/republishing IEEE copyrighted material for advertising or promotional purposes or for creating new collective works for resale or redistribution, please go to http://www.ieee.org/publications_standards/publications/rights/rights_link.html to learn how to obtain a License from RightsLink.

Copyright Clearance Center RightsLink®

Home | Account Info | Help

IEEE Requesting permission to reuse content from an IEEE publication

Title:	Benchmarking of a Commercially Available Stacked Dielectric Elastomer as an Alternative Actuator for Rehabilitation Robotic Exoskeletons *
Conference Proceedings:	2019 IEEE 16th International Conference on Rehabilitation Robotics (ICORR)
Author:	A. Behboodi
Publisher:	IEEE
Date:	June 2019

Logged in as:
Ahad Behboodi
LOGOUT

Thesis / Dissertation Reuse

The IEEE does not require individuals working on a thesis to obtain a formal reuse license, however, you may print out this statement to be used as a permission grant:

Requirements to be followed when using any portion (e.g., figure, graph, table, or textual material) of an IEEE copyrighted paper in a thesis:

1) In the case of textual material (e.g., using short quotes or referring to the work within these papers) users must give full credit to the original source (author, paper, publication) followed by the IEEE copyright line © 2011 IEEE.
2) In the case of illustrations or tabular material, we require that the copyright line © [Year of original publication] IEEE appear prominently with each reprinted figure and/or table.
3) If a substantial portion of the original paper is to be used, and if you are not the senior author, also obtain the senior author's approval.

Requirements to be followed when using an entire IEEE copyrighted paper in a thesis:

1) The following IEEE copyright/ credit notice should be placed prominently in the references: © [year of original publication] IEEE. Reprinted, with permission, from [author names, paper title, IEEE publication title, and month/year of publication]
2) Only the accepted version of an IEEE copyrighted paper can be used when posting the paper or your thesis on-line.
3) In placing the thesis on the author's university website, please display the following message in a prominent place on the website: In reference to IEEE copyrighted material which is used with permission in this thesis, the IEEE does not endorse any of [university/educational entity's name goes here]'s products or services. Internal or personal use of this material is permitted. If interested in reprinting/republishing IEEE copyrighted material for advertising or promotional purposes or for creating new collective works for resale or redistribution, please go to http://www.ieee.org/publications_standards/publications/rights/rights_link.html to learn how to obtain a License from RightsLink.

If applicable, University Microfilms and/or ProQuest Library, or the Archives of Canada may supply single copies of the dissertation.

BACK | CLOSE WINDOW